Crystallization Studies of Liquid Crystalline Polycarbonates Based on Substituted Stilbene Mesogen

by

Yao-Yi Cheng

B.S., Tsing Hua University, Hsinchu, Taiwan
(1990)

Submitted to the Department of Materials
Science and Engineering in partial fulfillment of
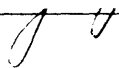the requirement for the degree of

DOCTOR OF PHILOSOPHY

at the

Massachusetts Institute of Technology
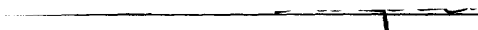
February, 1995

Signature of Author _____
Department of Materials Science and Engineering
January 13, 1995

Certified by _____
Associate Professor Peggy Cebe
Thesis Supervisor

Accepted by _____
Carl V. Thompson II
Professor of Electronic Materials, Chair, Departmental Committee on Graduate Students

MASSACHUSETTS INSTITUTE
OF TECHNOLOGY

JUL 2 0 1995

Science

Crystallization Studies of Liquid Crystalline Polycarbonates Based on Substituted Stilbene Mesogen

by

Yao-Yi Cheng

Submitted to the Department of Materials Science and Engineering
on January 13, 1995, in partial fulfillment of the requirement for the degree
of Doctor of Philosophy

Abstract

The purpose of this research is to investigate the relationship between the chemical structure variations and the macroscopic properties like thermal transition temperatures and crystallization kinetics for liquid crystalline polycarbonates based on substituted stilbene mesogen. The chemical variations include changes in the methylene spacer length and substitution on the mesogen. We are able to determine the role of the chemical variations on the thermodynamic stability of the mesophase and in the nucleation kinetics and growth of the crystalline phase.

For our liquid crystalline α-methyl stilbene (HMS) polycarbonates, there is a very narrow temperature range of stability for the mesophase. The mesophase, which is actually monotropic, can be only observed during cooling when three dimensional crystal growth is suppressed. The multiple melting endotherms seen in the heating scan are assigned either to the melting of more perfect crystals forming from the mesophase (melting at higher temperature) or to less perfect crystals forming from the isotropic phase (melting at lower temperature). The region of stability of the mesophase seen in the cooling scan becomes smaller, when the methylene spacer number, n, ranges from 5 to 8. When the length of spacer becomes greater than that of the mesogen ($n \geq 9$), all the transition temperatures drop. Using wide angle X-ray scattering and molecular modeling, we show that the orientation of the carbonate group and the length of the methylene spacer are both implicated in the rapid nucleation of crystals. When the length of the methylene spacer and the mesogen are comparable, a regularly packed intermeshed crystal structure occurs. This crystal structure forms rapidly from the mesophase which acts as a template for nucleation and growth of crystals from an already ordered melt. Using small angle X-ray scattering, we have found for the first time that HMS polycarbonates with odd-numbered methylene spacer have a higher value of crystal lamellar thickness than those with even-numbered one. The odd-even oscillation in lattice parameters and lamellar characteristics has not been reported before. Changes in long period, lamellar thickness, and linear crystallinity during non-isothermal crystallization and melting are explained by a model of dual lamellar thickness.

The steric effect of the second lateral methyl substituent on the stilbene mesogen lowers the stability of the mesophase of α,β-dimethyl stilbene (DMS) polycarbonates. Because of the steric effect, DMS polycarbonates do not have "odd-even" property oscillation with the methylene spacer length as HMS polycarbonates do.

Thesis Supervisor: Dr. Peggy Cebe

Title: Associate Professor of Polymer Physics

2

Acknowledgements

I would like first to thank my thesis supervisor, Professor Peggy Cebe, for her guidance and encouragement. I am very grateful for her advocate as my thesis advisor and mentor. Also, her assistance in correcting my thesis writing is deeply appreciated.

I wish to extend my thanks to my committee members, Professor Michael F. Rubner, Professor Anne M. Mayes, and Professor Lionel C. Kimerling, for their advice and encouragement.

I also appreciate the support from Dr. Schreuder-Gibson's group in the U. S. Army Natick R, D &E Center. The materials in this research are synthesized by them.

There is a lot of pleasant time with my colleagues, Dr. Peter P. Huo, Dr. Norene Lucas, Dr. Enid Sichel, Sharon Lu, Dave Rich, Mark Brillhart, Yoshi Aihara, Justyna Teverovsky, Linda Molnar, and undergraduate researchers Wendy Russell, Julie Holmes, Ingchie Kwan, Preston Li and Roland Desrochers. Ms. Amy Sklivas is also highly acknowledged. I would like to thank my other colleagues at MIT, among them are Dr. Yaping Liu, Dr. Ding-Kuo Ding, Peter Kloumann, Joe Adario, Michael Frongillo, John Martin, Ken Zemach, Bill Stockton, Stephanie Simmons and Sandy Schaefer Ung.

My family deserves much credit. The support from my parents have been greatly helpful. I also thank my wife, Crystal Liu, for her love and constant encouragement.

TABLE OF CONTENTS

4

.

List of Figures

10

List of Tables

13

Chapter 1
Introduction and Background

1.1   OVERVIEW

1.1.1 Introduction to Liquid Crystalline Polymers and Definitions

Liquid crystalline polymers (LCPs) may exhibit liquid crystalline order either as a function of concentration in solution (lyotropic LCPs) or as a function of temperature in the melt (thermotropic LCPs). The type of ordered structures that liquid crystalline polymers form may be represented as shown in Figure 1.1 [1]. Traditionally, the thermotropic liquid crystalline phase exhibited by small molecular rod-like mesogens can be classified as nematic, cholesteric, smectic A (an untilted nematic) or smectic C (a tilted layer). Disk-like molecules exhibit various discotic liquid crystalline phases.

These ordered liquid crystalline structures give birefringent melts and solutions when observed under crossed polarizers. As with small-molecule liquid crystals the most simple polymeric liquid crystal phase is the nematic phase. The molecule chain axes mutually align in relation to a simple director without long range positional order which might contribute to a crystal lattice. Schlieren texture is a characteristic of the nematic phase. When viewed between crossed polarizers, this texture shows an irregular network of black brushes branching out from a number of scattered points and passing continuously from one point to another. They correspond to extinction positions of nematic mesophase. These points are the intersections of vertical lines of singularity with the glass surfaces [2,3]. Possible topologies (molecular arrangements) about point singularities are given in Figure 1.2 [4]. Disclinations are point or line defects within a mesophase of a liquid crystalline sample. The strength of the disclination, S, is connected with the number of dark brushes meeting at one point [4]:
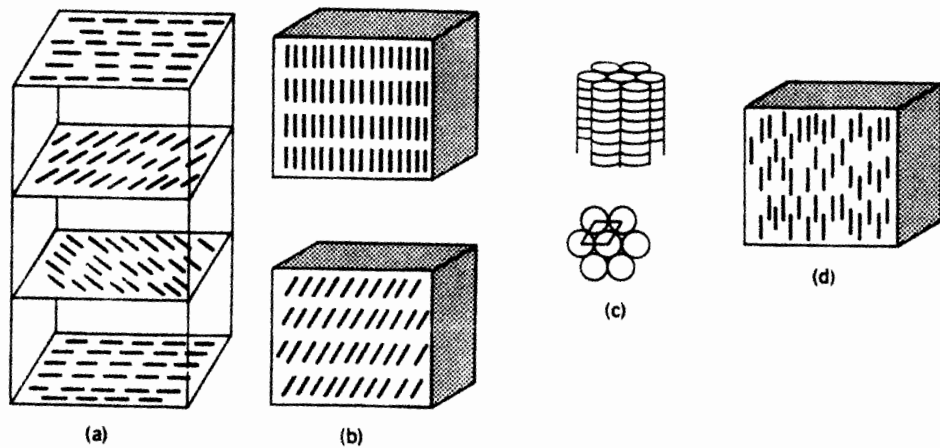
Figure 1.1   The type of ordered structures that LCPs form: (a) cholesteric;

(b) smectic A (top) and smectic C (bottom); (c) discotic; (d) nematic.

(Figure taken from Ref. 1, Figure 1)
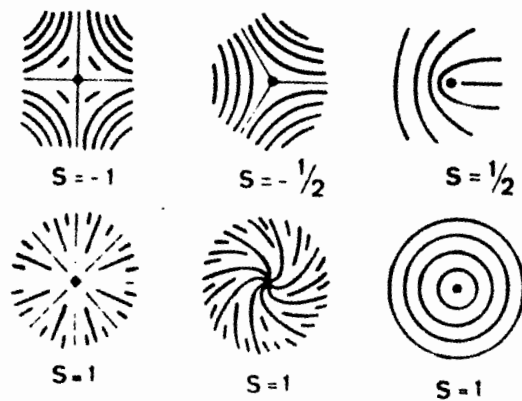
Figure 1.2   Possible topologies (molecular arrangements) about point singularities.

(Figure taken from Ref. 4, Figure 2.17)

$$| S | = \text{number of brushes} / 4 \qquad (1)$$

From the observation of singularities with $S = \pm 1/2$, the mesophase can be identified as a nematic phase. By electron microscopy using a decoration technique [5], disclination structures can be also observed.

One of the major commercial interests in LCPs is their processibility to form uniaxially oriented fibers (for example, see Ref. 1, P. 41). Because of the high chain continuity in oriented LCPs, a desired high stiffness and tensile strength can be achieved along the chain alignment direction. Melt processing is one of the easiest processing methods for thermotropic LCPs . Thermotropic LCPs can be simply extruded from the molten liquid crystalline state to form highly oriented fibers. LCPs can be blended with other polymers to improve processibility and to form high strength composites. One of the characteristics of an LCP fiber is its low coefficient of thermal expansion, which can meet the needs of dimensional stability and reduction of internal stress during cooling. Commercially, LCP fibers are generally more expensive than other fiber materials.

1.1.2 Review of the History of Liquid Crystalline Polymers

The history of LCPs started in 1956 when Flory published a paper on concentrated polymer solutions [6]. The lattice theory of Flory is applicable for quantitative treatment of phase separation phenomena in solutions of rodlike chain polymers, including melts [7-9]. The theory predicted that at a critical concentration V_p*, athermal solutions of polymer hard rods (no intermolecular attractions) of axial ratio x (length/diameter) show initiation of a stable anisotropic or liquid crystalline phase, i.e.,

$$V_p* = (8/x)[1-(2/x)] \qquad (2)$$

16

As the axial ratio of the polymer rod drops approaching to 6.4, the polymer composition of the isotropic phase and the liquid crystalline phase both get close to 1, which is undiluted. Therefore, for an undiluted system, which is thermotropic, the ordered liquid crystalline phase will always be stable with respect to the isotropic phase if the axial ratio of the rod exceeds 6.4. However, this ratio is obtained by considering only the repulsive, shape dominated, forces between the molecules.

Incorporation of possible directional attractive forces makes it possible that polymer rods of lower axial ratio can have a liquid crystalline phase. Groups in polymer chains with polarizabilities higher along their bond axes than along the perpendicular can contribute to the stability of the liquid crystalline phase. Examples of such groups are p-phenylene, -C≡C-, -N=N-, and -C≡N-. These interactions are important in semiflexible long-chain polymers. Therefore, high axial ratio is not required for liquid crystalline phase formation in the melt. The nature of the liquid crystalline phase appears to be dependent totally on the shape of the monomer unit. For example, consider the structure [10,11] shown below:

$$\pmb{+}CONH-Ph-COO(CH_2)_nOOC-Ph-HNOC-(CH_2)_m\pmb{+}_{dp}$$

These are polyesteramides having a smectic liquid crystalline phase for specific values of n and m. It is very likely that intermolecular hydrogen bonding plays an important role. In this case, strong interactions compensate for a weak steric drive to the liquid crystalline phase.

1.1.3 Introduction to Monotropic Liquid Crystalline Behaviors

In the polymer melt (the thermotropic system), how does the liquid crystalline phase stabilize as opposed to the crystal phase and the isotropic phase? In 1956 Flory

tried to answer this question [6]. As mentioned above, for rodlike chains, when a limiting concentration is exceeded, either a liquid crystalline phase or a crystalline phase separates from the isotropic phase. Crystallization may happen in two steps: 1) the polymer chains order cooperatively in a given region into a parallel alignment without change in the intermolecular interactions; and 2) the increase in intermolecular interactions is possible by the more efficient packing of the chains in the parallel state. The first step is similar for both the crystallization process and the formation of liquid crystalline phase. The second step is separation of a crystalline state or a liquid crystalline phase. With extensive chain alignment and good chain regularity, crystallization should proceed so fast that the two steps are inseparable.

Recently, from a thermodynamic point of view, the liquid crystalline phase can be identified to be either enantiotropic or monotropic [12,13]. The thermodynamic relation required is:

$$dG = VdP - SdT \qquad (3)$$

where G is the free energy, V is the volume, S is the entropy, P is the pressure and T is the temperature. Assume the phase transition happens at a constant pressure ($dP = 0$) . The free energies of the crystal (G_k), liquid crystal (G_{lc}), and isotropic (G_i) phases decrease with increasing temperature. The decrease of G_i (dG_i/dT) is steeper than G_{lc} and G_k, because

$$S_i > S_{lc} > S_k. \qquad (4)$$

As shown in Figure 1.3(a) (taken from Fig.1 of Ref.12), the enantiotropic liquid crystalline phase is thermodynamically stabilized with respect to the crystalline phase and

18
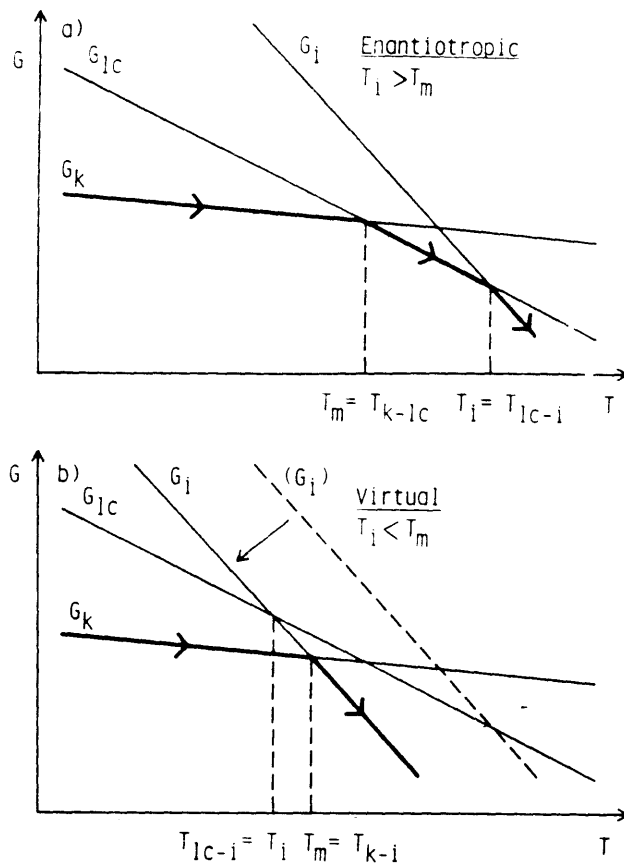
Figure 1.3   The diagram of the free energy vs. temperature used to explain

(a) the enantiotropic mesophase, (b) the virtual mesophase.

(Figure taken from Ref. 12, Figure 1)

19
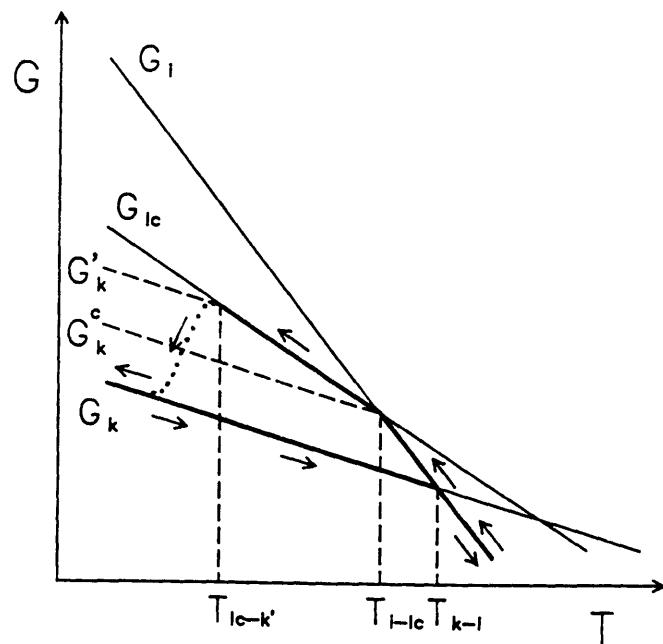
Figure 1.4   The diagram of the free energy vs. temperature used to explain the

monotropic mesophase. (Figure taken from Ref. 13, Figure 2)

the isotropic phase within the temperature range from T_m (T_{k-lc}) to T_i (T_{lc-i}). It is observed as reversible both on heating and on cooling. As shown in Figure 1.3(b), the virtual liquid crystalline phase is thermodynamically less stable than the crystalline phase and the isotropic phase. The monotropic liquid crystalline phase is a particular case of a virtual mesophase, which can only be observed on cooling, provided that the crystallization process is by-passed due to supercooling. Particularly in polymers, crystallization only happens at a certain supercooling temperature and the crystallization temperature can be appreciably below the equilibrium melting point. In contrast, the formation of liquid crystalline phase generally requires less supercooling. As shown in Figure 1.4 (taken from Fig.2 of Ref.13), an unstable or monotropic liquid crystalline phase can exist from T_{i-lc} to $T_{lc-k'}$ in cooling. As temperature drops further, crystallization will happen and the free energy may drop to the value of the perfect crystal G_k. During reheating, the perfect crystal melts directly into isotropic liquid at T_{k-i}.

It is possible that the free energy only drops in between two extremes, G_k and $G_{k'}$. If the free energy remains at a value above $G_k{}^c$ after crystallization, the liquid crystalline phase still can be seen during reheating. Then this liquid crystalline phase can be classified as enantiotropic. Therefore, it is possible that the improved perfection of crystals upon annealing can make this kind of enantiotropic liquid crystalline phase into a monotropic liquid crystalline phase.

1.2   OVERVIEW OF MAIN CHAIN THERMOTROPIC LIQUID CRYSTALLINE POLYMERS

1.2.1 Introduction

It is helpful to view liquid crystalline polymers as being constructed from the same rigid mesogenic groups that form small-molecule liquid crystals. The most basic

construction is to link the rigid mesogenic groups end to end to form a rigid polymer chain, which is the rigid rod polymer, as mentioned in 1.1.2. However, in practice this approach leads to a problem: although T_m and T_{lc-i} are both increased as a result of the polymerization, and the range of mesophase stability is in principle maintained or even enhanced, thermal degradation of the polymer tends to curtail this range and often prevents the liquid crystalline phase from being observed.

Therefore, the reduction of the transition temperature into an useful working range without destroying the liquid crystalline stability completely is one of the primary objectives in the design of LCPs. One route to make the chain less stiff is to introduce more mobile linking groups between the rigid units. A further modification involves the connection of the mesogenic units through spacers consisting of lengths of flexible polymer molecules. Such flexible spacers may be incorporated between the mesogenic groups to give a single linear molecule, which is used to form the so-called main chain LCPs. Or a flexible polymer chain can be used as a backbone to which the mesogenic sections are added as side groups, which is used to form side chain LCPs.

Insertion of substituents on the mesogen can modify its steric and electronic features [14-22], and therefore its potential as a mesogen. The steric factor generally plays a more important role for LCPs, which is also the case for small monomeric liquid crystals [18]. The lateral substituents usually reduce the thermal stability of the liquid crystalline phase.

1.2.2 Stilbene Containing Liquid Crystalline Polymers

Main chain thermotropic LCPs with various kinds of mesogens have been studied [23-47]. Stilbene-containing polymers have been widely studied due to the low cost of the monomer. Various linking groups that link the methylene spacer and the stilbene

22

α-methyl stilbene polyester
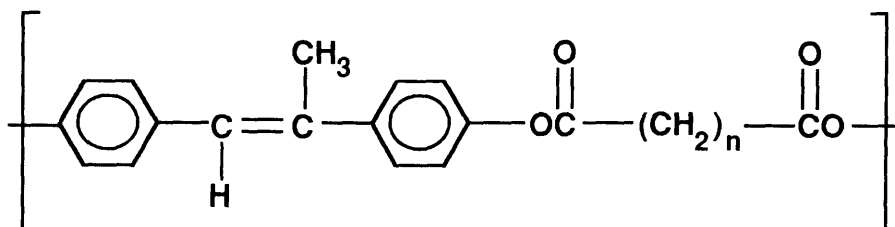
α-methyl stilbene polyether
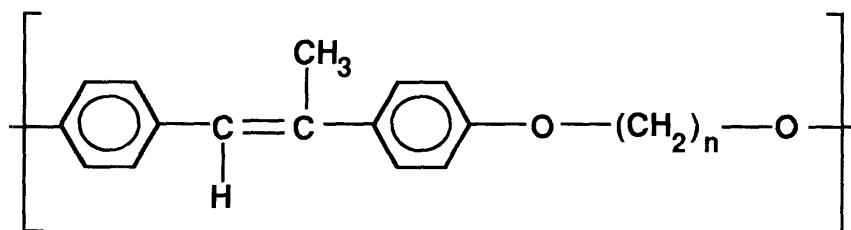
α-methyl stilbene polycarbonate (HMS-n)
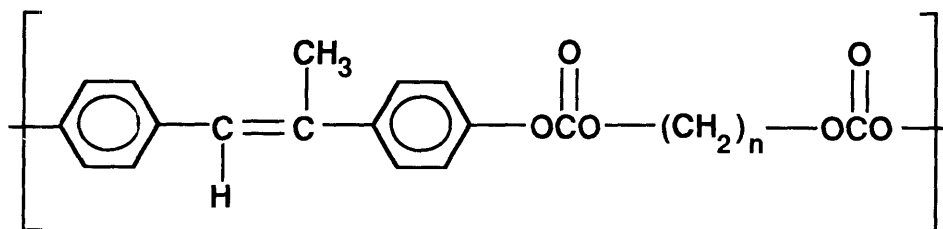
Figure 1.5 Chemical structure of stilbene containing polymers

α,β-dimethyl stilbene polycarbonate (DMS-n)
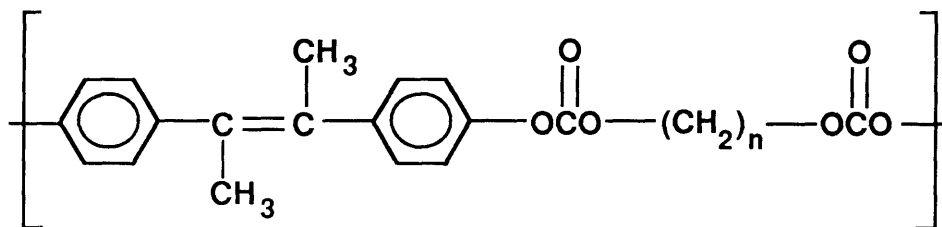
α-ethyl stilbene polycarbonate (HES-n)
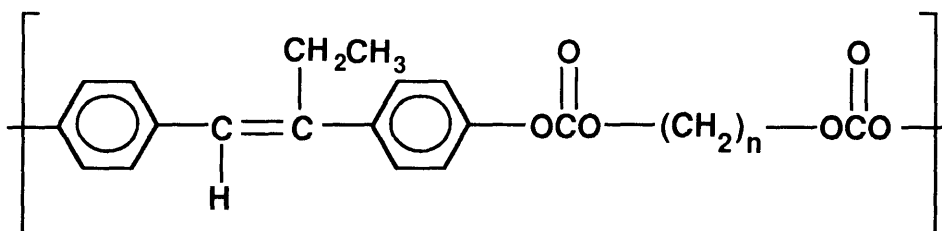
α,β-diethyl stilbene polycarbonate (DMS-n)
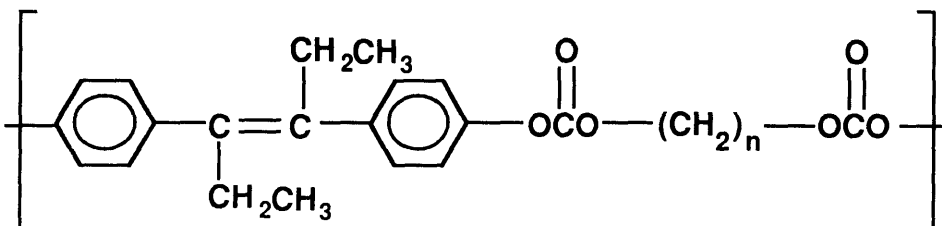
Figure 1.5, Continued

24

mesogen have been studied. Figure 1.5 shows the chemical structure for stilbene-containing polymers. Jackson's [48] stilbene polyesters were reported in the 1980's as high melting enantiotropic LCPs. These polyesters can produce reasonably high strength fibers and injection molding plaques. Polyesters of α-methyl stilbene [49] were found to melt at temperatures similar to Jackson's polyesters and were also enantiotropic LCPs. Percec's α-methyl stilbene polyethers [50] were reported to be lower melting enantiotropic LCPs of stilbene which can exhibit a nematic or smectic liquid crystalline phase. Like other main chain thermotropic LCPs, for these stilbene LCPs, both their melting temperature, T_m ($T_m = T_{k-lc}$), and their transition temperature from the liquid crystalline phase to the isotropic phase, T_i ($T_i = T_{lc-i}$), tend to decrease with increasing length of flexible spacer. Figure 1.6 is a plot of both T_m and T_{lc-i} vs. the number of -(CH$_2$)- units in the spacer for a homologous series of polyesters of α-methyl stilbene [14,49]. The zig-zag nature of the plots is an example of the odd-even effect, which was seen in all of the stilbene-containing polymers mentioned above. Both transition temperatures tend to be higher when there is an even number of -(CH$_2$)- units in the flexible spacers. Also notice that the temperature range for liquid crystal stability decreases with increasing length of the spacer. At n=12, T_{lc-i} first drops below T_m and the stability of the liquid crystalline phase is lost .

Insertion of a second substitution has a drastic depressive effect on T_i that causes α, β dimethyl stilbene polyesters not to have an enantiotropic liquid crystalline phase. For example, the α-methyl stilbene liquid crystalline polyester with -(CH$_2$)$_8$- flexible spacer has a melting point of 483K and isotropic temperature of 530K, while the α, β dimethyl stilbene polyester with the same flexible spacer has a melting temperature of 500K and a virtual liquid crystalline phase at T_i=454K [21]. In this work, no odd-even effect is discussed because of the limited flexible spacer number.

25
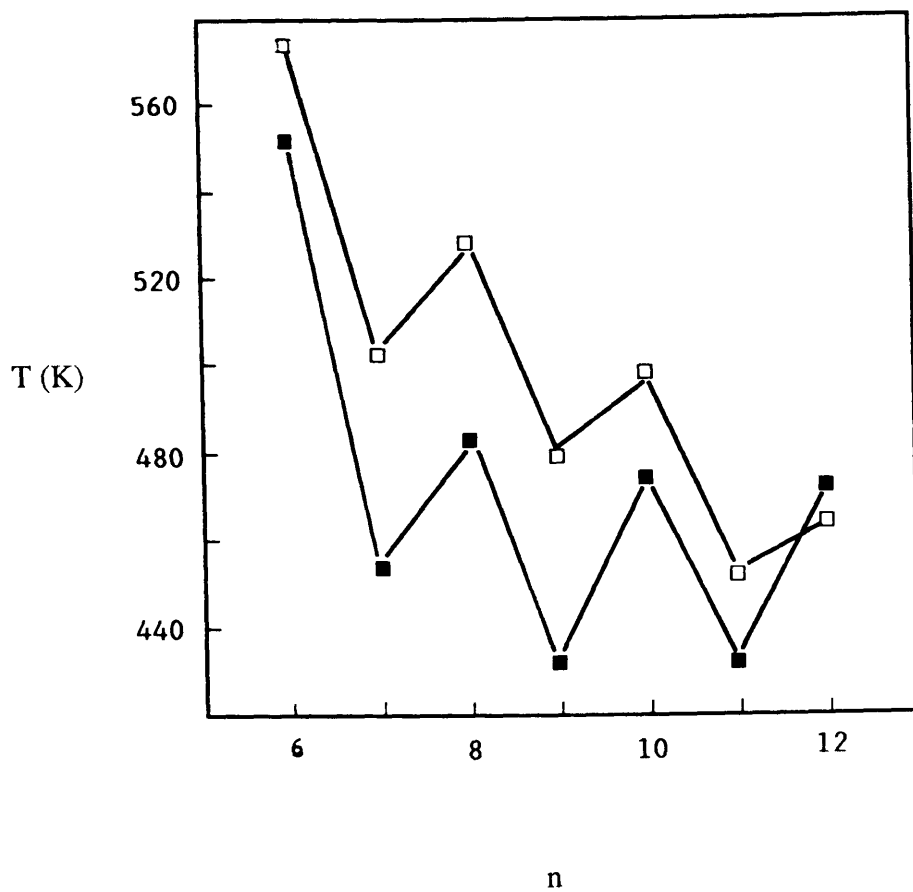
Figure 1.6   The diagram of T_m and T_{lc-i} vs. the number of $-(CH_2)-$ units in the

spacer for a homologous series of α-methyl stilbene polyesters.

(Figure taken from Ref. 14, Figure 4)

Expanding on the past work with stilbene-based polyesters and polyethers, a series of polycarbonates have been synthesized by Dr. Schreuder-Gibson with stilbene mesogen, mono- or di- substituted with methyl or ethyl groups, which are referred to as HMS-n, DMS-n, HES-n, DES-n, respectively [51]. Their chemical structures are shown in Figure 1.5. For stilbene polycarbonates containing the heptane flexible spacer, methyl substituted stilbenes (HMS-7 and DMS-7) are semicrystalline, while ethyl substituted stilbenes (HES-7 and DES-7) are amorphous [51].

1.2.3 Theoretical Concerns Relating to the Odd-even Effect

The odd-even effect can be easily understood by considering that the degree of alignment of the polymer chains within the mesophase is higher for the even series than for the odd series, when the methylene units in the flexible spacer have all trans conformation [52]. Although the methylene spacer has been found not to be restricted to the all-trans conformation in the anisotropic phase, its conformation is rather extended [53-57]. An all-trans sequence will only connect two mesogenic groups without introducing a kink in a polymer chain if it has an even number of methylene units. However, there are some theoretical bases which can explain the odd-even phenomenon [58-61].

Conformational energy calculations [58-61] have pointed out that the methylene spacer length and the linking group both have influence on the conformation of the methylene spacer. Three contributions to the total partition function, Z_T, can be considered :

$$Z_T = Z_{st} Z_{en} Z_{conf} \tag{5}$$

where Z_{st} is the contribution considering excluded volume effects, Z_{en} is the orientation-

27

dependent contribution, and Z_{conf} takes care of the configurational degree of freedom.

When the methylene flexible spacer (F) is attached to the mesogen (M) by M-O-F or M-O(O=)C-F linkage, the even-numbered methylene spacers have a significant population of highly extended conformations which makes the nearly parallel alignment of the mesogen along the macroscopic orientation axis favorable. These conformers help to promote a stable nematic phase and are most likely preferred over others in the nematic phase. The conformational energy and entropy change of the methylene spacer contributed from these conformers can significantly increase the enthalpy and the entropy change of the transition from the isotropic phase to the nematic phase. It has been found experimentally that the enthalpy and entropy changes of the isotropic-nematic transition for these polymers are much larger than those of the monomeric liquid crystal [26,30]. In contrast, for an odd-numbered methylene spacer, the number of highly extended conformers is much smaller. For these conformations, the mesogen is tilted by about 30° from the macroscopic orientation axis and the order parameter is smaller. (The order parameter can be defined as $1 - (1.5 * < \sin^2 \phi >)$, where ϕ is the angle between a chain segment and the macroscopic orientation axis). Therefore, the enthalpy and entropy change from the isotropic to nematic transition are much smaller for these polymers with odd-numbered methylene spacer than those with even-numbered one, as experimentally observed [23,26,30,49,62,63].

Interestingly, it has been found experimentally that when the the methylene flexible spacer (F) is attached by M-C(O=)O-F linkage, the tendency to form a nematic phase is significantly suppressed [16,32]. When a nematic phase occurs, the enthalpy and entropy change of the isotropic-nematic transition is larger for these polymers with odd-numbered methylene spacer than those with an even-numbered one [42]. From the conformational energy calculation, it is found that for these polymers with even-

numbered methylene spacer, the population of extended conformers is smaller than those polymers having a M-O-F or a M-O(O=)C-F link. It is ascribed to the fact that the trans conformation of O-C-C-C bonds is not the lowest energy conformation for the polymers having a M-C(=O)O-F link. Therefore, the enthalpy change of the isotropic-nematic transition is reduced for these polymers with even-numbered methylene spacer and the odd-even effect is reversed.

1.3 CHARACTERIZATION OF MAIN CHAIN THERMOTROPIC LIQUID CRYSTALLINE POLYMERS

1.3.1 Identification of Liquid Crystalline Phase

It is recommended to use various methods to identify the liquid crystalline phase in LCP systems because the coexistence of phases might obscure the observation under polarized optical microscopy at different temperatures. For example, when LCPs are oriented by shearing, a shear band structure might be observed under polarized optical microscopy and electron microscopy [64-66]. It is believed that the formation of the shear band is caused by the stress relaxation of polymer chains from the oriented state, which results in periodic thickness change. Recently, it was found that crystallization can also lead to the formation of banding morphology [67]. The banding was caused by the periodic buckling of polymer chains in the crystalline phase.

Two dimensional wide angle X-ray diffraction is also a popular method for the identification of liquid crystalline phases. The X-ray diffraction patterns of aligned nematic polymers will look similar to that shown in Figure 1.7 [52]. The important features which characterize the nematic structure are the presence of diffuse equatorial maxima, and sometimes layer lines which are centered on the meridian and diffuse along their length [68]. The existence of any sharp maximum is indicative of certain type of
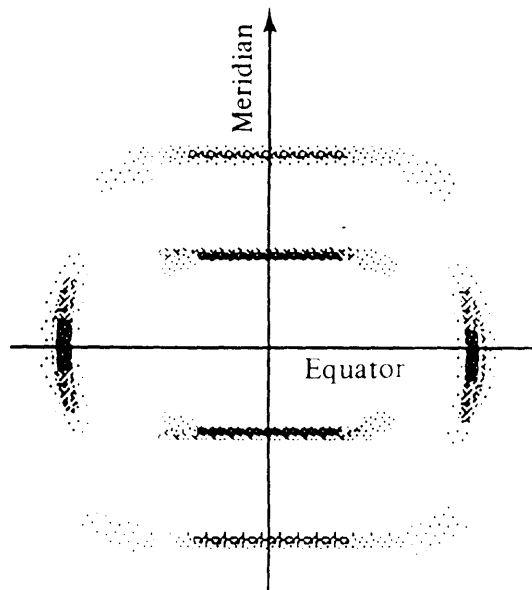
Figure 1.7   X-ray diffraction patterns of aligned nematic polymers.

(Figure taken from Ref. 52, Figure 2.5)

long range positional order, such as occurs in smectic structures or crystals, and will take the polymer out of the nematic classification. However, nematic polymers may be partially crystalline, and in that case sharp diffraction features or distinctly quadrantal reflections will then be superimposed on a basic nematic pattern.

1.3.2 Crystallization Kinetics and Crystalline Structures

Many crystallization studies of thermotropic LCPs have been done by using a differential scanning calorimeter (DSC). Typically, two kinds of studies were executed. First, many studies used several different cooling rates to try to find out the effect on the exotherm peak of crystallization and the isotropic to mesophase transition. This approach is especially useful for the study of a monotropic system [69]. The exotherm of crystallization is so suppressed by a higher cooling rate that the isotropic to mesophase transition is observable.

In the second study, the DSC was also used to study the isothermal kinetics of the mesophase formation and of the crystallization from the mesophase or isotropic state. Ideally, if the resolution of data is high enough in the beginning of crystallization, one can determine the Avrami parameter. The general results present some controversial points about the mechanism of the transformation and the resulting Avrami parameters [70]. Parallel studies of polarized optical microscopy and real time wide angle X-ray scattering (WAXS) are usually done. From these studies, it is generally suggested that crystallization from the liquid crystalline phase can preserve the local orientation in the crystalline phase.

By using two dimensional wide angle X-ray diffraction techniques, some packing principles of main chain LCPs in the crystalline phase are proposed by Ungar and Keller [71]. Two possible structures are proposed, as shown in Figure 1.8. In an "intermeshed"

31
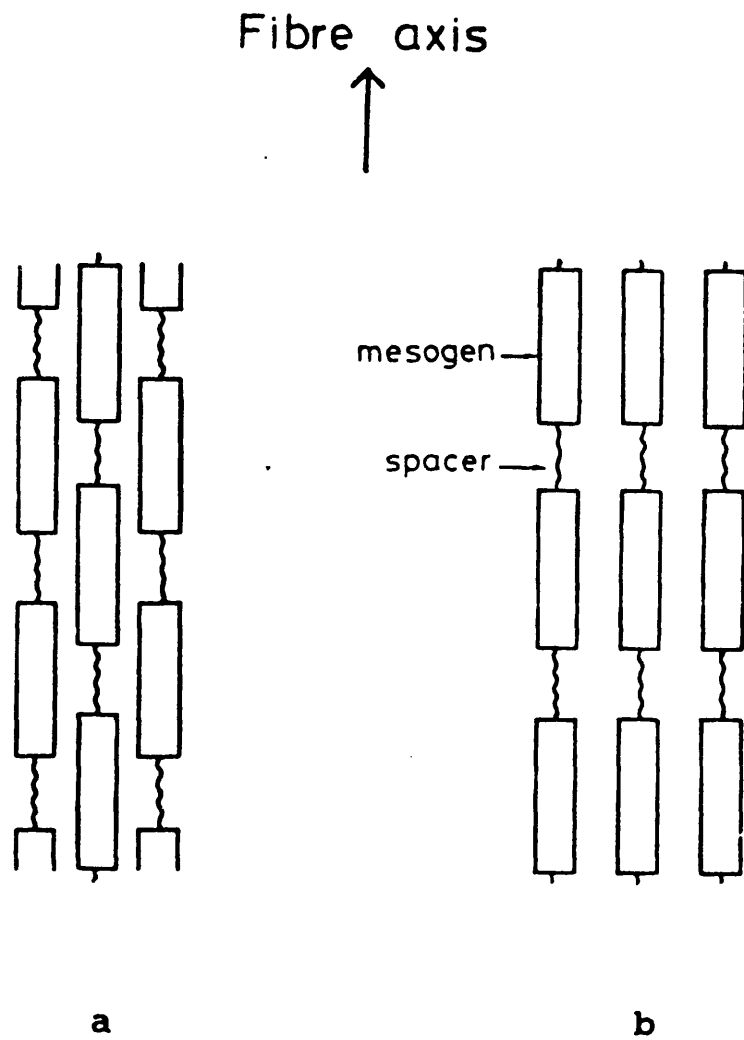
Figure 1.8   Mesogen - spacer packing in (a) intermeshed,

(b) layered structure. (Figure taken from Ref. 70, Figure 3)

structure, the rigid mesogen with bigger cross section matches the flexible spacer on adjacent polymer chains. In a "layered" structure, the rigid mesogen and the flexible spacer are coupled themselves in series on adjacent polymer chains. The "intermeshed" structure seems more stable thermodynamically because it will transform into the "layered" structure by an endothermic reaction.

A detailed study of the influence of the flexible spacer on the solid state structure has been made [72] for a series of mesogenic aromatic-aliphatic azomethine ether polymers (AZMEP-n), with methylene spacers number n =1-16. Unit cell parameters determined from the fiber patterns of annealed single filaments have been used to classify the polymers into distinct groups having different chain conformations and crystal systems. The even members of the series have C-centered monoclinic, I-centered monoclinic or triclinic unit cells changing with the increase of the length of spacer. When n is odd, the unit cells are orthorhombic, I-centered monoclinic or triclinic changing with the increase of the length of spacer.

1.4   Objective and Overview of This Research

Main chain LCPs have potential uses as high strength fiber forming materials because of their tendency to form ordered phases from the isotropic phase. Main chain LCPs can be extruded from the liquid crystalline state and form an extended chain structure in the solid state, which has high chain continuity and therefore high mechanical properties along the orientation direction. Generally, the wider the temperature range of stability for the liquid crystalline phase, the better the fiber forming capability for the LCP during melt processing. In our research, we incorporate the methylene flexible spacer in the LCP structure, which is connected with the stilbene mesogen by the carbonate linking group. This is a popular approach as mentioned in 1.2.1, because the

33

incorporation of the methylene spacer can lower transition temperatures and therefore ease the melt processing.

The purpose of this research is to investigate the relationship between the chemical structure variations and the macroscopic properties like thermal transition temperatures, crystallization kinetics, and fiber formation. The chemical variations include change in the methylene flexible spacer length, substitution on the mesogen and linking group chemistry. As mentioned in 1.2.2, it has been found both HMS and DMS polycarbonates are semicrystalline. Therefore, in this research, we are concentrating on these two groups of materials, especially on HMS polycarbonates. In our research, we are able to determine the role of the chemical variations on the thermodynamic stability of the liquid crystalline phase and in the nucleation kinetics and growth of the crystalline phase.

For our liquid crystalline α-methyl stilbene polycarbonates, there is a very narrow temperature range of stability for the liquid crystalline phase. The liquid crystalline phase can be only observed during cooling when three dimensional crystal growth is suppressed. Using wide angle X-ray scattering and molecular modeling, we show that the orientation of the carbonate group and the length of the methylene flexible spacer are both implicated in the rapid nucleation of crystals. When the length of the methylene spacer and the mesogen are comparable, a regularly packed crystal structure occurs in which the mesogen (M) and the flexible spacer (F) align as shown below:

-M-F-M-F-M-F-M-

-F-M-F-M-F-M-F-

This crystal structure forms rapidly from the liquid crystalline phase which acts as a template for nucleation and growth of crystals from an already ordered melt.

34

Using small angle X-ray scattering, we found that the orientation of the carbonate group and the length of the methylene spacer are also related to the larger dimension of crystals forming from the liquid crystalline phase. α-methyl stilbene polycarbonates with odd-numbered methylene spacer have a higher value of crystal lamellar thickness than those with even-numbered one.

The effect of the second methyl substituent on the mesogen for stilbene polycarbonates (DMS-n) is discussed in Chapter 5. In summary, the steric effect of the second methyl substituent lowers the stability of the liquid crystalline phase. The steric effect also reduces the effect of the carbonate group, and therefore DMS polycarbonates do not have the regular property change with the methylene spacer length as the HMS polycarbonates do.

Chapter 2
Crystallization Studies and Monotropic Liquid Crystalline Behavior of HMS Polycarbonates

2.1. INTRODUCTION

It has been found that the monotropic mesophase exists in several kinds of main chain thermotropic liquid crystalline polymers, such as poly(ester imides) [69], polyurethanes [73,74], and polyethers and copolyethers [75-79]. It has also been found that some enantiotropic LCPs can behave like monotropic LCPs after an annealing process [80].

The behavior of these monotropic LCPs is strongly related to the shape of the monomer unit and the conformation of the polymer chain. One interesting characteristic is the existence of a kink in the polymer chain, which plays an important role in the interaction between the polymer chains. A kink can permanently exist in a polymer chain, as, for example, in polyurethane LCPs [73,74]. This particular kink is caused by two urethane linkages in the meta positions with respect to the benzene ring. Due to the interchain hydrogen bonding forming within the urethane linkage by adjacent polymer chains, these LCPs form an ordered monotropic mesophase. The order is preserved in the crystalline phase which forms from the mesophase. A kink can also exist in a polymer chain as one of the conformational isomers. Percec's liquid crystalline polyethers and copolyethers [75-79] are examples. Instead of being linked by a rigid group, two benzene rings are connected by two methylene linkages to form a flexible rodlike mesogen. The formation of the monotropic mesophase depends on the degree of alignment of polymer chains caused by their cooperative movement.

It is well-known that for main chain LCPs, both the mesogen and the flexible spacer contribute to the orientational order that characterizes the transition from the isotropic (i) phase to liquid crystal (lc) mesophase. From the intercept and the slope of ΔH_{i-lc} and ΔS_{i-lc} versus the number of methylene units in the flexible spacer, Blumstein first obtained the contribution from the mesogen and the flexible spacer, respectively [81]. The former was assigned as the orientational contribution and the latter as the conformational contribution. Blumstein's polyesters showed an odd-even effect in ΔH_{i-lc} and ΔS_{i-lc} versus n, the number of methylene units in the flexible spacers [26,81]. The value is higher when n is even. This effect can be understood by considering that the degree of alignment of the polymer chains within the mesophase is higher for the even series than for the odd series, when the methylene units in the flexible spacer have all trans conformation [52,82]. This effect is usually observed and can be theoretically justified [58,59] for those polymers with rigid rod mesogen. However, for Percec's polyethers with flexible mesogen [79], ΔH_{i-lc} and ΔS_{i-lc} increase linearly with the number of methylene units in the flexible spacers. This phenomenon was explained by the coupled action of the flexible mesogen and the flexible spacer.

In this Chapter, we report on characterization and crystallization studies of α-methyl stilbene polycarbonates (HMS-n) whose synthesis has been reported previously [51]. The chemical repeat unit for these polymers is shown in 1.2.2. The flexible spacer number ranges from n = 4-10, 12. A monotropic mesophase was identified for these HMS polycarbonates. Like some other monotropic LCPs mentioned above, HMS-polycarbonates also have kinks in their polymer chains caused by the conformational isomers of the carbonate linkage. If the two bonds adjacent to the carbonate linkage have trans conformation, then HMS polycarbonates will have a linear shape.

37

In this Chapter, we report on the crystallization and melting behavior of α-methyl stilbene polycarbonates [51]. In contrast to the enantiotropic stilbene-based polyethers and polyesters, HMS polycarbonates are monotropic LCPs. Also, there is no odd-even effect seen in any of the transition temperatures vs. the flexible spacer number. Finally, there are different trends in the phase transition temperatures for n ≤ 8 compared with those of higher n value. These differences in thermal behavior can be related directly to differences in the chemical structure of the linking groups and to the relative lengths of the flexible spacer and mesogen.

2.2. EXPERIMENTAL SECTION

2.2.1 Materials

The synthesis of HMS polycarbonates was performed in Dr. Schreuder-Gibson's group [51] and followed the method of Sato [84]. The synthesis is described in the Appendix. The resultant LCPs were soluble in chloroform and obtained as fine white powders, except for n=7,9 which were obtained as white, very fibrous product. All polymers studied in this research have reasonably high molecular weight, in the range from 11,000 to 54,800 with distributions (M_w/M_n) close to 2 as reported previously [51].

2.2 Differential Scanning Calorimetry (DSC)

Thermal properties of materials were studied using a Perkin-Elmer DSC-4 or DSC-7. Indium was used to calibrate the temperature and the heat of fusion. All materials studied had a sample weight range of 2.5-6.5 mg. The studies that were done included heating and cooling at fixed rates, the effect of crystallization temperature on crystallization time and melting temperature, and the effect of crystallization time on melting temperature.

38

The first approach involved heating and cooling at fixed rates over a wide temperature interval. The sample was heated to 200°C and held at that temperature for 2.5-3 minutes, then cooled at a rate of 10°C/min to 50°C, then heated at 10°C/min to 200°C. This study was done for all HMS-n samples. In addition, HMS-6 through 9 were cooled and heated at 5, 20, and 50°C/min. This study was designed to test the dependence of the mesophase to isotropic transition on cooling rate.

The next study was isothermal crystallization for HMS-5 through 9. The sample was melted at 190°C for about 3 minutes, then quenched at -50°C/min to a crystallization temperature T_C and held isothermally until the crystallization was finished. The T_Cs were specifically chosen for each HMS sample in advance. Because all HMS-5 through 8 materials have close crystallization temperatures, we chose the same crystallization temperatures in the range between 138°C and 144°C for these samples. Exothermic heat flow as a function of time was measured. Here we were interested in the effect of the flexible spacer number on the isothermal crystallization kinetics.

The next study involved immediate rescan after isothermal crystallization for HMS-5, 6, 8 and 9. After staying at T_C isothermally until crystallization was finished, the sample was immediately heated at 5°C/min to 190°C without cooling. This immediate rescan technique avoids the formation of imperfect crystals during cooling to room temperature, and thus results in a cleaner endothermic response.

HMS-5 and HMS-9 were studied by a variety of other thermal approaches. HMS-9 was held at T_c = 114°C and HMS-5 at T_c = 140°C until crystallization was finished, then immediately heated at 1, 2, or 5°C/min. Finally, the effect of crystallization time was studied for HMS-9 at T_c =114°C and for HMS-5 at T_c = 147°C. Samples were held isothermally at the crystallization temperature for different times, and then immediately

39

heated at 5°C/min to 190°C immediately, without cooling to room temperature.

2.2.3 Optical Microscopy

A Zeiss microscope was equipped with a turret containing long working distance objective lenses, for use with the Mettler hot stage. The long working distance protects the lens from aberrations that might result from exposure to elevated temperatures. For HMS-n, samples of powder were placed on glass slides and covered with a glass cover slip. These were inserted into the hot stage at room temperature and the stage controller was set to heat and then cool the samples at a fixed rate. Samples were studied using polarized transmitted light geometry, and the analyzer was placed at 90° to the polarizer. The change in transmittance was recorded simultaneously as the sample heated.

Crystallization studies were done on HMS-5. The polymer was heated to 190°C and held at that temperature for 2.5 minutes, then cooled at 20°C/min for isothermal crystallization to 127°C, the temperature of the mesophase to crystal transition of HMS-5. Samples were also cooled at 20°C/min from 190°C to 157°C, the transition temperature of the isotropic phase to mesophase transition, and held for 40 minutes, then cooled at 20°C/min to 127°C for further isothermal crystallization.

2.2.4 Transmission Electron Microscopy (TEM)

TEM was performed on HMS-5, 7 and 9 using a JOEL 200CX transmission electron microscope operating at 200 KV. Samples were prepared by making a dilute solution of the polymer in chloroform. This was done by dissolving 1 mg of polymer in 2 ml of the solvent. Several drops of the polymer solution were then placed on a freshly cleaved mica surface that had been coated with a thin layer of carbon by thermal evaporation. The chloroform evaporated in about 1 minute leaving a thin film of polymer. The polymer on the mica was then subjected to heat treatment using a Mettler

hot stage. In all cases, the polymer was heated to 190°C and held at that temperature for 3 minutes. For HMS-5, cooling was done at -10°C/min. with isothermal holding at 157°C for 30 minutes. The procedure was repeated with an isothermal hold at 127°C. Cooling was also done for HMS-7 with isothermal holds at 155°C and at 136°C; and for HMS-9 with holding at 132°C and at 102°C. After holding at the specified temperature, the samples were removed from the hot stage and allowed to air-cool. The above temperatures correspond to peak temperatures of exotherms observed in a DSC cooling at -10°C/min. That is, HMS-5, 7 and 9 were assigned isotropic-to-nematic transitions at 157°C, 155°C and 132°C, respectively, and nematic-to-crystalline transitions at 127°C, 136°C, and 102°C, respectively.

2.3. RESULTS

2.3.1 Differential Scanning Calorimetry

DSC thermograms of HMS-4-12 are shown in Figures 2.1 and 2.2, for first cooling and second heating, respectively. Nearly all samples showed a dual exothermic response indicating a small higher temperature exotherm representing the isotropic to mesophase (i-lc) transition, followed by a large exotherm at the mesophase to crystalline (lc-k) transition. On the reheating scans, usually dual endotherms were observed. Notice that the upper melting temperature range is quite broad, and always covers the temperature range of the isotropic to mesophase transition seen in the cooling scan. Table 2.1 summarizes the melting and crystallization peak positions. Transition temperature vs. n is shown in Figure 2.3 (cooling) and Figure 2.4 (heating). There is only weak odd-even effect seen at the upper crystalline melting temperature in heating for low n, but no odd-even effect is seen in cooling. The stability range of the mesophase becomes smaller from n = 5 to 8 in the cooling scan. For n ≥ 9, all the transition temperatures drop. Table 2.2 lists the estimated $\Delta H_{i\text{-}lc}$ and $\Delta H_{lc\text{-}k}$.

41
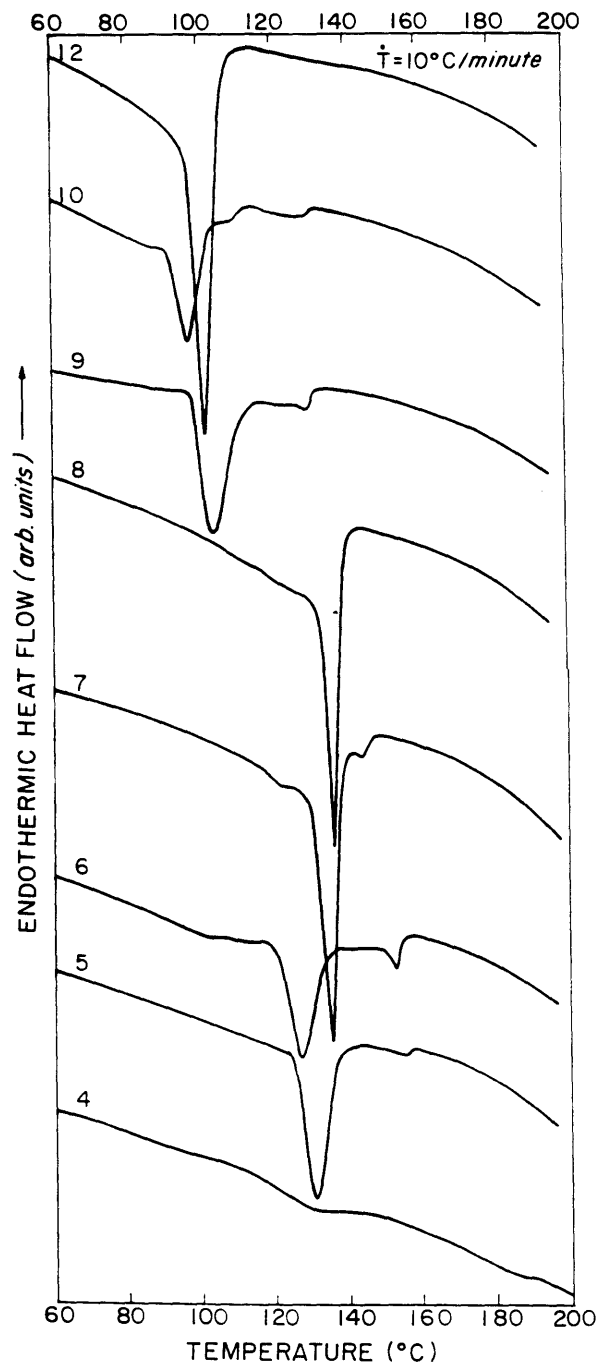
Figure 2.1   DSC thermograms of HMS-4-10,12 at 10°C/min cooling.
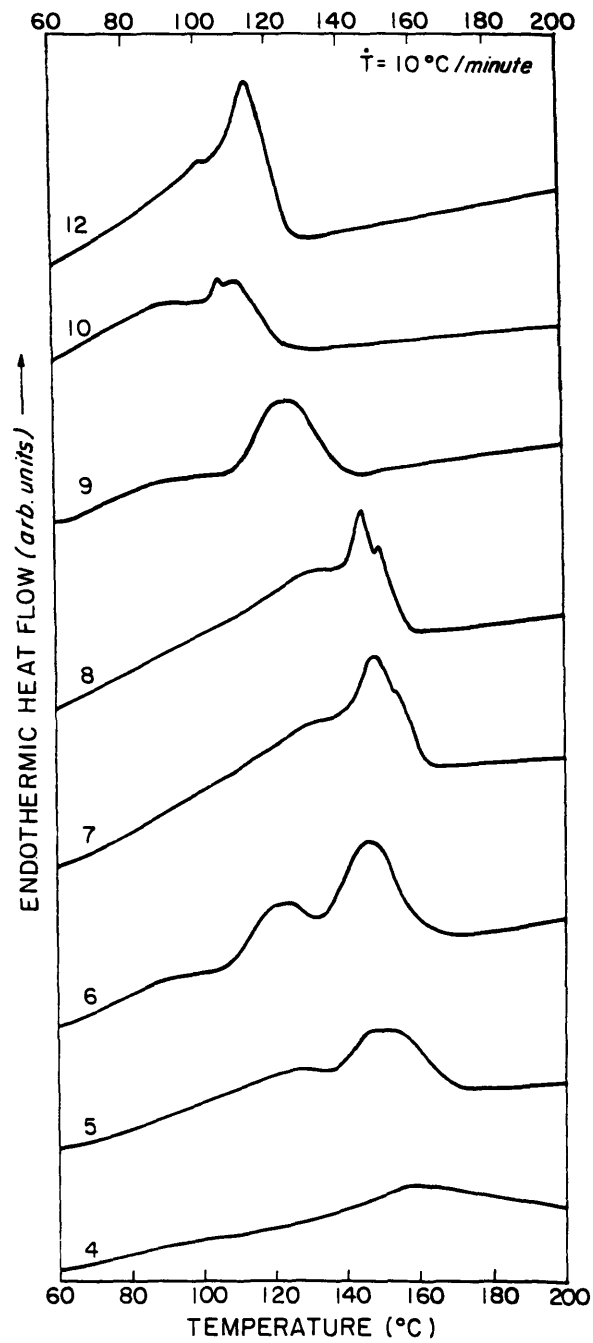
Figure 2.2   DSC thermograms of HMS-4-10,12 at 10°C/min heating.

Table 2.1

Thermal Transition Peak Temperatures for HMS Series Polycarbonates
at 10°C/minute Scan Rate

Sample	Crystallization Temp.(°C)		Melting Temp.(°C)	
n	T_c(upper)	T_c(lower)	T_m(upper)	T_m(lower)
	(±2°C)	(±1°C)	(±1°C)	(±1°C)
4	-----	129	159	-----
5	156	132	148	127
6	154	128	147	123
7	144	135	150	131
8	-----	138	146	136
9	131	106	125	90
10	131	99	109	97
12	-----	104	116	-----

------- No transition seen in this sample
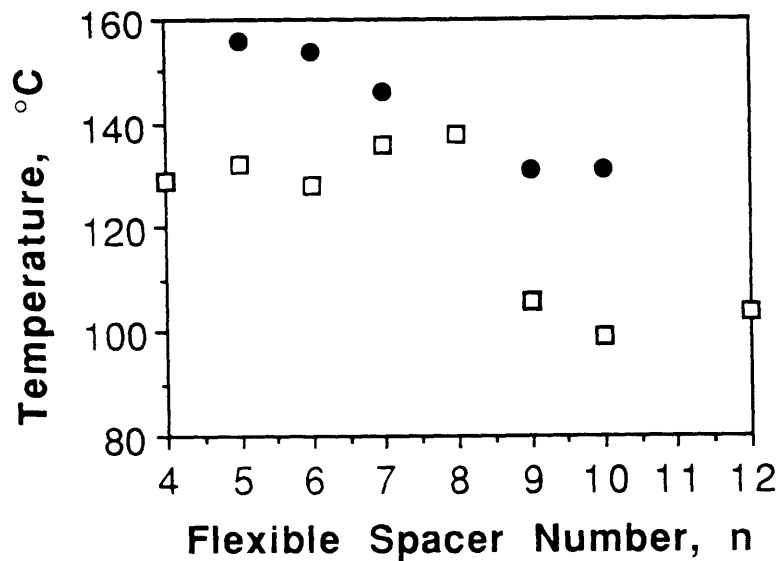
Figure 2.3   Transition temperatures vs. n during cooling:

($\bullet$) $T_{i\text{-}lc}$ and ($\square$) $T_{lc\text{-}k}$.
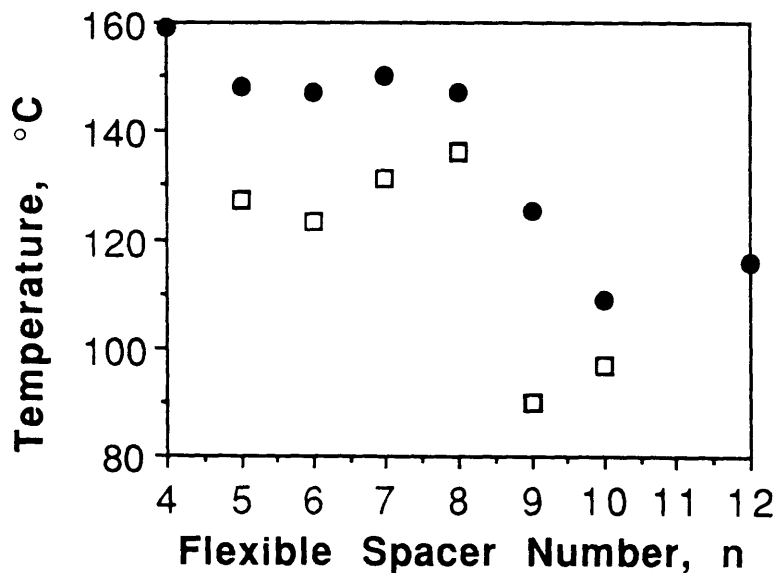
Figure 2.4   Transition temperatures vs. n during heating: ($\bullet$) upper melting

T_{m2} and ($\square$) lower melting T_{m1} peak position.

45

Table 2.2

**Estimated $\Delta H_{i\text{-}lc}$ and $\Delta H_{lc\text{-}k}$ for HMS Series Polycarbonates
at 10°C/minute Scan Rate**

Sample n	$\Delta H_{i\text{-}lc}$ (KJ/mole)	$\Delta H_{lc\text{-}k}$ (KJ/mole)
4	----	0.6
5	0.1	4.3
6	0.2	2.5
7	0.2	4.4
8	----	3.6
9	0.6	5.6
10	0.3	4.5
12	----	7.8

------- No transition seen in this sample

Figure 2.5 shows DSC scans at cooling rates of 5, 10, 20, and 50°C/min for HMS-9. There is little change for the isotropic to mesophase transition temperature (indicated by an arrow) with the cooling rate, but the onset of crystallization is suppressed by higher cooling rate. Similar results were seen in HMS-6. The liquid crystalline phase transition is not affected much by this variation of cooling rate for these two samples. However, the formation of three dimensional crystals is greatly affected by the cooling rate due to the strong temperature dependence of the rate of formation of secondary nuclei.

In Figure 2.1, we were unable to observe the isotropic to mesophase transition for HMS-8, which we had expected to see at the front shoulder of the large crystallization exotherm, as was the case for HMS-5 through 7. Given the dependency of the crystallization exotherm on cooling rate, we used a high cooling rate to suppress the exotherm of crystallization causing it to occur at a lower temperature. Figure 2.6 shows DSC scans of HMS-8 at cooling rates of 5, 10, 20, and 50°C/minute. At a cooling rate of 50°C/min HMS-8 now clearly shows the mesophase transition as a shoulder on the high temperature side of the crystallization exotherm. It is not seen at lower cooling rates because it overlaps with the crystallization phase transition and can not be separately identified. Similar effect of cooling rate was seen for HMS-7. The mesophase transition of HMS-7 can be observed at cooling rates of 5°C/min to 50°C/min (see Figure 2.1 for 10°C/min) but disappears at a slow cooling rate of 2°C/min. At this rate, the onset temperatures of the transitions from the isotropic to crystalline phase is about 143°C. Table 2.3 summarizes the onset temperatures of the transitions from the isotropic to mesophase (T_{i-lc}) and from the mesophase to crystalline phase (T_{lc-k}). All the heats of transition from the isotropic to mesophase are qualitatively the same with the cooling rates.
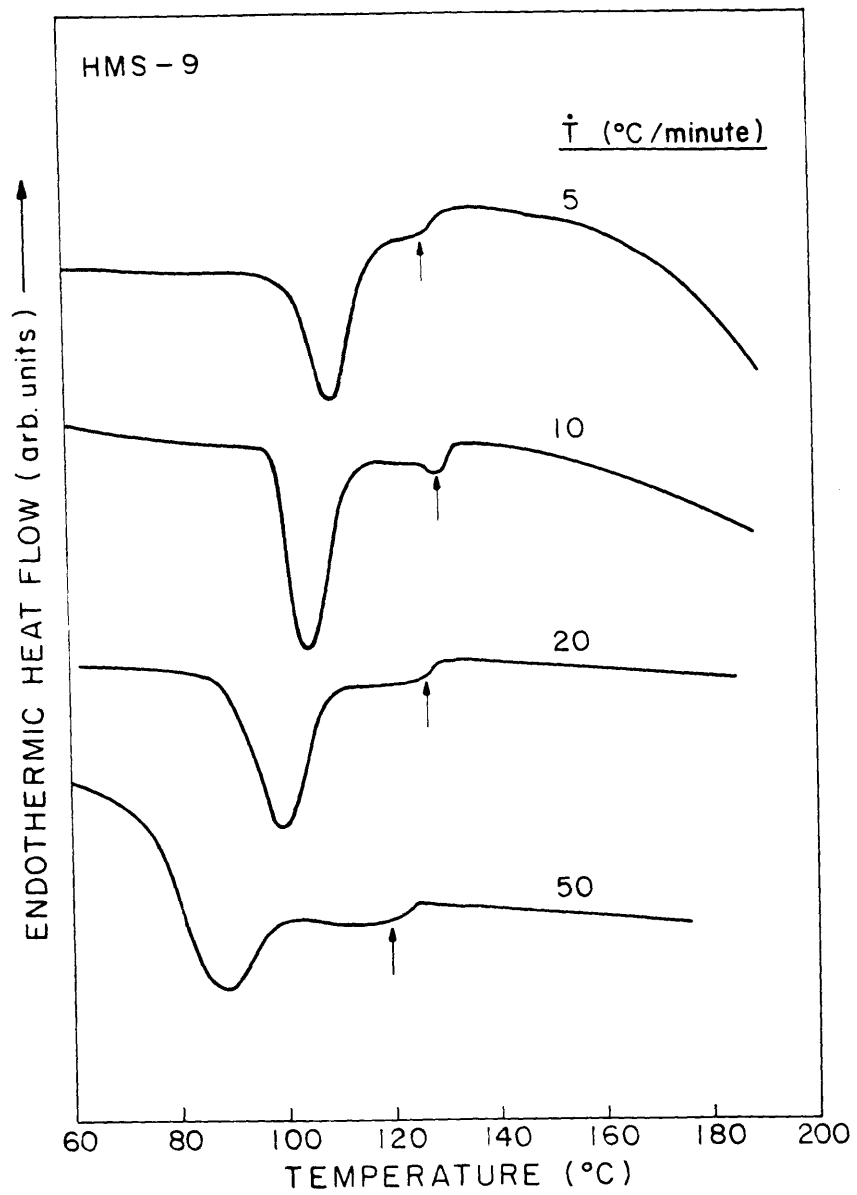
Figure 2.5   DSC thermograms of HMS-9 at various cooling rates.
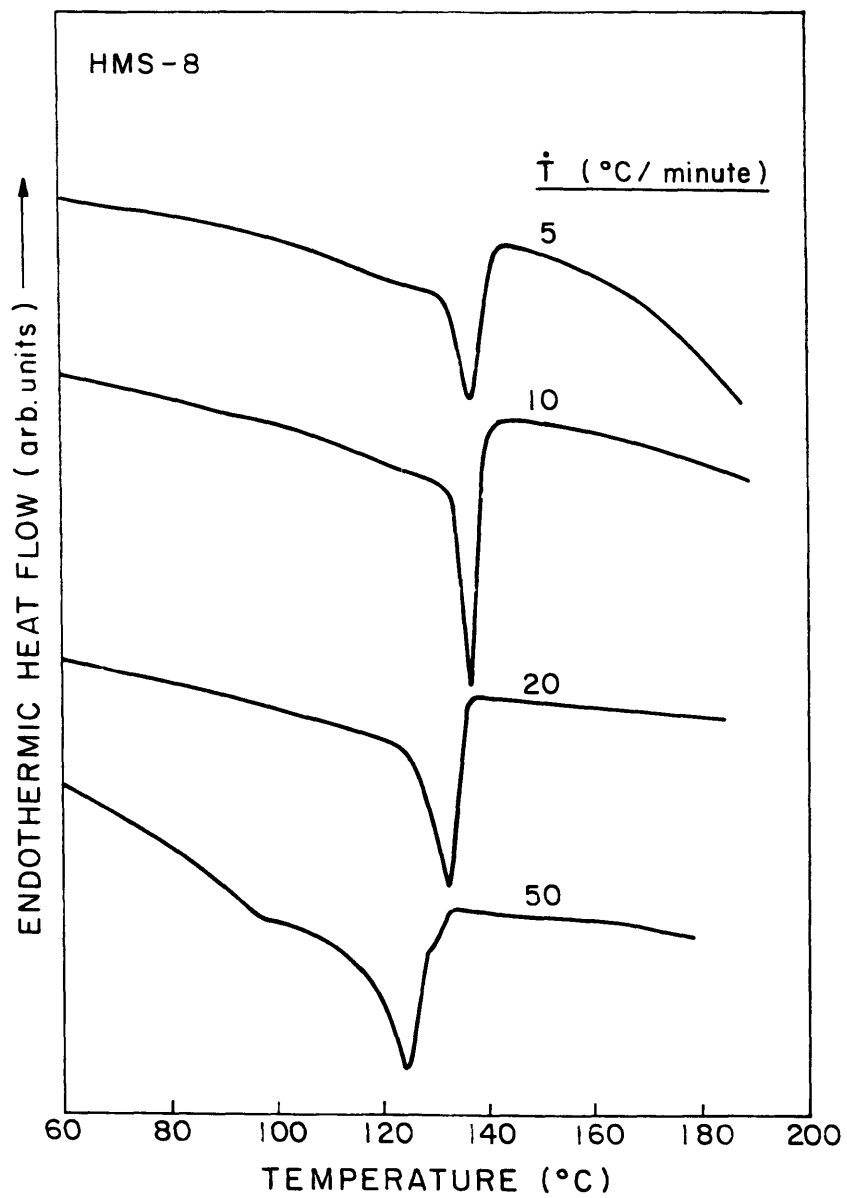
Figure 2.6   DSC thermograms of HMS-8 at various cooling rates.

Table 2.3

Onset Temperatures of Transitions of HMS-6 Through 9 at Different Cooling Rates

Cooling rate (°C/min)	HMS-6		HMS-7		HMS-8		HMS-9	
	T_{i-lc}(°C) (±1°C)	T_{lc-k}(°C) (±1°C)	T_{i-lc}(°C) (±1°C)	T_{lc-k}(°C) (±1°C)	T_{i-lc}(°C) (±1°C)	T_{lc-k}(°C) (±1°C)	T_{i-lc}(°C) (±1°C)	T_{lc-k}(°C) (±1°C)
5	156	137	144	141	-----	143	133	120
10	156	137	143	138	-----	142	134	114
20	153	123	139	132	-----	136	133	112
50	150	111	132	121	132	128	126	99

----- No transition seen at this rate

During isothermal crystallization, the crystallization time, t_c, is the time after which no further exothermic heat flow can be detected. As the crystallization temperature increases, the crystallization time increases, and the exothermic peak area decreases and finally becomes undetectable. Figure 2.7 shows the isothermal crystallization heat flow versus time for HMS-9 crystallized at 108°C and 120°C. As the crystallization temperature increases, the crystallization kinetics become slower, and the area under the exothermic peak also becomes smaller. Tables 2.4 and 2.5 summarize the time to maximum exothermic heat flow and crystallization time as a function of the crystallization temperature from the isothermal study of HMS-5 through 8. Table 2.6 summarizes both the time to maximum exothermic heat flow and crystallization time as a function of the crystallization temperature for HMS-9.

Figure 2.8 shows DSC scans of HMS-9 at a heating rate of 5°C/min after staying at the crystallization temperature isothermally until crystallization was finished. The sample is not cooled before scanning, therefore this technique is called an 'immediate rescan'. These thermograms represent the immediate rescans after isothermal crystallization at 108, 112, 114, 116, 118, 120 and 123°C. We can see that there are two major peaks in nearly all the immediate rescan endotherms. We will designate the lower one as T_{m1} and the upper one as T_{m2}, according to the peak position. T_{m2} is broader and extends to the bottom of T_{m1}. The area under T_{m2} becomes smaller as the crystallization temperature increases. Finally, when crystallization temperature equals 123°C, only the lower peak remains. Also, the temperature range of T_{m2} becomes smaller, and appears to have a fixed upper limit. We observed similar results for the DSC scans of HMS-5, 6 and 8. In each case, there are two endotherms, the upper one of which becomes relatively smaller as crystallization temperature increases.
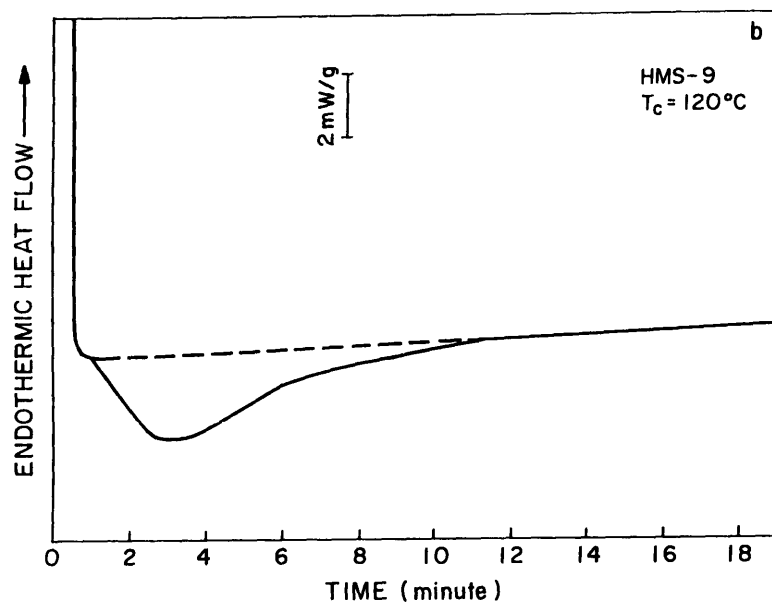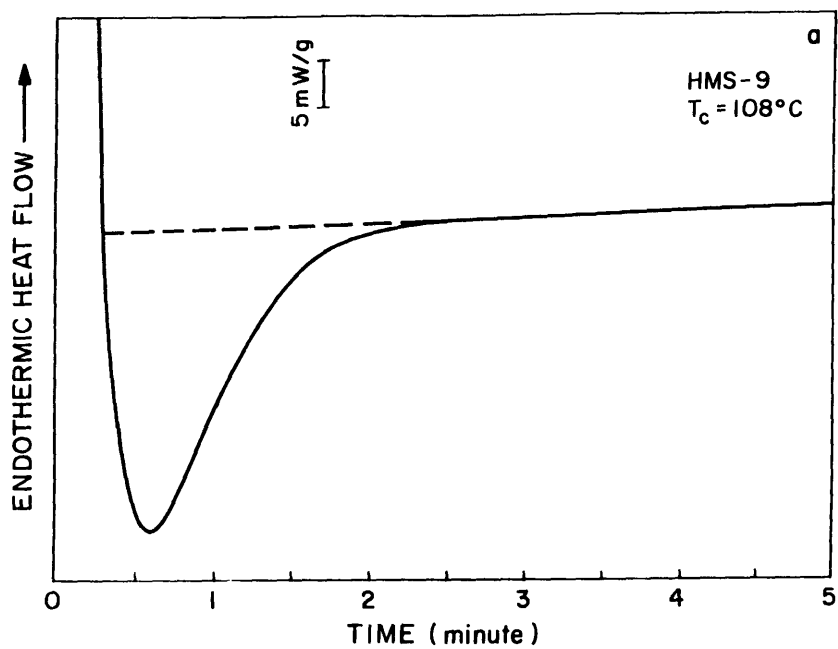
Figure 2.7   DSC heat flow vs. time, during isothermal crystallization

of HMS-9 at (a) 108°C and (b) 120°C.

Table 2.4

**Time to Maximum Exothermic Heat Flow (minutes)
as a Function of Crystallization Temperature for HMS-5 through 8**

Sample	Crystallization Temperature (°C)						
	130	134	138	140	142	144	147
HMS-5	-----	0.7	0.7	0.9	1.2	1.4	2.2
HMS-6	0.4	0.8	1.3	1.6	1.9	2.1	-----
HMS-7	-----	-----	0.9	1.0	1.4	1.7	3.4
HMS-8	-----	-----	0.2	0.4	0.7	1.2	2.6

------ Not tested at this temperature

53

Table 2.5

Crystallization Time (minutes) as a Function of Crystallization Temperature for HMS-5 through 8

Sample	Crystallization Temperature (°C)						
	130	134	138	140	142	144	147
HMS-5	------	2.1	2.8	3.0	4.0	8.6	13.7
HMS-6	2.8	4.8	6.3	7.7	8.6	9.3	------
HMS-7	------	------	4.4	5.0	6.3	8.0	12.4
HMS-8	------	------	2.0	2.8	4.1	8.2	17.8

------ Not tested at this temperature

Table 2.6

**Time to Maximum Heat Flow and Crystallization Time (minutes)
as a Function of Crystallization Temperature for HMS-9**

Crystallization Temperature (°C)	Time to Maximum Exothermic Heat Flow (minutes)	Crystallization Time (minutes)
108	0.3	2.2
112	0.5	2.5
114	0.6	4.7
116	1.0	6.7
118	1.4	7.5
120	2.1	10.8
123	2.2	14.2
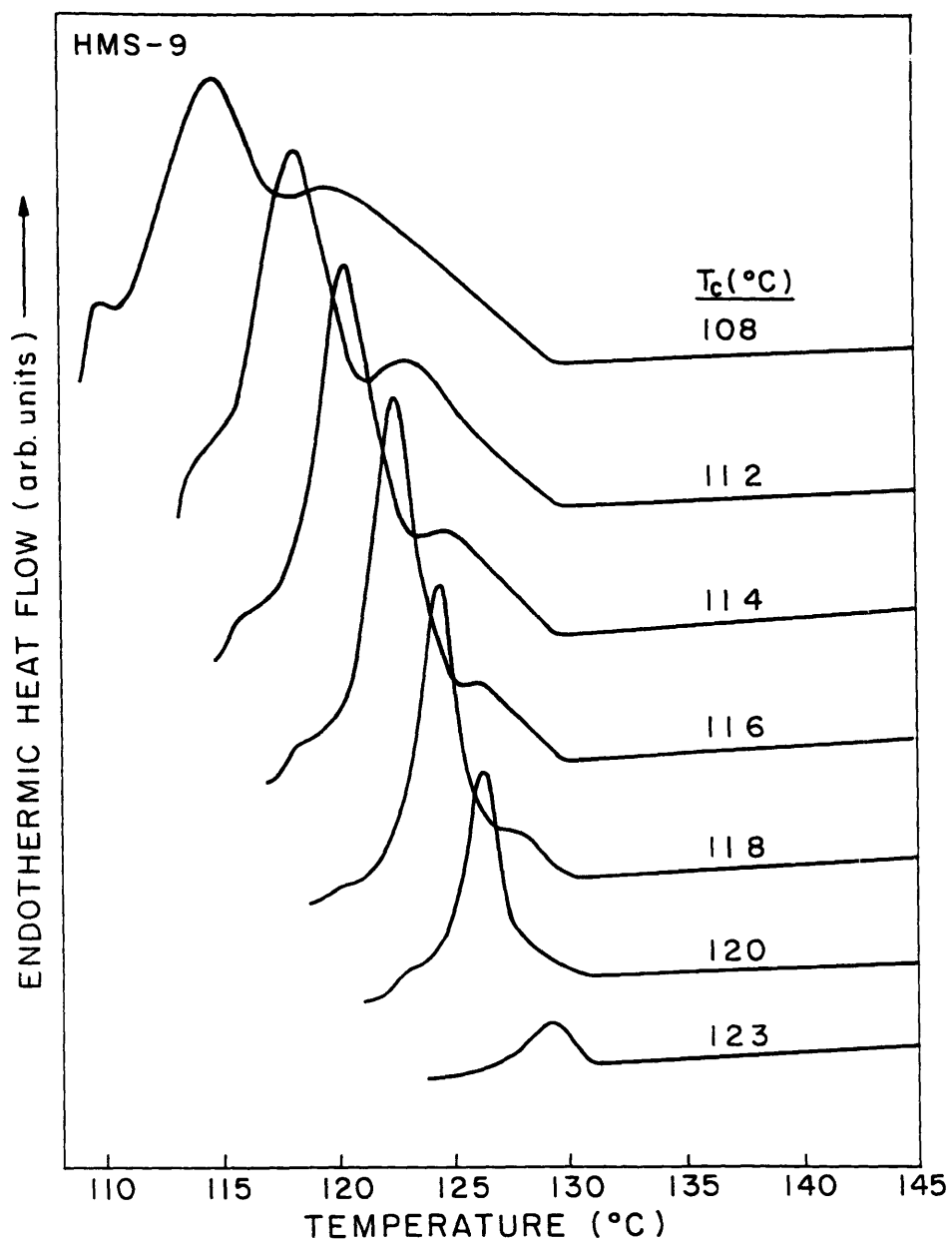
Figure 2.8   Immediate rescan DSC thermograms of HMS-9 at 5°C/min

heating rate after isothermal crystallization at the

temperatures shown.

The relationship between the melting point and the crystallization temperature is found from the Hoffman-Weeks equation [85] as:

$$T_m = T_m^0 (1 - 1/\gamma) + T_c / \gamma \qquad (1)$$

where T_m^0 is the infinite crystal melting point and γ is the thickening factor of the lamellae. The thickening factor is found from the reciprocal of the slope, and the infinite crystal melting point is found from the intersection of the T_m vs. T_c curve with the line $T_m = T_c$. Here we use T_{m1} as T_m. Table 2.7 summarizes the infinite crystal melting points and thickening factors for HMS-5, 6, 8 and 9. The thickening factors are all very close to 1.

Figure 2.9 shows the immediate rescans at heating rates of 1, 2, and 5°C/min for HMS-9 which was isothermally crystallized at a crystallization temperature of 114°C. There is little change in T_m and also the area under the melting peak is almost the same with these heating rates. Similar results were also seen for HMS-5. Therefore, we suggest that there is little or no reorganization during this process. This is consistent with studies on other kinds of main chain thermotropic LCPs [86,87].

Figure 2.10 shows DSC scans at heating rate of 5°C/min for HMS-9 after being held at T_c = 114°C for 0.5, 1.0, 2.0 or 4.7 minutes. For HMS-9 at this crystallization temperature, the time to maximum exothermic heat flow is 0.6 minutes as determined from isothermal crystallization studies. From this study of HMS-9, we see that there are two peaks developing at the same time. By comparing the melting peaks after different crystallization time, we see that the upper peak, T_{m2}, with wider and higher range, stops growing earlier than the lower one, T_{m1}. The upper peak develops most of its area before the time to maximum exothermic heat flow, while the lower peak develops significant area after this time.

Table 2.7

**Infinite Crystal Melting Point and Thickening Factor
for HMS-5, 6, 8 and 9**

Sample	Infinite Crystal Melting Point, T_m° (°C)	Thickening Factor, γ
HMS-5	203	1.2
HMS-6	231	1.1
HMS-8	215	1.1
HMS-9	262	1.0
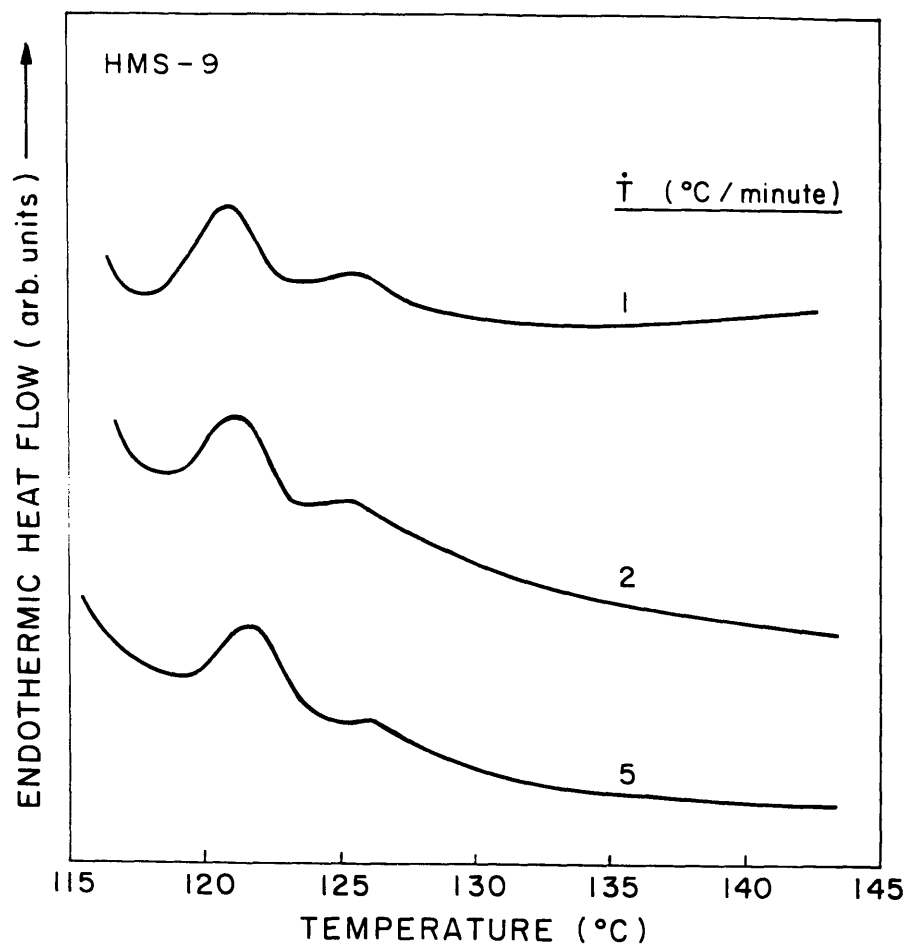
Figure 2.9   DSC thermograms of HMS-9 after isothermal crystallization at

114°C for 4.68 minutes. Immediate rescan at the indicated rates.
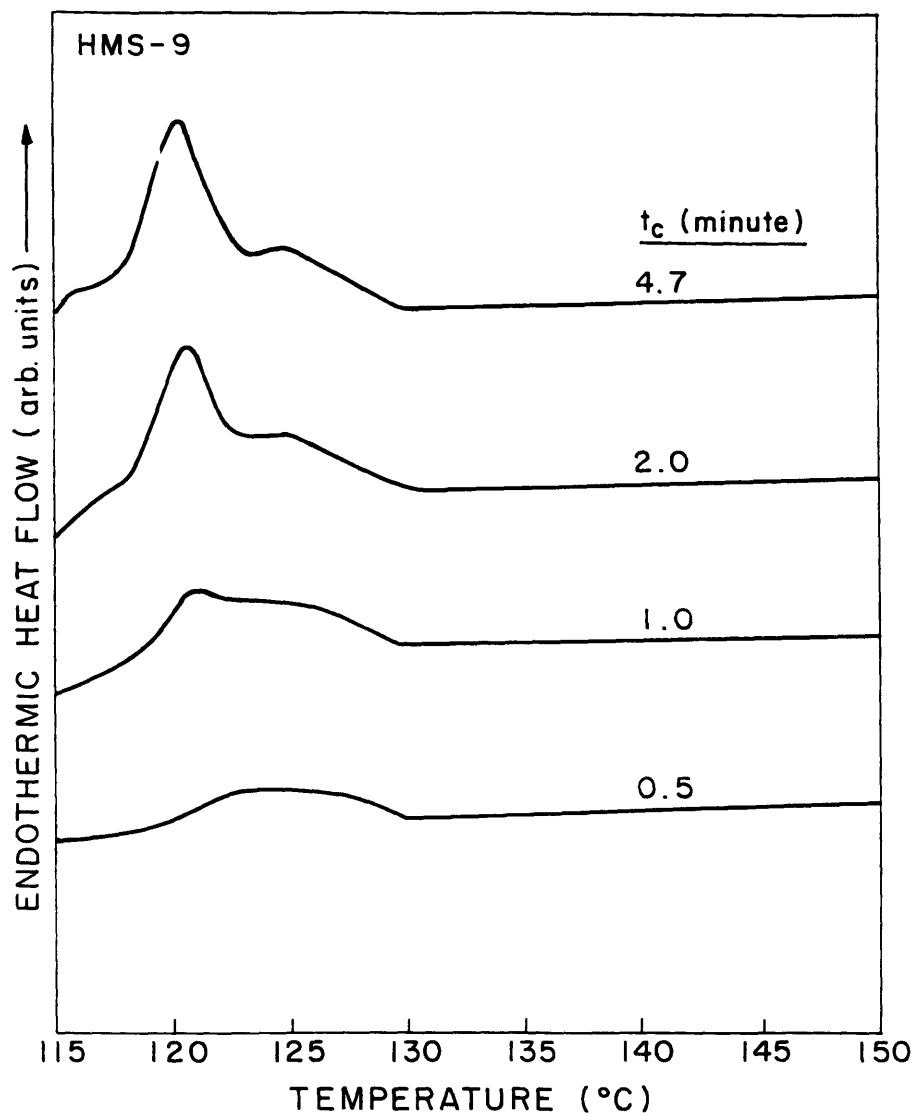
Figure 2.10   Immediate rescan of HMS-9 at 5°C/min heating rate after

isothermal crystallization at 114 °C for the indicated times.

60

2.3.2 Optical Microscopy

Optical Microscopy revealed a fine grained pattern of birefringence whose intensity (recorded with a photodetector) changed rapidly near the isotropic to mesophase transition and more gradually near the mesophase to crystalline transition. Poorly formed spherulites were seen in HMS-5, 6, 7 and 8. None were seen in HMS-4, 9, 10 and 12.

In Figure 2.11(a) and (b), we show optical micrographs of HMS-5 at magnification of 320x between crossed polars. We can see Schlieren texture in Figure 2.11(a), which is a characteristic of the nematic mesophase [4]. As shown in Figure 2.11(a) and (b), spherulites developing at crystallization temperature 127°C without annealing were much bigger than those developing at 127°C after prior annealing at 157°C, which is the isotropic to mesophase transition temperature. When the sample was annealed at 157°C, many small highly birefringent spots formed at this temperature. Upon cooling to 127°C, the birefringence increased and crystals filled the entire field of view, as shown in Figure 2.11. We conclude that the locally forming mesophase serves as nucleation site for subsequent crystallization.

2.3.3 Transmission Electron Microscopy

Islands of different sizes with similar morphology were formed for HMS-5, 7, and 9 samples for both isothermal-annealing temperatures. The smaller islands demonstrate a sheath-like texture which suggests that polymer chains align parallel to each other and may crystallize to cause periodic thickness change, as described in Chapter 1. There appears to be an increase in thickness from the edge to the center of the larger island as is apparent from the increase in mass/thickness contrast. We can clearly see sheath-like texture around the edge, and even the interior part of these larger islands. We can also observe faint diffraction spots from the smaller islands and stronger diffraction spots from the larger islands. Furthermore, in the center of the larger islands, we can see the lamella-
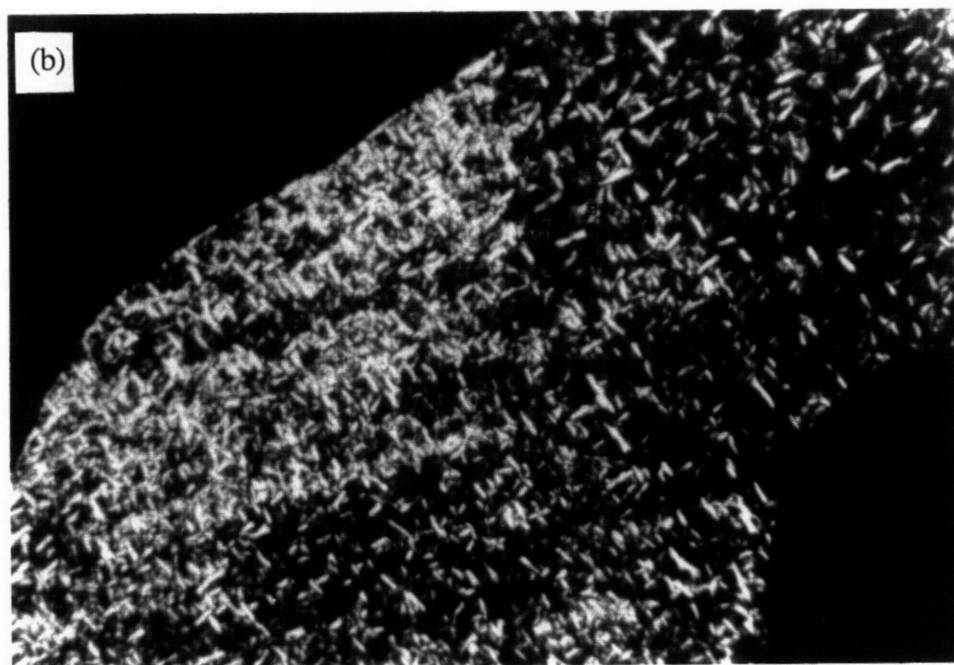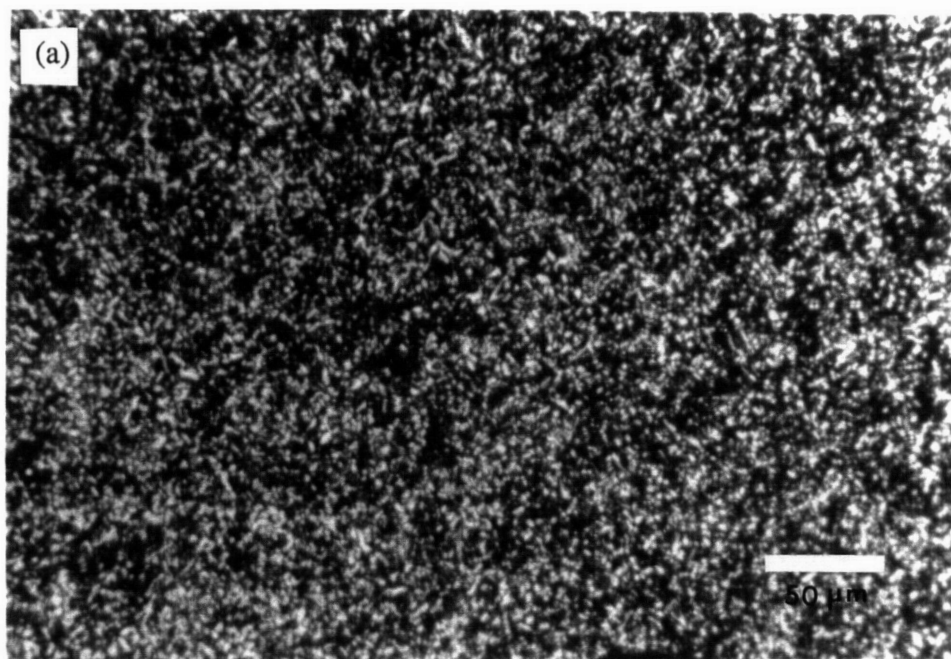
Figure 2.11   Optical micrograph of HMS-5 crystallized at 127°C for 40 minutes.

(a) Sample annealed at 157°C for 40 minutes prior to crystallization

at 127°C. (b) Sample cooled directly to 127°C without annealing.

Scale marker is the same for both figures.

like structure or some sharp crystal edges. Therefore, crystals with different degrees of perfection have developed in the whole sample. Also, we know that these crystals are from the parallel aligned polymer chains, which suggests that the nematic phase serves as crystal nuclei. Figure 2.12 shows a TEM micrograph of HMS-5, which was annealed at 157°C for 30 minutes and then air-cooled.

2.4. DISCUSSION

2.4.1 Relationship Between Transition Temperatures and Flexible Spacer Number

In our HMS polycarbonate polymers, no odd-even effect is seen in any of the transition temperatures, as shown in Figures 2.3 and 2.4. In contrast, all of the HMS polyethers [50] and polyesters [49,82] showed an odd-even effect in both the melting temperature and the transition temperature from the liquid crystalline phase to the isotropic phase. We suggest that the conformation of the carbonate linkage causes the loss of the odd-even effect. As mentioned in the Introduction, for most LCPs with rigid rod mesogen, polymers with an even number of methylene units in the flexible spacer have a higher degree of alignment than those with an odd number. Moreover, as with Percec's polyethers [75-79], when a polymer has a flexible mesogen, the liquid crystal mesophase is formed by the coupled action of the flexible mesogen and the flexible spacer. The flexible mesogen can result in significant conformational changes of the polymer chain, which will affect the formation of the liquid crystal mesophase. Similarly, for the HMS polycarbonates reported here, the carbonate linkages positioned beside the methyl-stilbene mesogen can cause considerable conformational change. In order to form the mesophase, the carbonate linkages have to adopt the conformation that causes the polymer chain to be aligned and stabilized. The specific conformation in the carbonate linkage might be the reason why the odd-even effect is lost within the HMS polycarbonate polymers. The loss of the odd-even effect in the transition temperatures
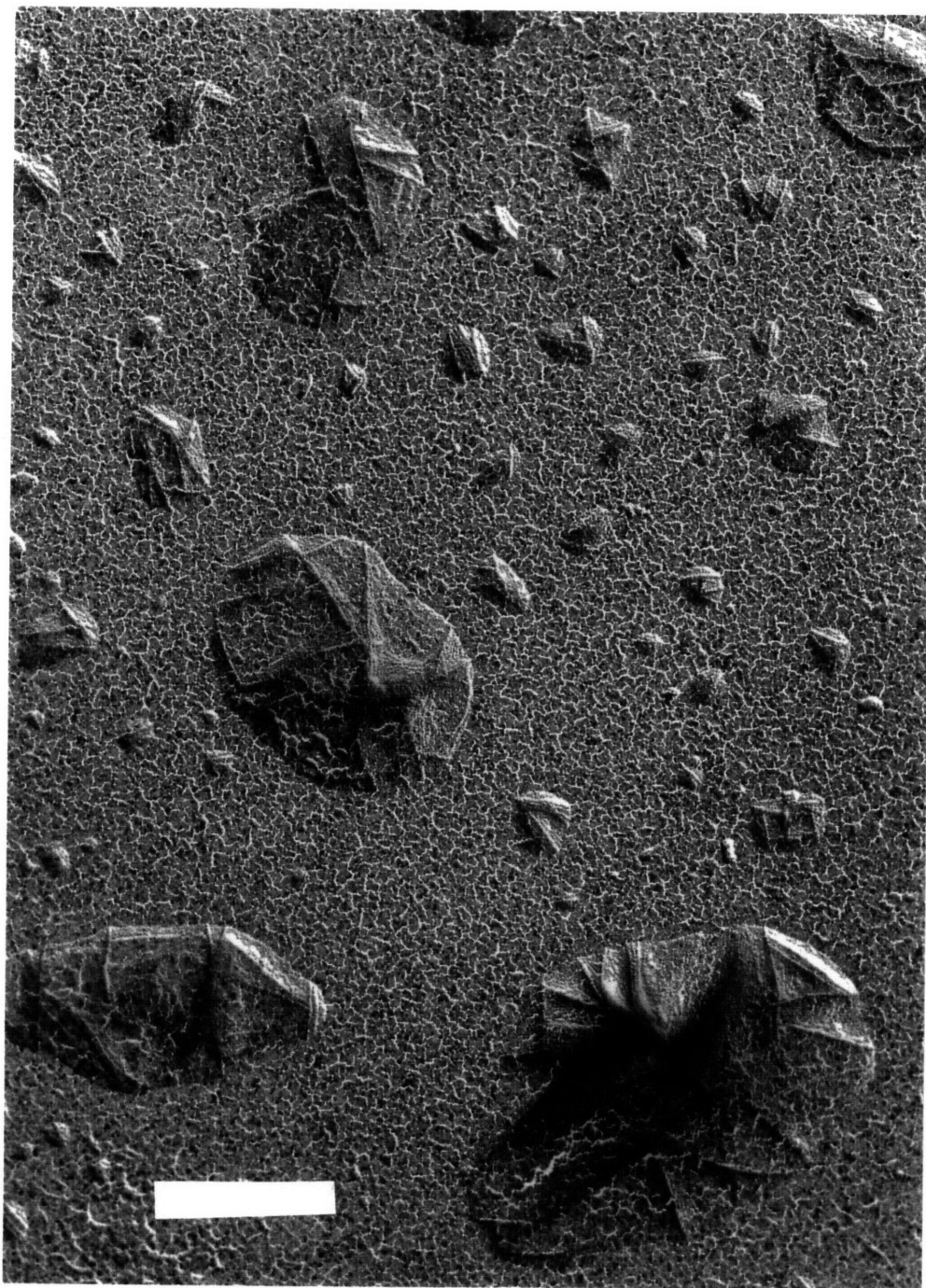
Figure 2.12   TEM micrograph of HMS-5 annealed at 157°C for 30 minutes

and then air-cooled. Bar = 1 μm

has also been seen in enantiotropic liquid crystalline polycarbonates [49].

Next, we consider the cause of the melting point reduction in HMS polycarbonates compared to HMS polyethers or polyesters. At the equilibrium melting temperature T_m, the crystal phase is in equilibrium with the melt. Setting the Gibbs free energy change equal to zero, we write:

$$T_m = \Delta H_f / \Delta S_f \qquad (2)$$

where ΔH_f and ΔS_f are the differences in enthalpy and entropy, respectively, between the melt and the crystal phase. Better intermolecular interaction leads to the higher absolute value of ΔH_f which would tend to increase the melting point. ΔS_f reflects the greater randomness in the isotropic phase [52]. The carbonate linkage contributes more conformational entropy change between the crystalline phase and the isotropic phase, and between the isotropic phase and the mesophase, than either ester or ether linkages. This effect not only causes the lower melting transition temperature of HMS polycarbonates, but also might cause the stable range of their mesophases to become narrowed. Actually HMS polycarbonates are monotropic liquid crystalline polymers. The local intermolecular interaction is the driving force for crystallization which leads to monotropic behavior. The effect of intermolecular interaction on mesophase behavior has been studied by other groups [88].

A change in properties occurs when the flexible space number exceeds eight. First, from polarizing optical microscopy, small but ill-formed spherulites are seen for n=5, 6, 7, and 8. No spherulites large enough to be identified by optical microscopy were seen for n=9, 10 or 12. Second, in both cooling and heating, the transition temperatures of HMS-polycarbonate LCPs drop sharply when n is greater than eight. In HMS

polyethers [50], which have an enantiotropic mesophase, the transition temperatures also drop when n > 8. Lowering of the crystallization and melting temperatures, and inability to form large spherulites imply that crystal size and perfection are reduced when n exceeds eight.

In terms of the repeat unit structure of the HMS polycarbonates, we note that the change in properties occurs when the length of the flexible spacer group exceeds the length of the stilbene mesogen, for chains in the all trans conformation. From the standpoint of energy minimization, this conformation represents one of the most probable conformations resulting in extended polymer chains, for most liquid crystalline polymers in the mesophase [25,59,79]. The fact that the same effect is seen in HMS polycarbonates and in HMS polyethers is related to similarity of their chemical structures. Both of these LCPs have linking groups that are symmetric. Crystal perfection is related to interchain packing, and in both HMS polycarbonates and polyethers the interchain packing is affected by the relative lengths of the flexible spacer and mesogen. For HMS polyethers, when the mesogen length is greater than the flexible spacer, the most stable crystal structure is 'intermeshed', in which the interchain packing is tight [71]. However, this kind of crystal structure does not exist in those polymers with the flexible spacer length longer than its mesogen, which have layered structure. Similarly, HMS polycarbonates with flexible spacer longer than the mesogen do not seem to have intermeshed structure. In support of this view, we note that in the plot of d-spacing for two major interchain reflections versus flexible spacer number, n, the interchain spacing shows an odd-even effect for low n value, but levels off when n ≥ 9 [89]. These results will be more completely discussed in a subsequent publication [90] on x-ray diffraction of HMS polycarbonates.

When the length of the flexible spacer gets close to that of the mesogen from n =

5 to 8, the stability range of the liquid crystal phase seen in the cooling scan becomes smaller. For HMS-7 and 8, the closeness of the length between the mesogen and the spacer increases the crystallization rate and makes the mesophase transition and the crystallization transition indistinguishable for the lower cooling rates. For these two samples, the liquid crystalline phase is much more unstable than in other samples, as suggested by the results of cooling rate studies in Table 2.3. We suggest that the difference is related to the difference of the spacer length, which results in difference in crystal structure. When the length of spacer becomes close to that of the mesogen, intermolecular interaction is affected, causing fast crystallization. In Chapter 3, we will describe our experiments in x-ray diffraction of HMS polycarbonates LCPs in which we investigate change of crystal structure with the number of methylene units in the flexible spacer [90].

2.4.2 Crystal Formation

For nematic liquid crystalline polymers, the crystallization from the nematic phase has been widely studied [86,87,91-94]. The nematic phase usually serves as a nucleus for subsequent crystallization. Without the formation of the nematic phase, the polymer crystallizes much more slowly from the isotropic phase. The crystals forming from the nematic phase usually have structure similar to their nematic phase. For monotropic liquid crystalline polymers, the crystallization from the liquid crystalline phase is rapid. Therefore, their liquid crystalline phase is considered to be more ordered than that of enantiotropic nematic LCPs [72].

Our HMS polycarbonate polymers are monotropic liquid crystalline polymers. As shown in Figures 2.1 and 2.2, the range of the transition from isotropic phase to nematic phase seen in the cooling scan overlaps the range of the upper melting peak of the crystals seen in the heating scan. The transition from the isotropic phase to liquid crystal phase is

very close in temperature to the transition from the liquid crystal phase to the crystal phase for the heating and cooling rates used in this study.

For main chain thermotropic liquid crystalline polymers, dual endotherms are usually seen in the DSC heating scan. As shown in Wendorff's crystallization studies on liquid crystalline copolyesters [91], two groups of crystals develop in sequence. The upper melting crystals form first from the nematic phase and restrict the growth of the later crystals forming among the first crystals by an annealing process. The closeness of the peak temperatures of the dual endotherms is a characteristic of our HMS polycarbonate LCPs. Whether we heat by immediately rescanning after isothermal crystallization, or heat after cooling from the melt, two crystal populations are observed. Each crystal population melts predominantly to form one of the dual endotherms. We conclude that the first crystal group using the nematic phase as the nuclei for crystallization has faster crystallization rate. The second crystal group grows more slowly due to the slower rate of formation of secondary nuclei from the isotropic phase.

The upper peak seen in the immediate rescan after isothermal crystallization is from the melting of the crystals developing from the nematic phase, while the lower peak is from the crystals growing from the isotropic phase. These two groups of crystals are both stable, which is why we observe no 'reorganization' during the rescan process. The upper melting crystals develop earlier than the lower melting crystals, as shown in Figure 2.10. Both crystal populations grow fast provided the crystallization temperature is below the transition temperature from the isotropic phase to the nematic phase. As the crystallization temperature increases, the population of upper melting crystals, using the nematic phase as the nuclei for crystallization, gradually diminishes, as shown in Figure 2.8. This result is in agreement with observation of decreased exothermic area shown in Figure 2.7. The mesophase transition covers a broad temperature range of about 10

68

degrees (see Figure 2.1). The amount of seed nuclei from the mesophase decreases as the isothermal crystallization temperature increases through the mesophase transition range, and this causes reduced ultimate crystallinity. However, the crystallization rate of the lower melting crystal group also slows down. Therefore, the formation of secondary nuclei is also related to the ability of the polymer to form aligned structures.

From the above discussion, we can conclude that the crystals using the nematic phase as the nuclei for crystallization are the crystals which cause the major exotherm right after the transition from the isotropic phase to the nematic phase seen in the cooling scan, as shown in Figure 2.1. These crystals are also the crystals which cause the upper melting peak in the heating scan, as shown in Figure 2.2. The lower endotherm, which overlaps greatly with the upper endotherm, is from the melting of those crystals developing from the secondary nuclei forming from the isotropic phase. The closeness of the melting point of these two groups of crystals can be understood by considering the structure of HMS polycarbonate. Due to the flexibility caused by the carbonate linkage, the first group of crystals develops from the nematic phase in regions quite scattered throughout the melt. These crystals have widely varying degrees of perfection, which causes a broad upper endotherm. And these crystals restrict the growth of the later crystals, but not as much as Wendorff's copolyesters do [91]. In the copolyester LCPs, clearly separate dual endotherms are observed.

The upper melting crystals are very stable and the crystals developing later from the remaining isotropic phase can only develop in a restricted geometry among the first crystals. There is further evidence provided by the crystallization study using optical microscopy. Bigger spherulites were seen within those samples crystallizing without annealing at the isotropic to nematic transition temperature. The annealing caused scattered nematic phases to form locally, which later crystallize and restrict the

development of large spherulites. The mechanism of crystallization whereby the secondary crystals develop among the first crystals was actually seen in a transmission electron microscopy study of PEEK [95]. The dual endotherm was also seen in the heating scan of PEEK which had been crystallized from the melt [96-98]. This mechanism of crystallization is common in those polymers with low degree of crystallinity and generally results in observation of broad endotherms.

2.5. CONCLUSIONS

1. HMS polycarbonates are monotropic liquid crystalline polymers, while HMS polyesters and polyethers have an enantiotropic liquid crystal phase.

2. The conformation in the carbonate linkage strongly affects the stability of the liquid crystal phase, and causes the loss of the odd-even effect. The spacer length also affects the crystallization kinetics. The crystallization from the nematic phase becomes faster when the length of spacer gets close to that of the mesogen. When the former exceeds the latter, all the transition temperatures drop.

3. The melting of crystals forming directly from the nematic phase causes the high temperature endotherm seen in the heating scan. These crystals grow fast and restrict the development of the later crystals forming from the isotropic phase. The later crystals are less perfect and melt to form the lower temperature endotherm.

70

Chapter 3
Structure Development in HMS Polycarbonates
by Wide Angle X-ray Scattering (WAXS)

3.1. INTRODUCTION

In our HMS polycarbonates, the monotropic nature of the mesophase prevents observation of some of the thermal transitions [99]. Therefore, the odd-even effect in the thermal properties is not obvious because of their monotropic liquid crystalline behavior [99]. However, we did observe that all transition temperatures dropped when n exceeded eight [99]. In addition, in our HMS polycarbonates an interesting odd-even effect has been observed (and reported in preliminary form [89]) in the two dominant interchain d-spacings from the wide angle X-ray scattering powder diffraction pattern when n ranges from 5 to 8. When n exceeded eight, the major interchain d-spacings leveled off.

HMS polyethers, polyesters, and polycarbonates all contain the same stilbene mesogen and the same flexible spacer group. These LCPs differ only in their linking groups. The question arises concerning the aspects of chain structure that cause our HMS polycarbonates to be monotropic LCPs, and to show weak (or no) odd-even effect in their thermal transitions, compared to their chemical relatives. In Chapter 2, we suggested previously that the stability of the liquid crystalline phase is affected by the carbonate linkage, which causes fast crystallization resulting from intermolecular interaction [99]. In this Chapter, we explore this idea further by a combined approach using wide angle X-ray scattering and molecular modeling. We show here that the HMS polycarbonate chains pack together in an intermeshed structure. The disposition of the carbonate group differs from n-even to n-odd, and this we suggest is responsible for the odd-even effect in the two dominant interchain d-spacings from the wide angle X-ray scattering powder

71

diffraction pattern when n ranges from n = 5 to 8.

3.2. EXPERIMENTAL SECTION

3.2.1 Reflection Mode WAXS

Wide angle X-ray scattering, WAXS, studies were made in reflection mode for all unoriented HMS polycarbonates. A Rigaku RU-300 rotating anode X-ray generator was used to examine samples in $\theta/2\theta$ reflection mode. The diffractometer has a diffracted beam graphite monochromator. Copper K_α radiation ($\lambda = 1.54\text{Å}$) was used with a step scan interval of 0.1 degree, at a scan rate of 1 degree/minute over the 2θ range from 3 to 53 degrees. HMS powder was melted on a teflon substrate then cooled, and the resulting solid piece was fixed to an aluminum frame for examination by WAXS.

3.2.2 WAXS Fiber Analysis

WAXS in transmission mode was performed at room temperature on selected oriented HMS fibers, using a Philips PW1830 X-ray generator operated at 45kV and 45mA with Ni-filtered CuK_α radiation. The Statton camera used in this study consists of a pinhole collimator over which the sample is placed, and a flat film (Kodak DEF-5) to record the scattering pattern. The sample to film distance is calibrated using Si powder reference standard (from National Institute of Standards & Technology) rubbed on the sample surface. The first 2θ value for Si is 28.44°. HMS fibers were hand drawn from the mesophase using tweezers. It was relatively easy to draw fibers for HMS-5,7, and 8 but quite difficult to draw HMS-6. The hand drawn fibers cooled rapidly in air, and will be referred to as raw fiber. Raw fibers were subsequently annealed below the melting temperature. WAXS was performed on both the raw and annealed fibers.

3.2.3 Molecular Modeling

CERIUS™, a commercial software package distributed by Molecular Simulations Inc., was used for indexing of experimental X-ray diffraction patterns and determination of the crystal structure. Because the experimental c-axis repeat unit is close to the end to end distance of the fully extended monomer unit, a initial structure close to all-trans conformation was assumed for X-ray diffraction simulation work. By comparing the experimental powder and oriented fiber diffraction pattern with the simulated patterns, we first determined the crystalline cell symmetry and then refined the crystal lattice parameters.

3.3. RESULTS

3.3.1 Reflection Mode WAXS

The WAXS diffractometer scans of HMS-5-12 are shown in Figure 3.1. WAXS scans in reflection mode generally show two sharp and dominant interchain reflections. In addition, several HMS polycarbonates show a number of much weaker peaks. Considering only the two dominant interchain reflections, we show in Figure 3.2 a plot of d-spacing vs. flexible spacer number, n. An odd-even effect is observed in the d-spacing for n = 5 to 8. The assignment of Miller indices of (020) and (110) will be explained later. When n ≥ 9, the two major d-spacings get closer to one another and level off.

3.3.2 WAXS Fiber Analysis

Next, we show the flat film fiber patterns of raw (unannealed) fibers, and annealed fibers. In Figure 3.3 WAXS of selected raw fibers is shown. HMS-5 raw fiber is shown in Figure 3.3a and HMS-8 is shown in Figure 3.3b. HMS-5 raw fiber WAXS shows a single diffuse equatorial maximum and no meridional reflections, which is characteristic of a nematic mesophase. HMS-8 raw fibers have two diffuse equatorial
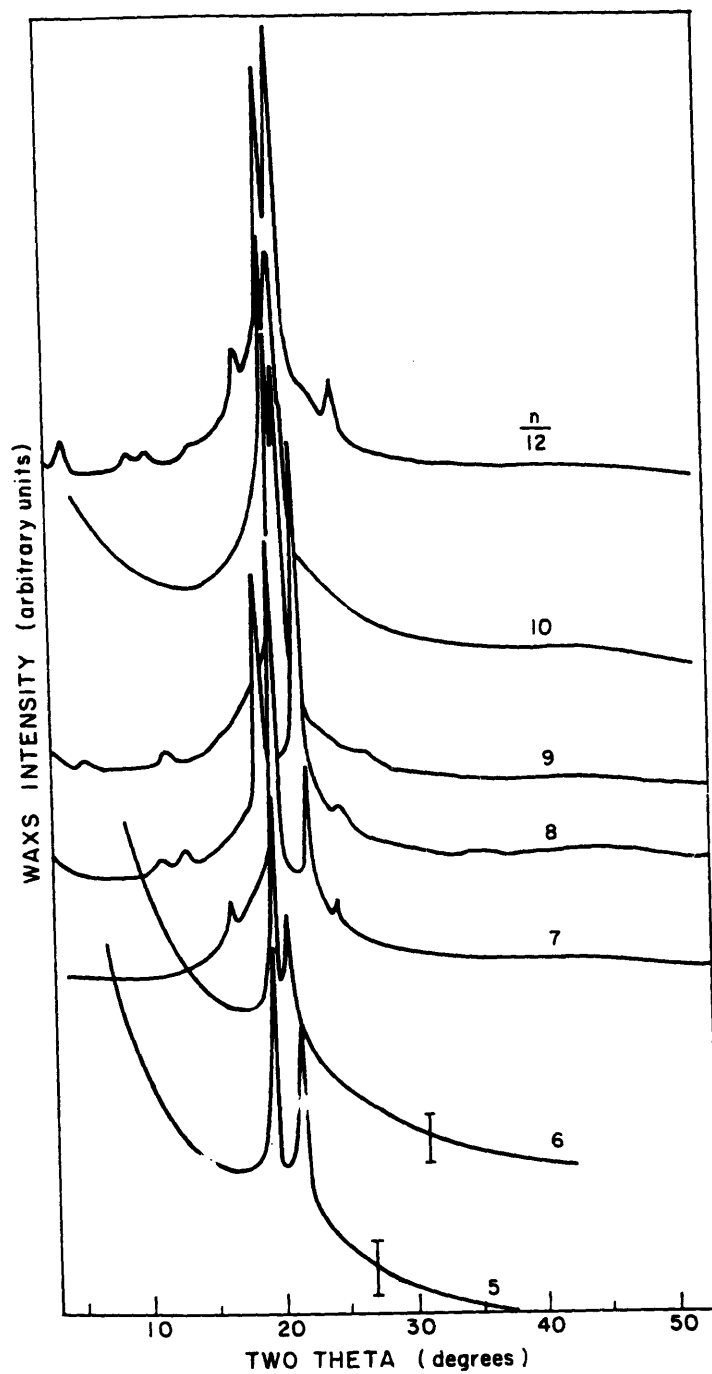
Figure 3.1   WAXS intensity versus two theta for HMS-4-10, -12.
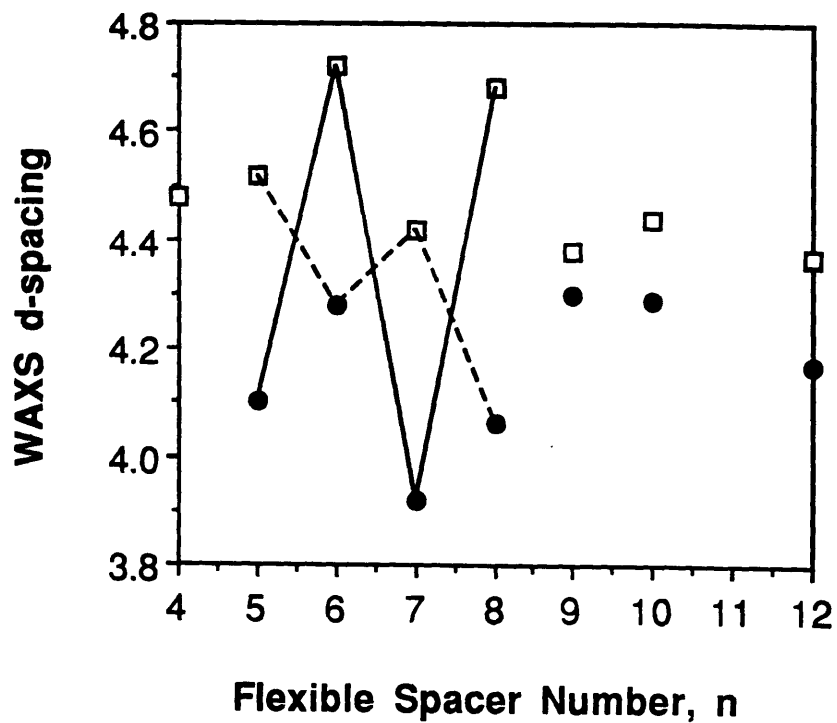
Figure 3.2   Interplanar spacing, d, versus flexible spacer number, n,

for the two major interchain reflections shown in Figure 3.1.

(□) higher value d-spacing and (●) lower value d-spacing.

d-spacing (020) - solid line; d-spacing (110) - dashed line.
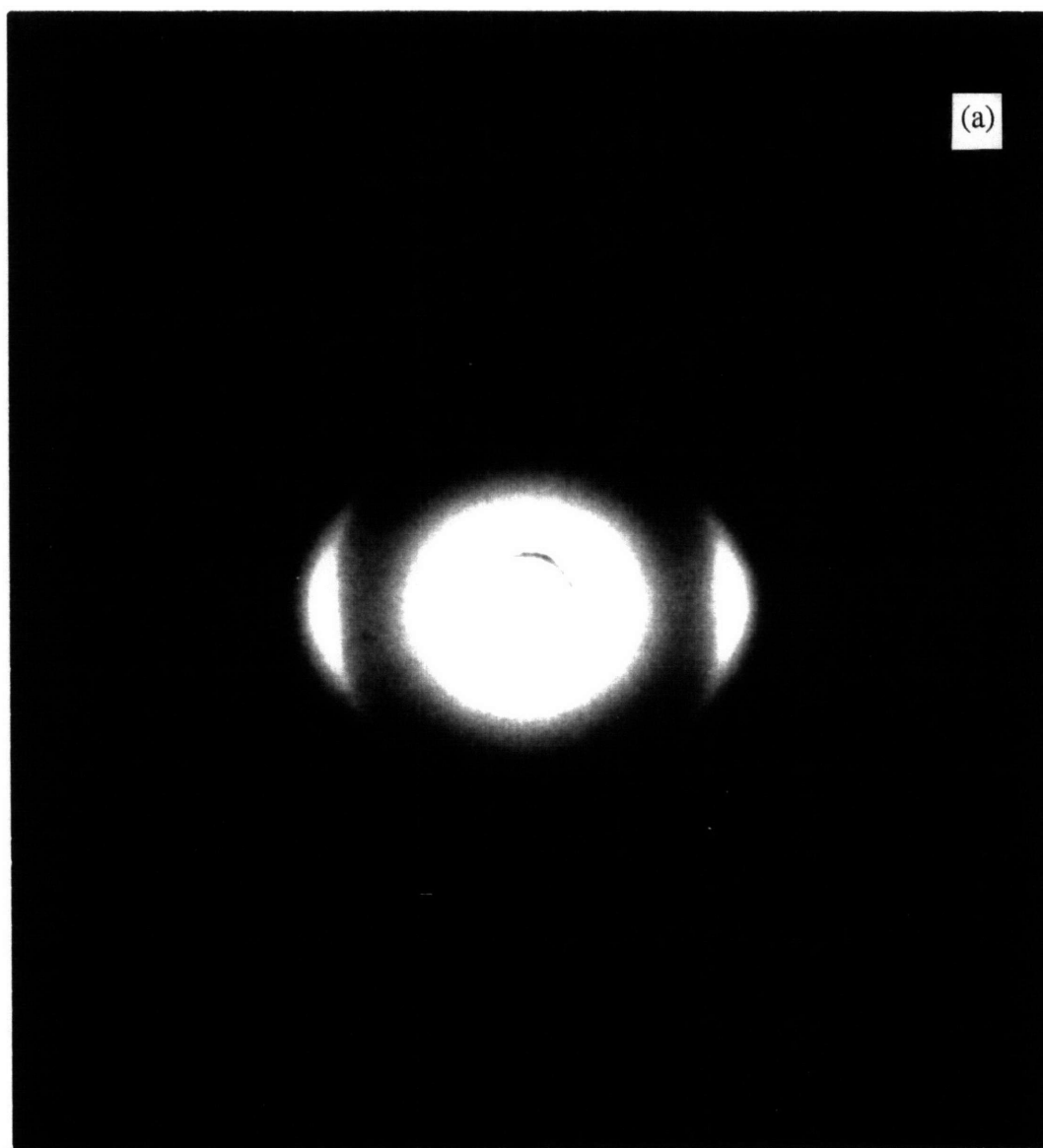
Figure 3.3   Flat film WAXS of hand drawn raw fibers:

(a) HMS-5, (b) HMS-8. Fiber axis is vertical.

(b)
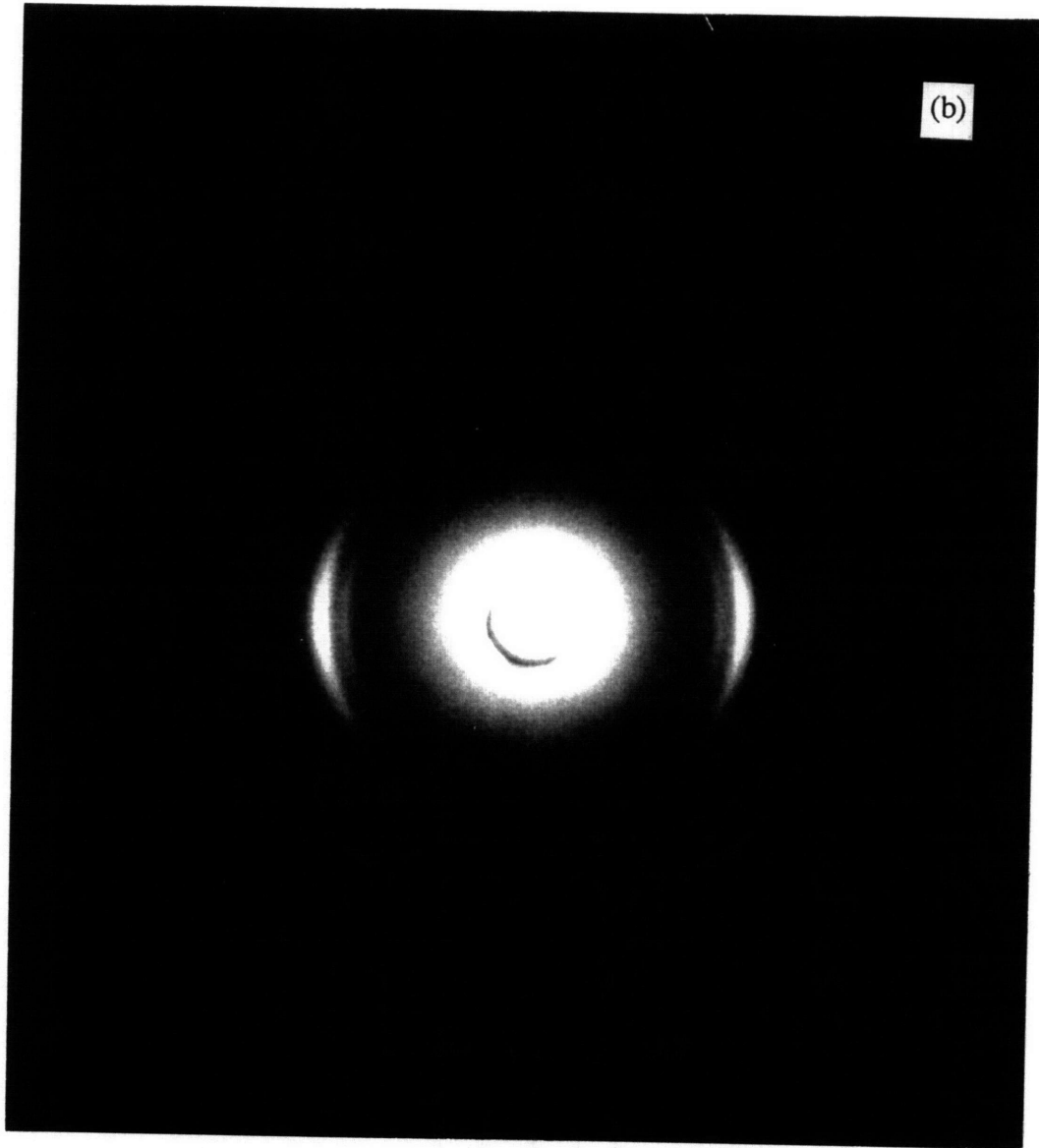
Figure 3.3, Continued

reflections and no meridional reflections. The appearance of two diffuse equatorial maxima in HMS-8 indicates a better interchain registry between the polymer chains in these fibers. For the sake of brevity, HMS-6 and HMS-7 are not shown. HMS-6 raw fiber was similar to HMS-5, and HMS-7 was similar to HMS-8.

WAXS patterns of selected annealed HMS fibers are shown in Figure 3.4 Once the raw fiber is annealed, crystalline reflections are observed though some are too weak to be seen in the reproduction. In Figure 3.4a, HMS-5 annealed fiber WAXS is shown along with a sketch of the reflections in Figure 3.4b. One meridional reflection is seen in annealed HMS-5 along with two equatorial and five quadrantal reflections. In Figure 3.4c, annealed fiber WAXS of HMS-8 is shown, with a sketch in Figure 3.4d. Two equatorial and six quadrantal reflections are identified in HMS-8. There were no meridional reflections in HMS-8. HMS-6 and HMS-7 patterns are not shown. HMS-6 did not form highly oriented fibers upon annealing, though numerous crystalline reflections were seen as broad arcs. HMS-7 annealed fiber pattern is similar to that of HMS-8. The experimental 2θ angles and corresponding d-spacings for HMS-5, 6, 7, and 8 are listed in Table 3.1-3.4, respectively, for the annealed fibers.

In the raw fibers shown in Figure 3.3, there is an absence of three dimensional crystalline order. Two raw fibers, HMS-5 and 6, showed a single equatorial reflection, an indication that the nematic mesophase could be described by a single average interchain separation distance. The other two raw fibers, HMS-7 and 8, displayed two strong equatorial reflections, an indication that for these fibers the nematic mesophase would best be described by two different average interchain separation distances. These probably reflect a higher level of order in the packing for HMS-7 and 8. When the three dimensional crystals form out of the nematic phase, which serves as the template on which crystals will nucleate, the average interchain spacing of the crystals is represented

78
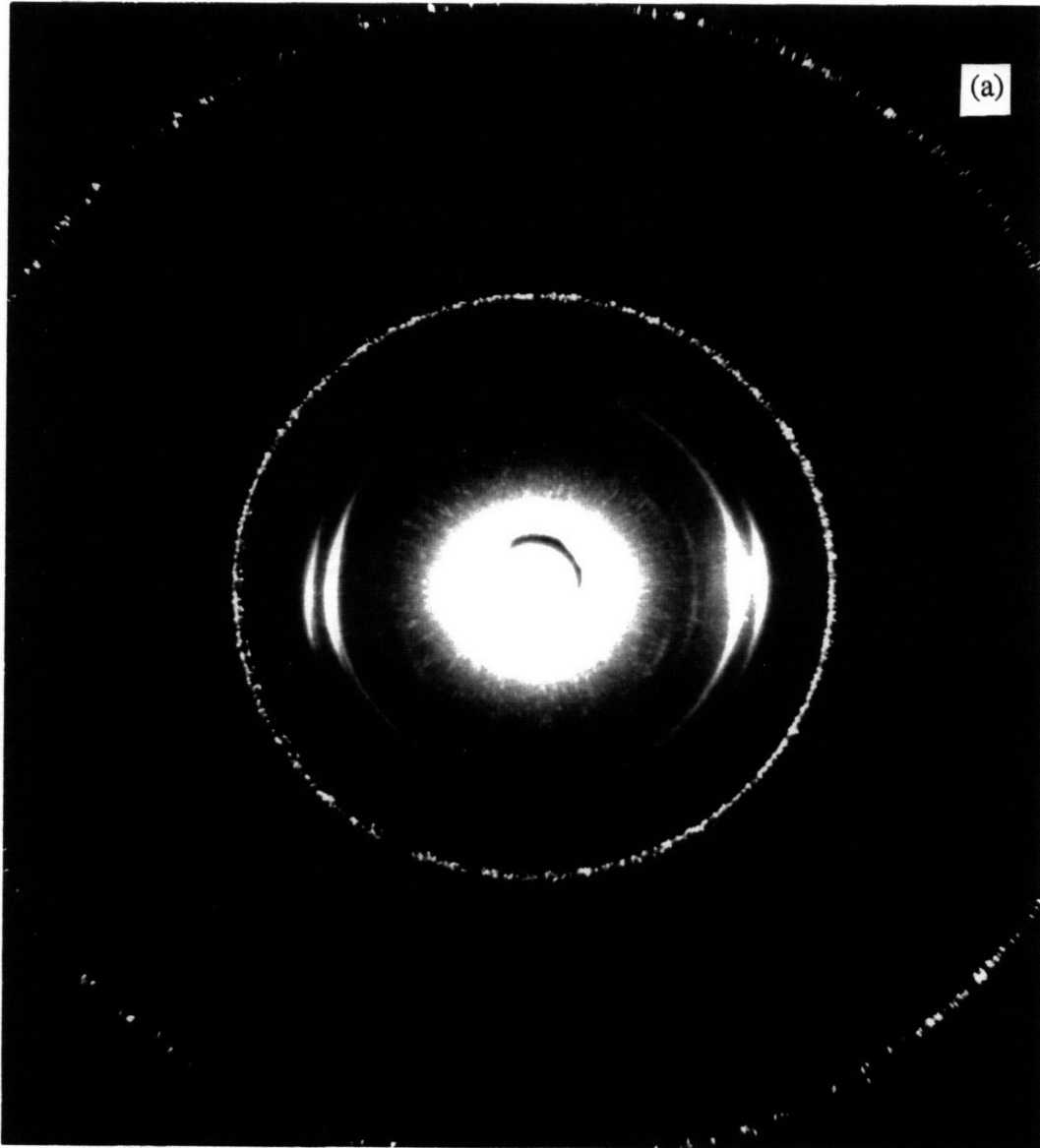
Figure 3.4   WAXS of hand drawn annealed fibers:

(a) HMS-5 experimental pattern, (b) Sketch of HMS-5 pattern,

(c) HMS-8 experimental pattern, (d) Sketch of HMS-8 pattern.

Fiber axis is vertical. Spotty ring is from Si calibration standard.

79

B

Si

(1 2 1)
(0 2 3)
(0 2 2)
(0 2 0)
(1 1 0)
(1 0 1)

(002) (012)

Figure 3.4, Continued

80

Figure 3.4, Continued

D

Si

(130)

(OII)

(10$\bar{1}$)
(110)
(021)
(020)
(101)

(114)

Figure 3.4, Continued

82
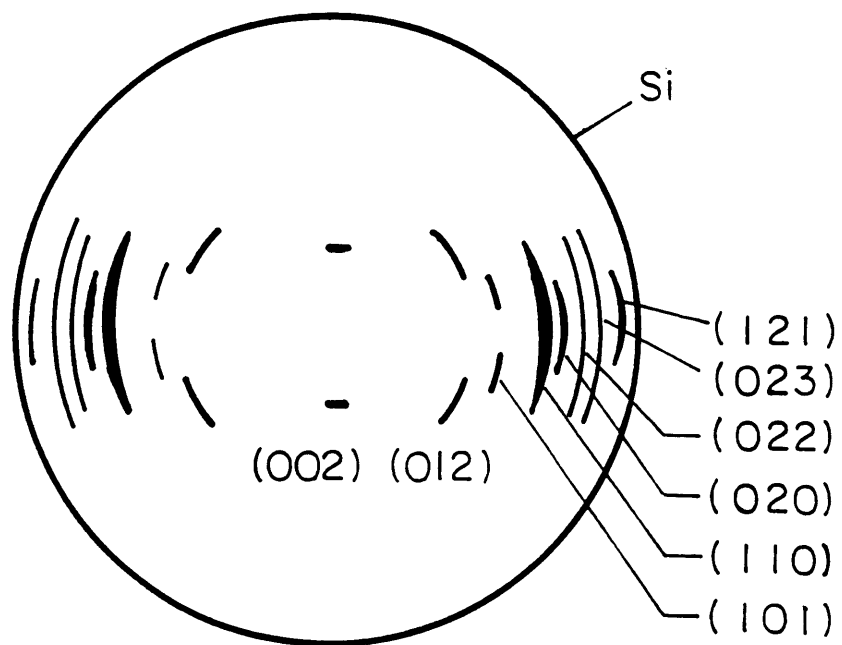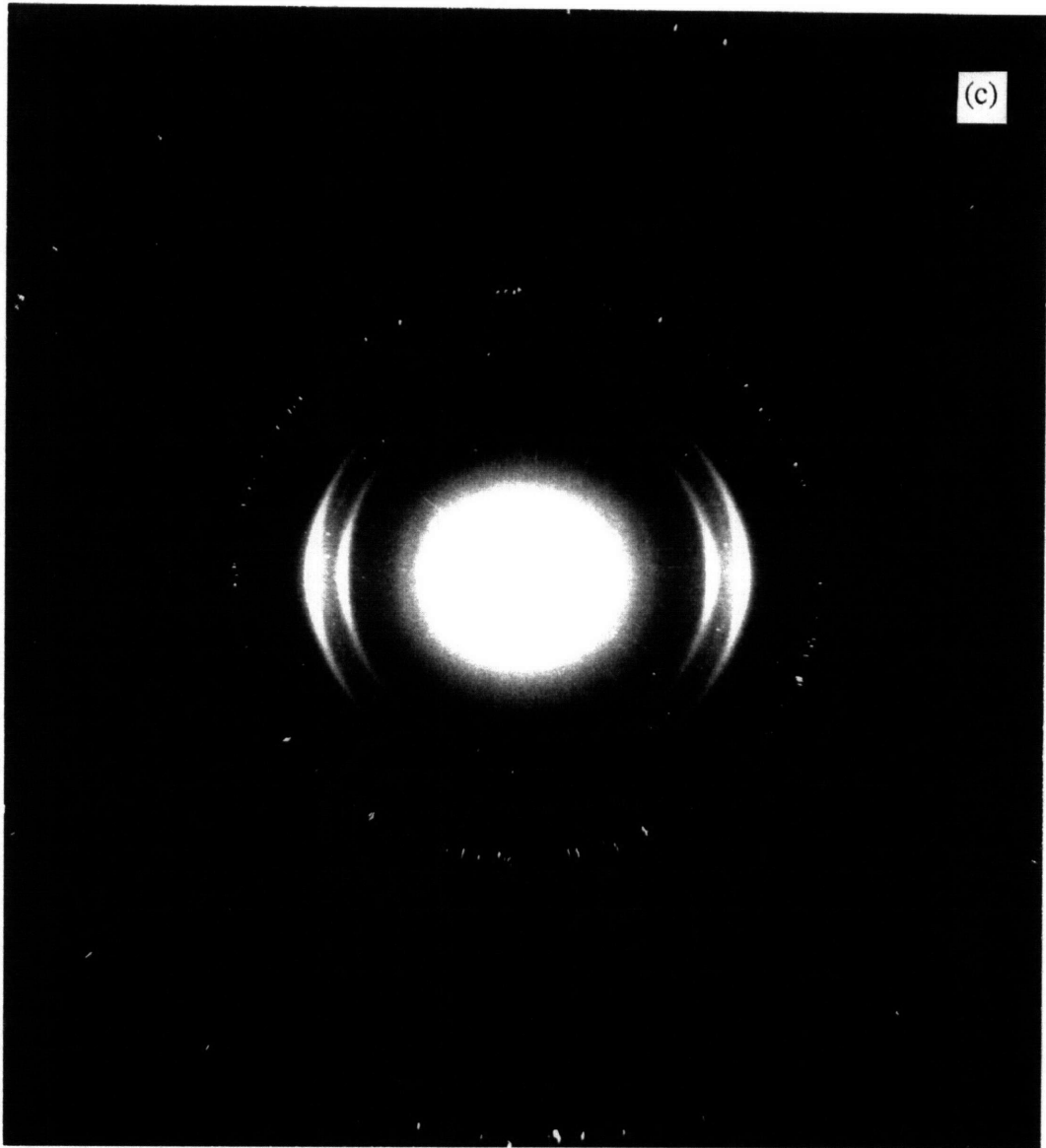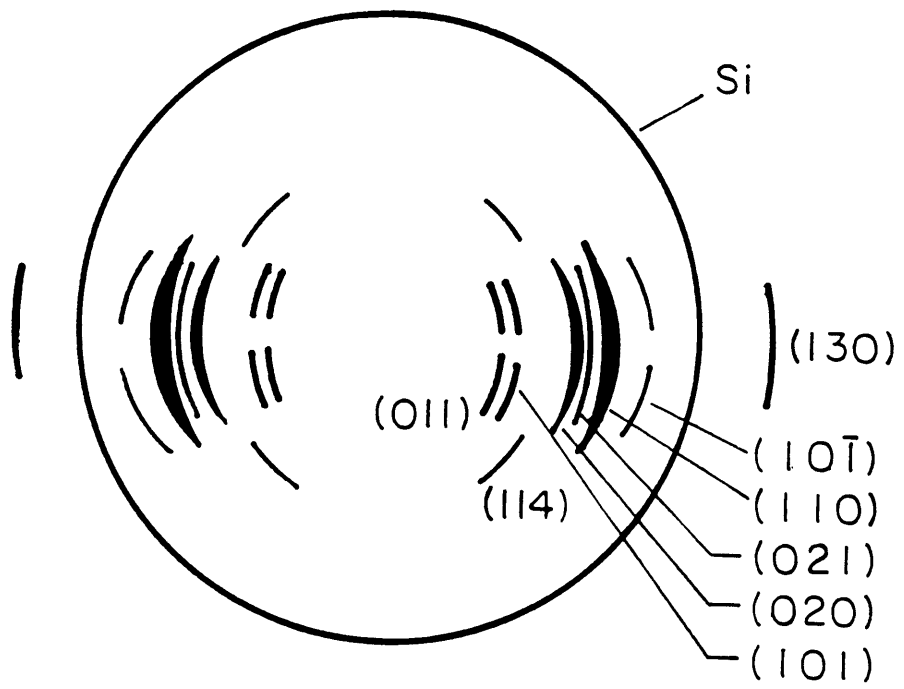
Table 3.1

Experimental and Model Crystallographic Parameters

of a Crystal Unit Cell of HMS-5

Miller Index*	2θ (°)		d-spacing (Å)	
(h k l)	data	model	data	model
(1 0 1)	16.4 (±0.2°)	16.6	5.4 (±0.1Å)	5.4
(1 1 0)	19.9 (±0.2°)	19.8	4.5 (±0.1Å)	4.5
(0 2 0)	22.2 (±0.6°)	22.8	4.0 (±0.1Å)	3.9
(0 0 2)	7.6 (±0.2°)	7.6	11.6 (±0.2Å)	11.7
(0 1 2)	14.3 (±0.6°)	13.7	6.2 (±0.3Å)	6.5
(1 2 1)	27.7 (±0.6°)	28.3	3.2(±0.1Å)	3.2
(0 2 2)	24.6 (±0.5°)	24.1	3.6 (±0.1Å)	3.7
(0 2 3)	25.7 (±0.3°)	25.5	3.5 (±0.1Å)	3.5

* Miller indices are assigned based on orthorhombic structure with lattice parameters given in Table 3.5

Table 3.2

Experimental and Model Crystallographic Parameters

of a Crystal Unit Cell of HMS-6

Miller Index*	2θ (°)		d-spacing (Å)	
(h k l)	data	model	data	model
(1 1 0)	21.3 (±0.3°)	21.2	4.2 (±0.1Å)	4.2
(0 2 0)	19.3 (±0.2°)	19.3	4.6 (±0.1Å)	4.6
(0 1 2)	12.2 (±0.2°)	12.0	7.2 (±0.1Å)	7.3
(0 1 3)	14.9 (±0.4°)	14.5	5.9 (±0.2Å)	6.1
(1 3 1)	35.3 (±0.5°)	34.9	2.5 (±0.1Å)	2.6
(0 1 4)	16.7 (±0.6°)	17.4	5.3 (±0.2Å)	5.1
(1 1 4)	25.8 (±0.3°)	25.8	3.5 (±0.1Å)	3.5
(1 3 4)	38.7 (±0.6°)	38.0	2.3 (±0.1Å)	2.4

* Miller indices are assigned based on orthorhombic structure with lattice
parameters given in Table 3.5

Table 3.3

Experimental and Model Crystallographic Parameters

of a Crystal Unit Cell of HMS-7

Miller Index*	2θ (°)		d-spacing (Å)	
(h k l)	data	model	data	model
(1 0 1)	12.2 (±0.2°)	12.1	7.3 (±0.1Å)	7.3
(1 1 0)	20.0 (±0.3°)	20.2	4.4 (±0.1Å)	4.4
(1 1 1)	16.5 (±0.2°)	16.5	5.4 (±0.1Å)	5.4
(0 2 0)	22.6 (±0.3°)	22.5	3.9 (±0.1Å)	4.0
(1 0 2)	9.5 (±0.2°)	9.5	9.3 (±0.1Å)	9.3
(1 1 2)	14.7 (±0.2°)	14.7	6.0 (±0.1Å)	6.0
(1 2 1)	24.9 (±0.6°)	25.6	3.6 (±0.1Å)	3.5
(0 2 2)	26.0 (±0.4°)	25.7	3.4 (±0.1Å)	3.5
(2 1 6)	24.0 (±0.3°)	23.9	3.7 (±0.1Å)	3.7

*   Miller indices are assigned based on monoclinic structure with lattice
       parameters given in Table 3.5

Table 3.4

Experimental and Model Crystallographic Parameters

of a Crystal Unit Cell of HMS-8

Miller Index*	2θ (°)		d-spacing (Å)	
(h k l)	data	model	data	model
(0 1 1)	11.4 (±0.2°)	11.5	7.8 (±0.2Å)	7.7
(1 0 1)	13.5 (±0.5°)	14.0	6.6 (±0.3Å)	6.3
(1 1 0)	21.9 (±0.4°)	21.5	4.1 (±0.1Å)	4.1
(0 2 0)	19.0 (±0.2°)	19.1	4.7 (±0.1Å)	4.7
(0 2 1)	20.6 (±0.4°)	20.2	4.3 (±0.1Å)	4.4
(1 3 0)	34.8 (±0.3°)	34.8	2.6 (±0.1Å)	2.6
(1 0 -1)	25.0 (±0.3°)	25.2	3.6 (±0.1Å)	3.5
(1 1 4)	16.6 (±0.2°)	16.6	5.3 (±0.1Å)	5.3

*   Miller indices are assigned based on monoclinic structure with lattice parameters given in Table 3.5

by the two strong equatorial reflections which are associated with the (020) and (110) planes.

The interchain spacing of the nematic mesophase seen in the raw fiber WAXS (Figure 3.3) can be compared to the interchain spacings of the crystalline phase seen in the annealed fiber WAXS (Figure 3.4). For HMS-5 (Figure 3.3a) and HMS-6 (not shown) the single equatorial reflection seen in the pattern of the raw, unannealed fiber has a d-spacing which lies in between the d-spacings of the two strongest reflections seen in the annealed fiber powder pattern. The inner spot on the equator of HMS-8 raw fiber pattern (Figure 3.3b), lies on the (020) position of annealed fiber pattern (Figure 3.4b). The outer diffuse spot has a d-spacing which lies in between the d-spacings of the two strongest reflections seen in the powder pattern just as the single equatorial reflection does in the HMS-5 and 6 raw fiber pattern. In contrast, the two spots on the each side of equator in the HMS-7 raw fiber pattern have d-spacings close to the d-spacings of the two strongest reflections seen in the powder pattern. For annealed fibers HMS-8 (Figure 3.4b) and HMS-7 (not shown) the d-spacings of the two strongest equatorial reflections correspond to the two strongest reflections observed in the powder patterns of Figure 3.1.

3.3.3 Molecular Modeling

Molecular modeling and X-ray simulation work was undertaken to determine the unit cell lattice parameters and crystal structure of the HMS polycarbonates that could be obtained as highly oriented fibers. Crystal structure was determined for HMS-5 through 8. We found the experimental c-axis repeat unit was very close to the end to end distance of a fully extended monomer unit. Therefore, an initial structure with a conformation close to all-trans was used to build the unit cell for X-ray diffraction simulation by CERIUS[TM]. By comparing the experimental powder and oriented fiber diffraction patterns with the simulated patterns, we derive the crystal structures for these polymers.

HMS-5 and 6 have an orthorhombic structure with two chains per cell, while HMS-7 and 8 have a monoclinic structure, also with two chains per cell. Figure 3.5a-c contain the a-b, a-c, and b-c projections, respectively, of HMS-5.

Agreement of intensity between the experimental and simulated X-ray diffraction patterns required the crystal unit cells of HMS-5 through 8 to have two polymer chains at (0,0,0) and (1/2,1/2,1/2) positions. Miller indices were assigned using the model lattice parameters. The predicted scattering angle, 2θ, and d-spacings are shown in Tables 3.1-3.4 for HMS-5-8, respectively, for direct comparison with the experimental data. Excellent agreement is obtained between the model and experimental d-spacings. In Table 3.5, we list crystal lattice parameters, a, b, c and angles α, β, γ, for HMS-5 through 8. The last column of the table lists the value of $a\sin\beta$.

The length of the b-axis of the unit cells shows an odd-even alternation for n = 5 to 8. In the orthorhombic system (for HMS-5 and 6) the lengths of the a- and b-axes are an indication of the interchain separation distances for the corner chains of the unit cell. For the monoclinic system (HMS-7 and 8), the quantity $a\sin\beta$ represents the perpendicular distance between the corner chains lying in the a-c plane. An odd-even alternation is observed in $a\sin\beta$ for n = 5 to 8.

In the crystal unit cell, HMS-5-8 have an extended chain structure. In Figure 3.6a-b we show the extended chain structures for monomer units of HMS-5 and 6, respectively. Note that for odd numbered n the two carbonyl oxygens lie on the same side of the monomer chain axis, while for even numbered n they lie on opposite sides of the chain as shown by the arrows. The carbonate linkage, which distinguishes this HMS series from the HMS-polyethers and HMS-polyesters, has important consequences for the unit cell symmetry, chain packing, and mesophase stability. When HMS-polycarbonate
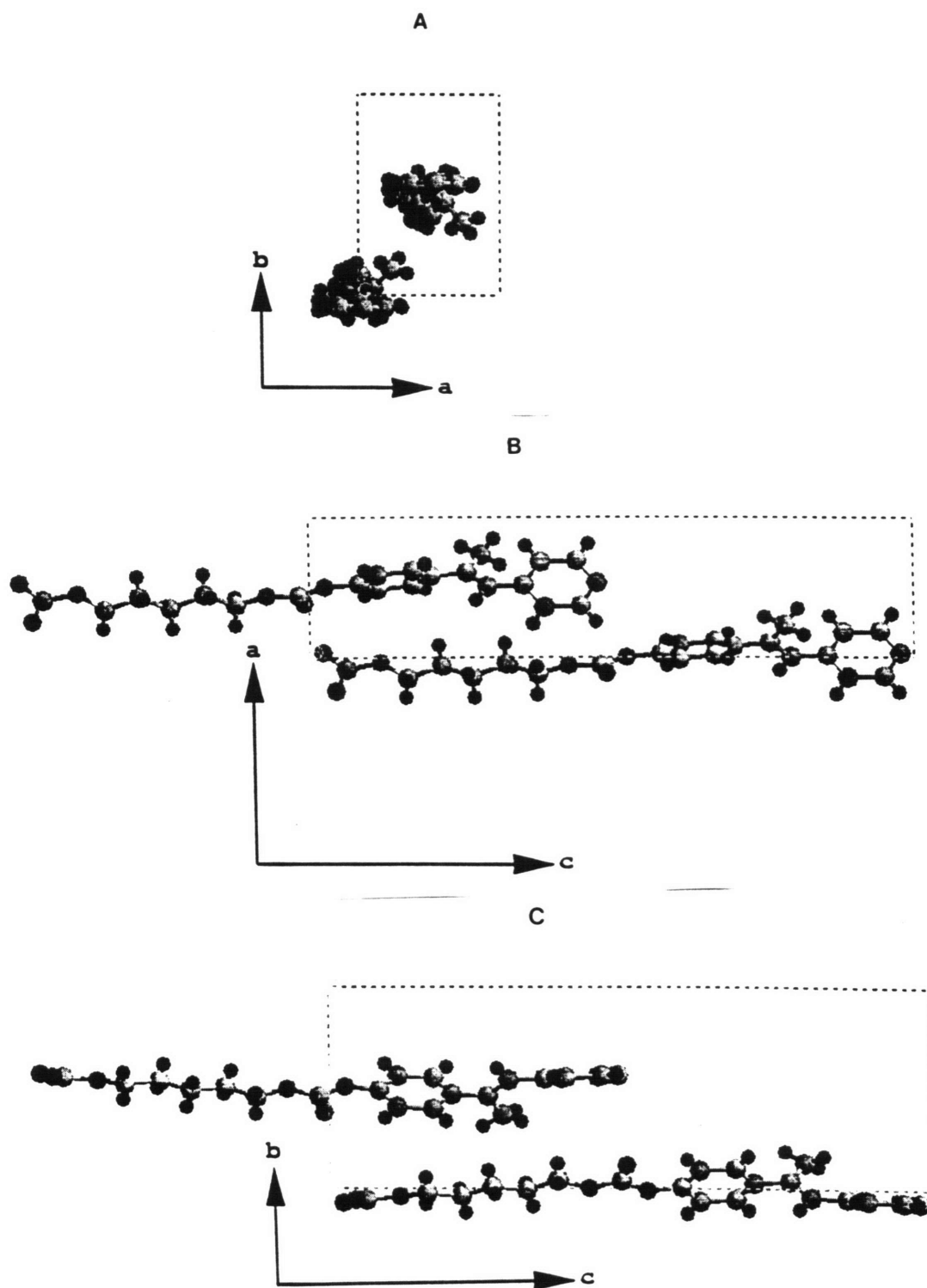
Figure 3.5   Projections of model unit cell of HMS-5.in the:

(a) a-b plane, (b) a-c plane, (c) b-c plane.

Table 3.5

Crystal Lattice Parameters of HMS-5-8

Sample n	a (Å)	b (Å)	c (Å)*	α (°)	β (°)	γ (°)	a sin β
5	5.5	7.8	23.4	90.0	90.0	90.0	5.5
6	4.7	9.2	24.4	90.0	90.0	90.0	4.7
7	9.4	7.9	25.6	90.0	34.3	90.0	5.3
8	9.1	9.3	26.8	90.0	30.4	90.0	4.6

* determined from model structure
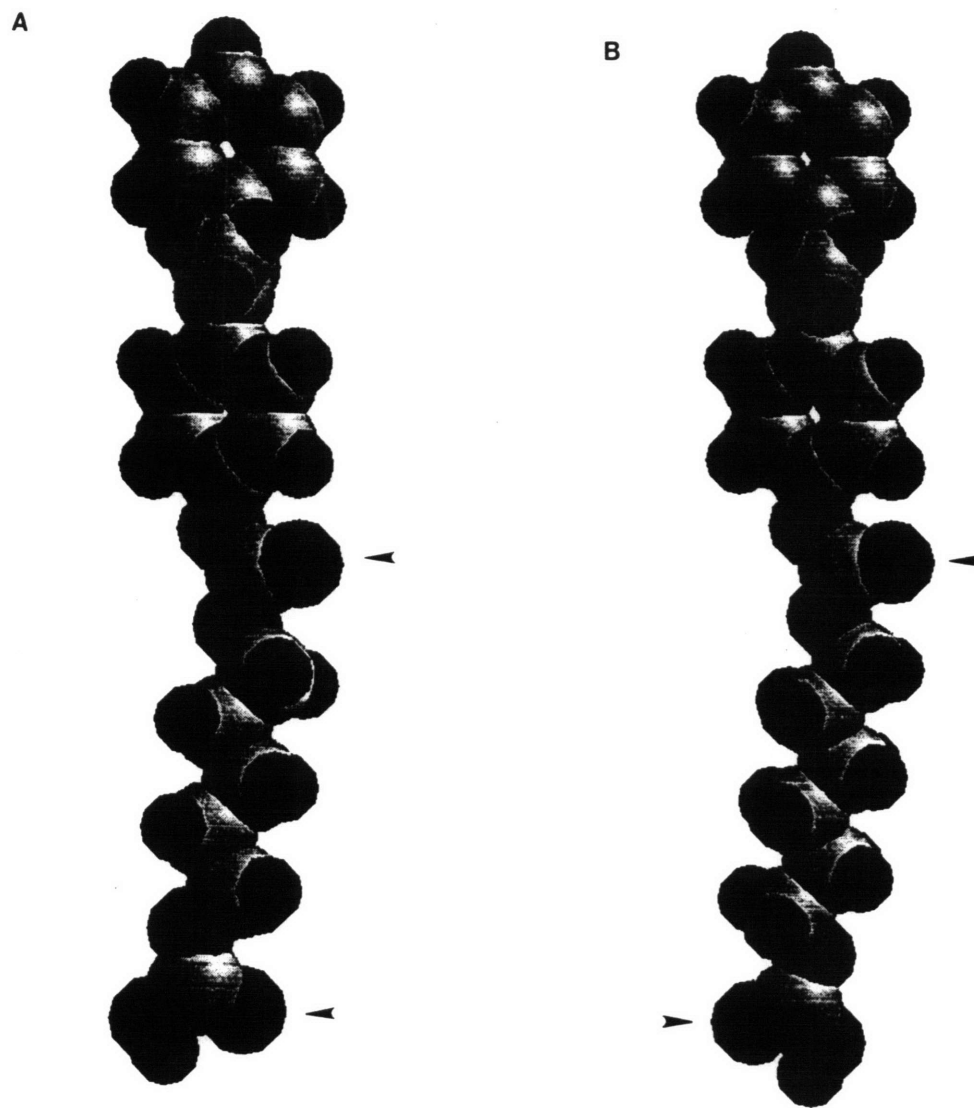
Figure 3.6   Model repeat unit structures for HMS-n: (a) HMS-5, (b) HMS-6.

monomers pack into the crystalline unit cell, the crystal symmetry is such that the center chain occupies a position shifted along the molecular chain axis, relative to the position of the corner chain. This causes HMS-5 to 8 have an *intermeshed* structure, which is similar to that observed in other main chain LCPs [71,72]. In Figure 3.7 the corner and center chains of the unit cell of HMS-7 are shown in a projection along the b-c plane. As seen in Figure 3.7, in the intermeshed crystal unit cell, the center and corner chain stilbene mesogens are intermeshed with the flexible spacer group. The stilbene mesogen of one chain is adjacent to the flexible spacer group of the neighboring chain.

3.4   DISCUSSION

A stable intermeshed structure can exist if the length of the flexible spacer is not too large compared with the length of the mesogen, as suggested by Unger and Keller [70]. The methyl stilbene mesogen has a unit length of about 11.6 Å. We can categorize the HMS-polycarbonates into three groups according to the relative lengths of the mesogen and the other portions of the chain. First, HMS-4 has a length of flexible spacer and linking groups of 10.8 Å that is quite short compared to the methyl stilbene mesogen. DSC studies show that while HMS-4 forms a nematic mesophase, the short flexible spacer group causes very slow crystallization kinetics [99]. Very poor crystals form over a wide temperature range from the melt, leading to very low ultimate degree of crystallinity. In the second group, HMS-9, 10, and 12 have flexible spacer lengths ranging from 12.6 Å to 16.5 Å, which are all very long compared to the methyl stilbene mesogen. As shown in Figure 3.2, the interchain d-spacings level off when $n \geq 9$. Furthermore, for $n \geq 9$ no large spherulites were seen with polarized optical microscopy and transition temperatures observed in DSC cooling and heating scans drop sharply [6]. These facts suggest that crystal size and perfection are reduced for HMS-9, 10 and 12. Here the flexibility of the chain leads to rapid crystallization kinetics and relatively less

92
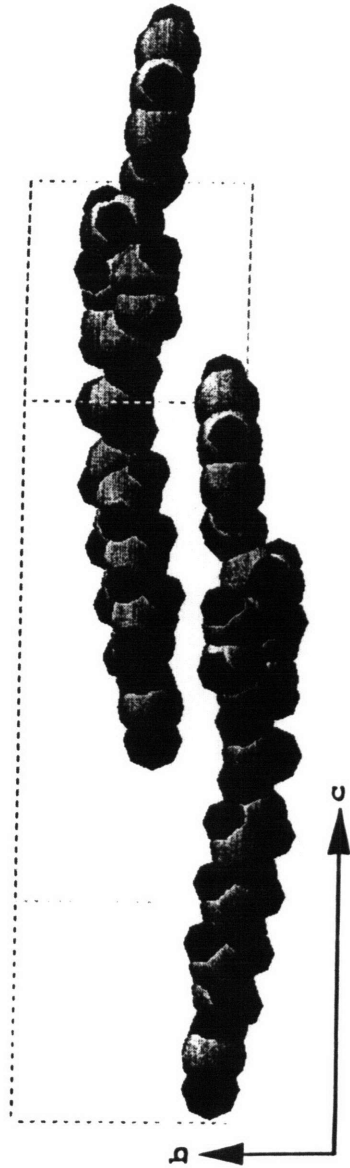
Figure 3.7   Disposition of the corner and center chains of the unit cell, viewed in projection in the b-c plane for HMS-7.

perfect crystals. However, the intermeshed structure is not stable in these members of the series. The flexible spacer is too long to allow proper overlap of the carbonates on adjacent chains.

Finally, in the third group are the series members HMS-5 through 8 in which the length of the mesogen is close to the length of the other groups, leading to a favorable overlap of the adjacent carbonates. HMS-8 has a stable intermeshed crystal structure, because the extended $-(CH_2)_8-$ length is about 11.3 Å which is close to the methyl stilbene mesogen. At the short end of this grouping, the extended $-(CH_2)_5-$ length is only about 7.4 Å yet a stable intermeshed structure is still observed. The carbonate linking group plays an important role in determining whether or not a stable intermeshed structure can be formed. In the HMS-5 member of the series, the carbonate-pentane-carbonate length is about 11.8Å, which matches the mesogen length quite well.

The carbonyl oxygen in the carbonate linkage is of partial negative charge while the remaining atoms in the carbonate linkage are of partial positive charge. This leads to a dipole moment transverse to the molecular chain axis at the position of the carbonate group. As shown in Figure 3.6, in HMS-5 and 7, consecutive carbonate dipoles on the chain point in nearly the same direction while in HMS-6 and 8 consecutive dipoles point in nearly opposite directions. This affects the way in which the corner and center chains are positioned relative to one another, and creates an odd-even effect in the packing of the cell. In HMS-5 and 7, the center and corner chains have dipole moments aligned, and pointing along [010]. In HMS-6 and 8, the dipole moments on adjacent carbonate units between chains can have a more favorable interaction when the center chain rotates relative to the corner chain. This rotation is demonstrated in Figure 3.8 where we show a view of the unit cells of HMS-7 and 8 for comparison, projected along the c-axis. The rotation of the adjacent chains of HMS-6 and 8, causes the length of the b-axis of the unit

cell to increase, and the quantity asinβ to decrease, compared with HMS-5 and 7.

HMS-7 and 8 have a higher degree of overlap of the carbonate linkage between adjacent polymer chains than is found in HMS-5 and 6. This is caused by the very close match between the length of the mesogen and the length of the flexible spacer. We suggest this is the reason why HMS-7 and 8 have a less stable mesophase than HMS-5 and 6. As seen in the differential scanning calorimetry cooling studies [99], the temperature stability range of the mesophase decreases from HMS-5 to 8. More over, as mentioned above, only a diffuse maximum is seen in the raw fiber pattern of HMS-5 and 6, which suggest that in the mesophase of these LCPs, the polymers chains arrange themselves randomly in two dimensions. The diffuse maximum represents the average distance between chains in the nematic mesophase. However, both HMS-7 and 8 show two spots on each side of the equator in the raw fiber pattern, which is evidence that in the mesophase of these two, there already exists a more regular arrangement of polymer chains in two dimensions. This would lead to faster crystallization from the mesophase, and therefore, a mesophase of reduced stability.

Although we clearly observe an odd-even effect in the crystal unit cell parameters, there is no obvious odd-even effect observed in the melting transitions, as shown in Chapter 2. This is probably because the broad melting endotherms from different crystal populations obscure this effect.
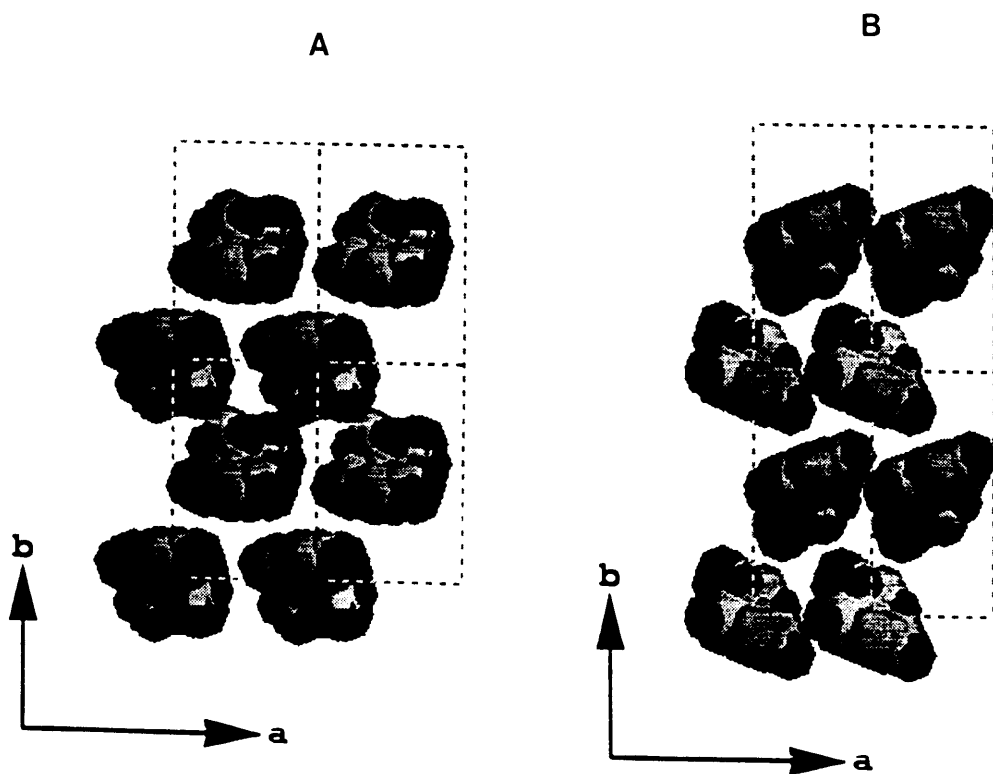
Figure 3.8   (a) HMS-7, and (b) HMS-8, projection view along the c-axis.

3.5. CONCLUSIONS

HMS polycarbonates with 5 to 8 methylene flexible spacer units have a stable intermeshed crystal structure. Within this structure, the disposition of the carbonate group differs from n-even to n-odd and causes the odd-even effect of the crystal unit cell parameters, b and asinβ. Furthermore, the higher degree of overlap of the carbonate linkage of HMS-7 and 8 than HMS-5 and 6 between adjacent polymer chains may be the reason why HMS-7 and 8 have less stable mesophase than HMS-5 and 6.

Chapter 4

Structure Development in HMS Polycarbonates
by Small Angle X-ray Scattering (SAXS)

4.1 INTRODUCTION

The monotropic liquid crystalline phase is not thermodynamically stable when compared either to the crystalline phase or to the isotropic phase at any temperature [12]. Therefore, the monotropic liquid crystalline phase can be only observed in cooling provided that the crystallization process is suppressed during cooling. Monotropic liquid crystalline behavior has been recently characterized for several main chain thermotropic LCPs [69,73-80]. It is worthwhile to reflect why our α-methyl stilbene polycarbonates are unable to form an enantiotropic liquid crystalline phase, whereas α-methyl stilbene polyethers and polyesters do form such phases. As suggested in Chapter 2 [90,99], the reason could be two fold. First, the flexibility of the carbonate linkage might cause the liquid crystalline phase to be thermodynamically less stable compared with the crystalline phase and the isotropic phase. Second, the carbonate linkage can cause fast crystallization resulting from improved intermolecular interaction.

The structure of the resulting crystals depends on the flexible spacer number, n. Both the stability of phases and the crystal unit cell packing depend upon n. As mentioned in Chapter 3, we found the methylene spacer length can affect the stability of the liquid crystalline phase and crystalline phase. The stability of the liquid crystalline phase relative to the crystalline phase decreases as the methylene spacer length gets close to that of the mesogen, from n = 5 to 8. When the length of the spacer becomes greater than that of the mesogen (n $\geq$ 9), all the transition temperatures drop. Formation of the crystalline phase is highly related to the existence of the liquid crystalline phase, which

serves as crystal nuclei or as a template for crystallization. The amount of seed nuclei decreases as temperature increases and as a result the crystallization rate slows down and the ultimate crystallinity is reduced.

It is also mentioned in Chapter 3 that an odd-even oscillation has been observed for HMS-5 to 8 in the two crystalline unit cell lattice parameters which determine the interchain distance. This phenomenon is caused by the disposition of the carbonate group which is different from n-even to n-odd in the crystalline phase [90]. In this Chapter, we report on the use of real-time synchrotron small angle X-ray scattering (SAXS) to study the development of crystal structure in HMS polycarbonates. An interesting odd-even effect is observed in lamellar thickness and linear crystallinity.

Real-time synchrotron SAXS has been widely used to investigate fast structure changes of homopolymers [100-113] and polymer blends [114-118]. For example, research on time resolved crystal structure and morphology development using synchrotron SAXS have been done for polyethylene (PE) [100-102], poly(ethylene terephthalate) (PET) [103,104], poly(aryl ether ether ketone) (PEEK) [105-107], poly(butylene terephthalate) (PBT) [108], poly(phenylene sulfide) (PPS) [109], thermoplastic polyimide (New-TPI) [110-111], and thermotropic polyethers based on semiflexible mesogen [74].

4.2 EXPERIMENTAL SECTION

The X12B beam line at Brookhaven National Synchrotron Light Source (NSLS) was used to obtain small angle X-ray scattering data in transmission mode. For high temperature work, a Mettler hot stage was supported in the X-ray beam path by an aluminum holder, and the beam passed through the sample, which was sealed between

two pieces of Kapton^{TM} tape. A two-dimensional histogramming gas-filled wire detector was used. All samples studied here were isotropic, so circular integration of the intensity was used to enhance the signal to noise ratio. The beam profile was treated according to pinhole geometry. The sample to detector distance was either 1.85 m or 1.46 m, and was calibrated by cholesterol meristate and collogen fiber. X-ray wavelength was either 1.53Å or 1.49Å.

SAXS scans at room temperature were taken for HMS-4 through 10 and 12, which were non-isothermally crystallized by cooling at -5°C/min from the melt to room temperature. Real-time SAXS data were taken during cooling at -5°C/min for HMS-5 and 6, and during heating at 5°C/min for crystallized HMS-5 to 9. Real-time studies were also done during isothermal crystallization. HMS-5 to 8 samples were melted at 190°C for 2.5-3 minutes, then cooled at -20°C/min to 140°C and held there until crystallization was finished. Crystallization times had been determined in our prior study [99]. Data were collected during cooling from 170-140°C and during the whole isothermal crystallization process. The data collection time was 120 seconds for static experiments, and 30 seconds for cooling and heating experiments, and 10 seconds for isothermal crystallization experiments.

SAXS intensity was corrected for background, sample adsorption, variation of incident beam intensity and thermal density fluctuations. The slope of Is^4 versus s^4 plot (where s is the scattering vector, $s = 2 \sin\theta/\lambda$) was used to get the diffraction intensity contribution from thermal density fluctuations [119,120]. The corrected intensity is used for quantitative analysis.

4.3 RESULTS AND DISCUSSION

4.3.1 Room Temperature SAXS

We show in Figure 4.1 the Lorentz corrected SAXS intensity, Is^2, versus s at room temperature for HMS-5 which had been cooled at $-5°C/min$ from the melt to room temperature. A well developed intensity maximum occurs at about s=0.005. For s less than about 0.005, intensity drops steadily until s is about 0.0025. The beam stop obscures real intensity data for s less than about 0.0025. We assume that HMS polycarbonates have a lamellar structure in which stacks of lamellae alternate with amorphous material. This assumption is reasonable considering that spherulites have been observed by both optical microscopy and transmission electron microscopy [99]. To obtain parameters characterizing the lamellar stacks, we use the one-dimensional electron density correlation function, $K(z)$, derived by discrete Fourier transform of the Lorentz corrected intensity. z is a dimension along the normal to the lamellar stacks. The intensity here is the corrected intensity obtained after the background and thermal density fluctuation corrections. The intensity versus s data then were linearly extrapolated to s = 0. Also, Porod's law, $I(s) \sim s^{-4}$ was employed to extrapolate the intensity data to high s. The resulting correlation function starts off with a z-spacing of 1/(maximum s value), but a spline interpolation fills in the missing values in the regime of interest.

In Figure 4.2a, we show a general plot of $K(z)$ vs. z, and in Figure 4.2b $K(z)$ versus z for HMS-5. The parameters characterizing the lamellar stacks are the long period, L, lamellar thickness, l_c, and linear crystallinity, χ_c. These are obtained according to the method proposed by Strobl and Schneider [121]. The average long period, L, is the z value where the first maximum in $K(z)$ occurs for z > 0. The invariant, Q, is related to the linear crystallinity, χ_c, and the electron densities of the crystal and amorphous phases, ρ_c and ρ_a, respectively, according to:
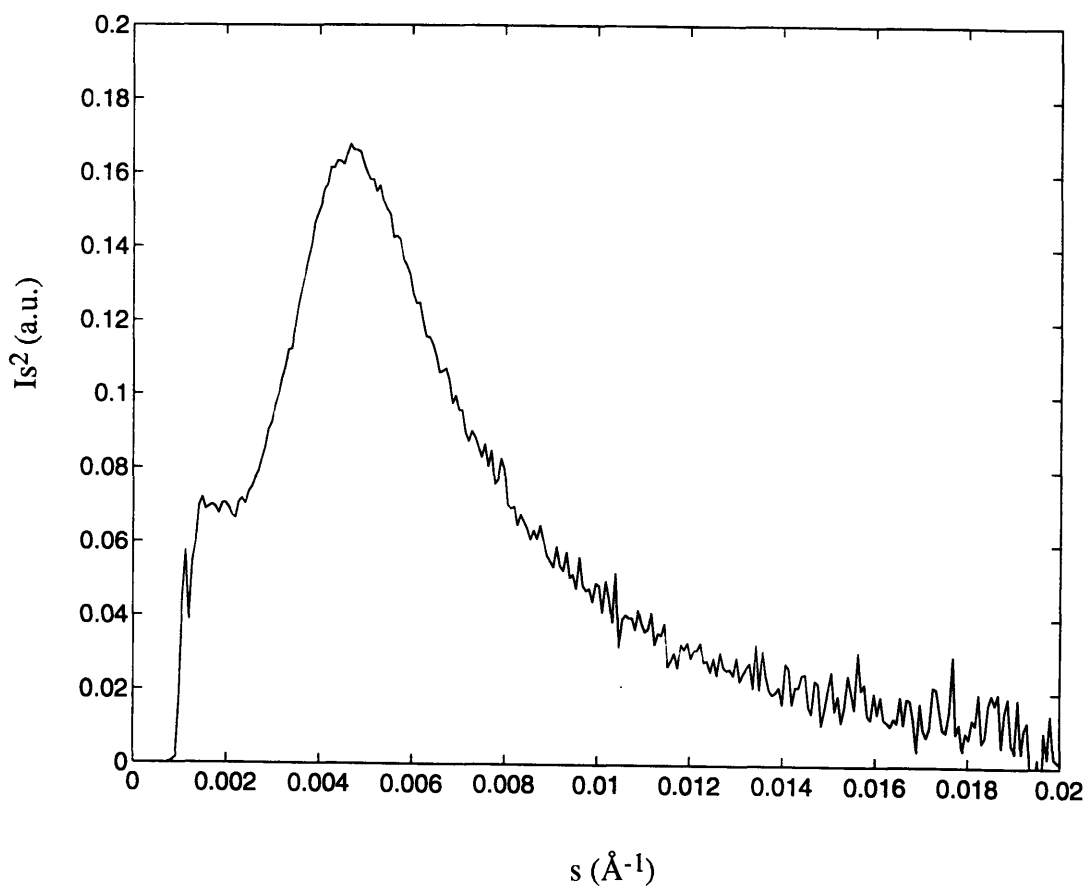
Figure 4.1   Lorentz corrected SAXS intensity vs. scattering vector s at room

temperature for HMS-5 cooled at -5°C/min from the melt.
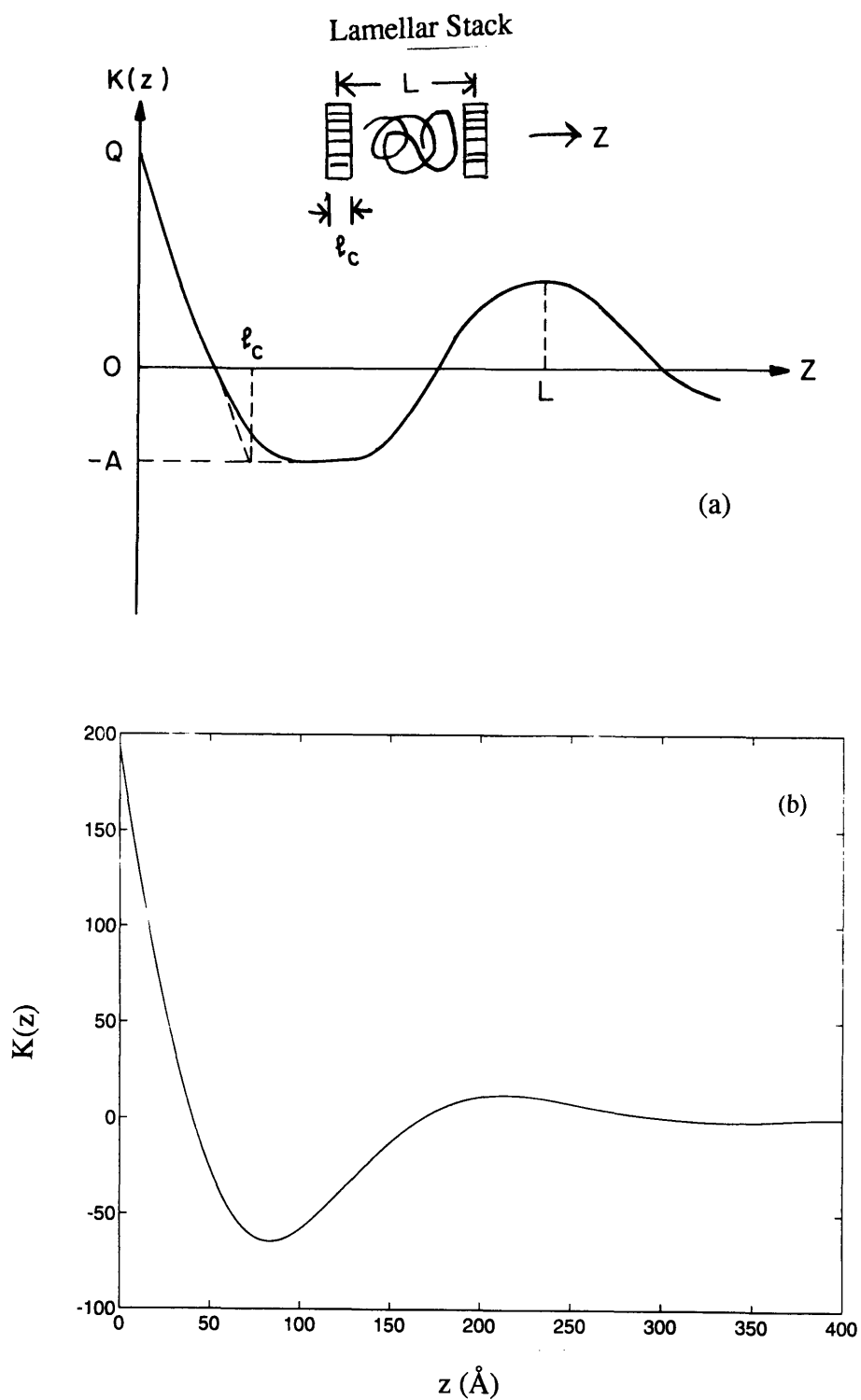
Figure 4.2   One-dimensional electron density correlation function, K(z) vs. z:

(a) schematic plot, (b) HMS-5 at room temperature.

$$Q = \chi_c (1 - \chi_c) (\rho_c - \rho_a)^2. \tag{1}$$

As shown in Figure 4.2a, Q is found from the intercept of extrapolation of the K(z) vs. z curve at small z value to z=0. The coordinate of the horizontal line tangent to the first minimum of K(z) vs. z is -A, where A is related to linear crystallinity and density by:

$$A = \chi_c^2 (\rho_c - \rho_a)^2. \tag{2}$$

Using equations (1) and (2), the linear crystallinity is found from:

$$A/(A+Q). \tag{3}$$

The definitions of L, l_c, Q and A are illustrated in Figure 4.2a. In Figure 4.2b, K(z) is shown for HMS-5.

In Table 4.1, we list long period, linear crystallinity and lamellar thickness at room temperature for HMS-4-10 and 12 crystallized by cooling at 5°C/min from the melt to room temperature. Lamellar thickness and linear crystallinity show an odd-even effect from HMS 4-10, as shown in Figure 4.3a, b, which has never been found before. In both parameters, the value at n=9 is quite large, more than 20% greater than the values of the odd members of the series for n<9. The variations in l_c and χ_c are well outside the error bars on the measurements which are shown by the vertical markers.

4.3.2 Real-time SAXS during Cooling and Heating

Figure 4.4 shows differential scanning calorimetry (DSC) cooling scans of HMS-5 and 6 for the purpose of comparison with SAXS data taken at the same cooling rate. The curves are vertically offset for clarity, but are drawn to the same vertical scale. The scale is shown by the vertical marker indicating heat flow of 50 mW/g. The cooling scan

104

Table 4.1

Long Period, Linear Crystallinity and Lamellar Thickness for Crystallized HMS-4-10 and 12 Cooled at 5°C/min from Melt to Room Temperature

Sample n	L(Å) (±5Å)	X_c (±0.01)	l_c(Å) (±2Å)
4	270	0.18	34
5	214	0.26	44
6	215	0.21	33
7	234	0.25	46
8	230	0.18	29
9	175	0.32	54
10	197	0.26	47
12	194	0.25	49
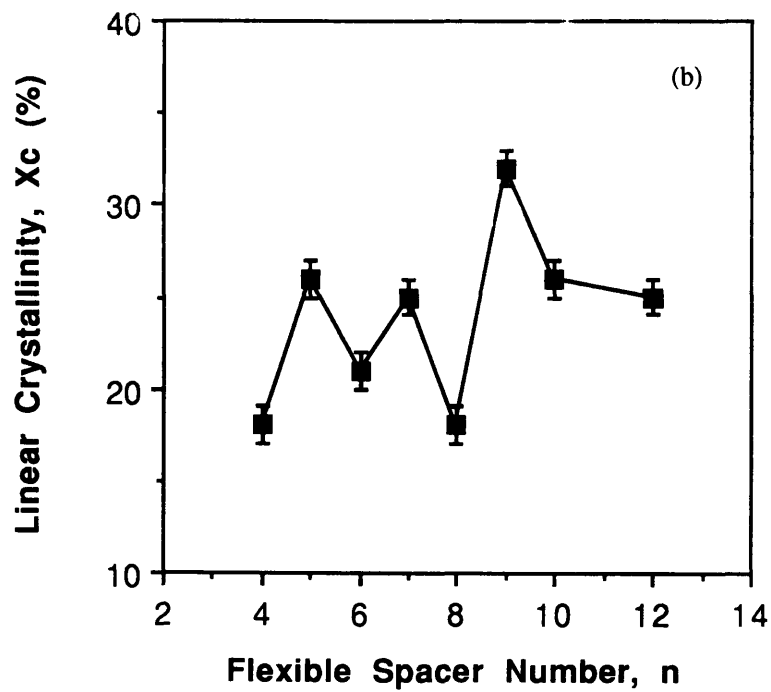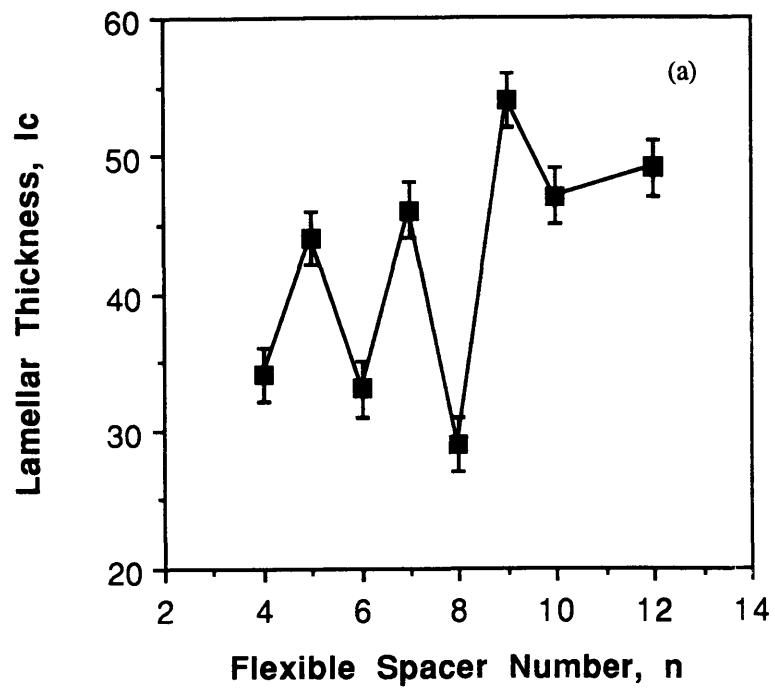
Figure 4.3   (a) Lamellar thickness and (b) linear crystallinity vs. n.
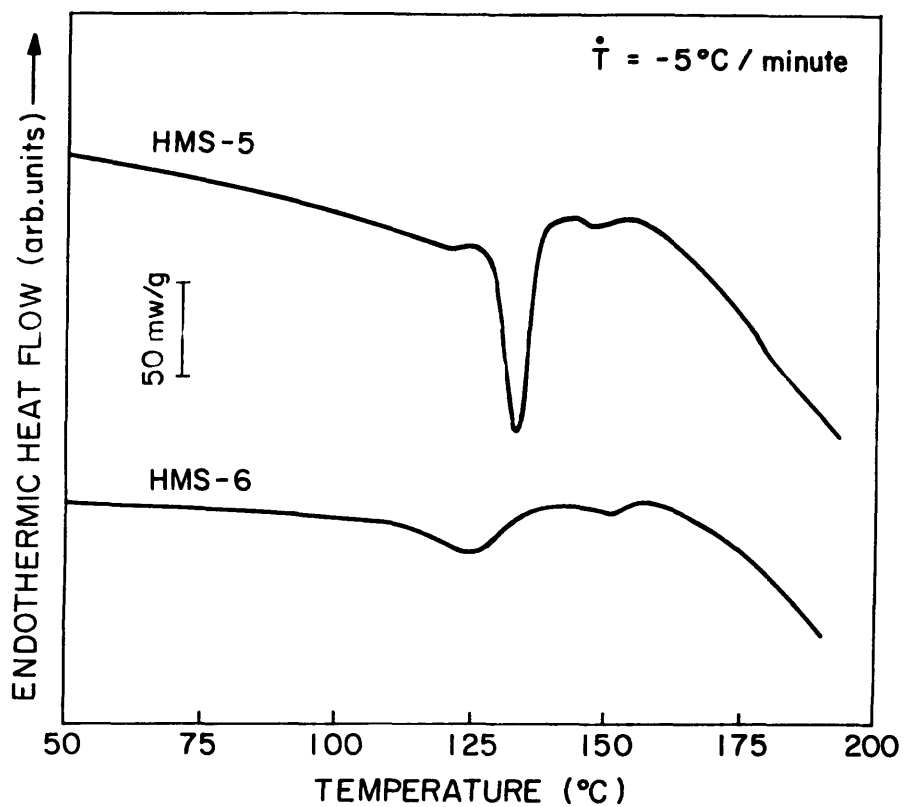
Figure 4.4   DSC thermograms of HMS-5 and 6 at 5°C/min cooling rate.

of HMS-5 shows a small exothermic transition at 155°C ($T_{i\text{-}lc}$) and a much larger, and sharper, crystallization exothermic peak at 132°C ($T_{lc\text{-}k}$). The area under the crystallization peak is 6.9 J/gram. HMS-6, in comparison, shows a broad small exothermic transition at 155°C ($T_{lc\text{-}k}$) and a broad crystallization peak at 127°C ($T_{lc\text{-}k}$). The crystallization exotherm area for HMS-6 is 3.4 J/gram, considerably smaller than that of HMS-5. These two LCPs have their thermal transitions, i-lc and lc-k, at about the same temperatures during cooling from the melt. Their heats of crystallization are, however, very different. Since the heat of fusion of the perfect crystal is unknown for these polymers, we can not determine the degree of crystallinity of HMS-5 compared to HMS-6. To gain further insight into the crystallization process, we use real-time SAXS to determine the development of crystal structure during cooling.

In Figure 4.5a, we show the Lorentz corrected intensity versus s data at selected temperatures during the cooling scan for HMS-5. As the temperature drops from 170°C to 115°C, the intensity increases. For temperatures greater than 135°C, any peak in the intensity (if one exists) is hidden by the beam stop. Only a very strong shoulder appears and grows up as temperature drops from 170°C to 135°C. At 135°C, the intensity peak finally emerges and continues to shift to higher s value as the temperature drops. Intensity reaches a maximum at about 115°C, then as temperature decreases below 115°C, the intensity in the peak drops during the later stages of crystallization. Figure 4.5b shows K(z) versus z at several temperatures at which a clear maximum in intensity was observed. As temperature decreases, the long period (L) shifts to lower values.

Figures 4.6a-c show long period (L), lamellar thickness (l_c), and linear crystallinity (χ_c), respectively, for HMS-5 (circles) and 6 (stars) during cooling for all measurement temperatures less than 140°C. From 170°C to 140°C, no long range periodic order can be seen (no clear peak appears in Is^2 vs. s) so the correlation function
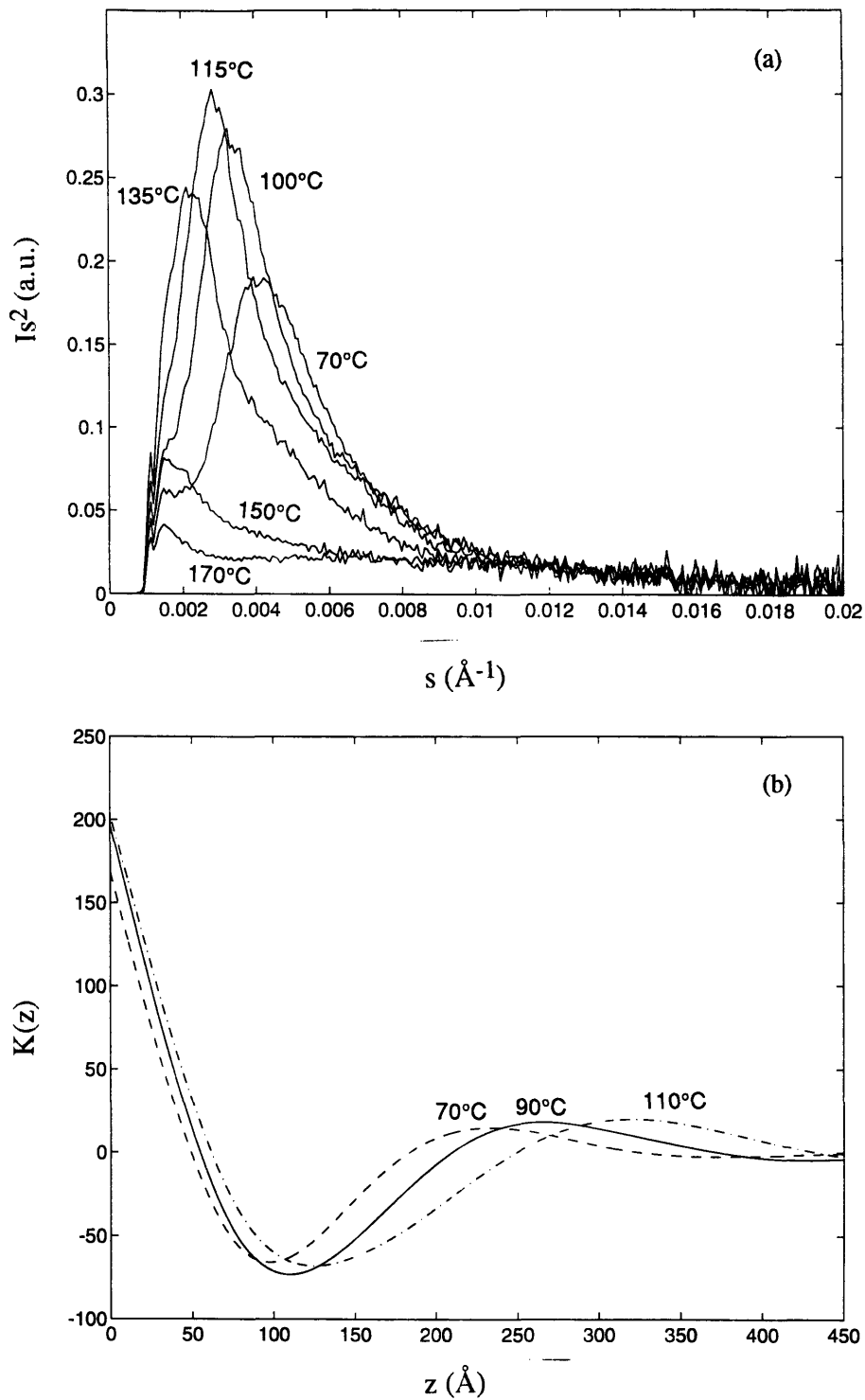
Figure 4.5   (a) Lorentz corrected SAXS intensity vs. s for HMS-5 during cooling

at -5°C/min from the melt. (b) One-dimensional electron density

correlation function for HMS-5 at several temperatures.
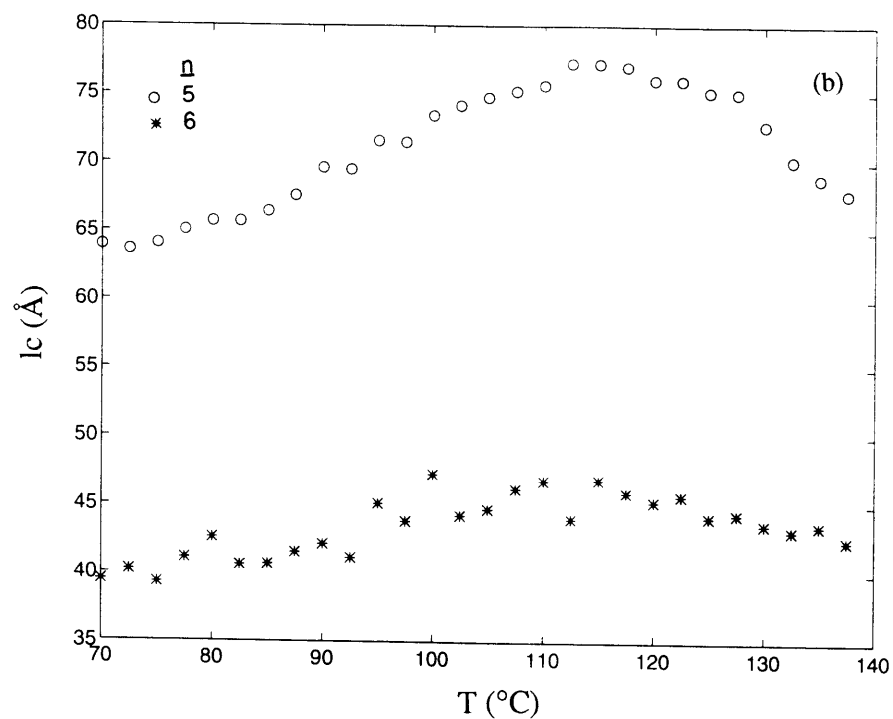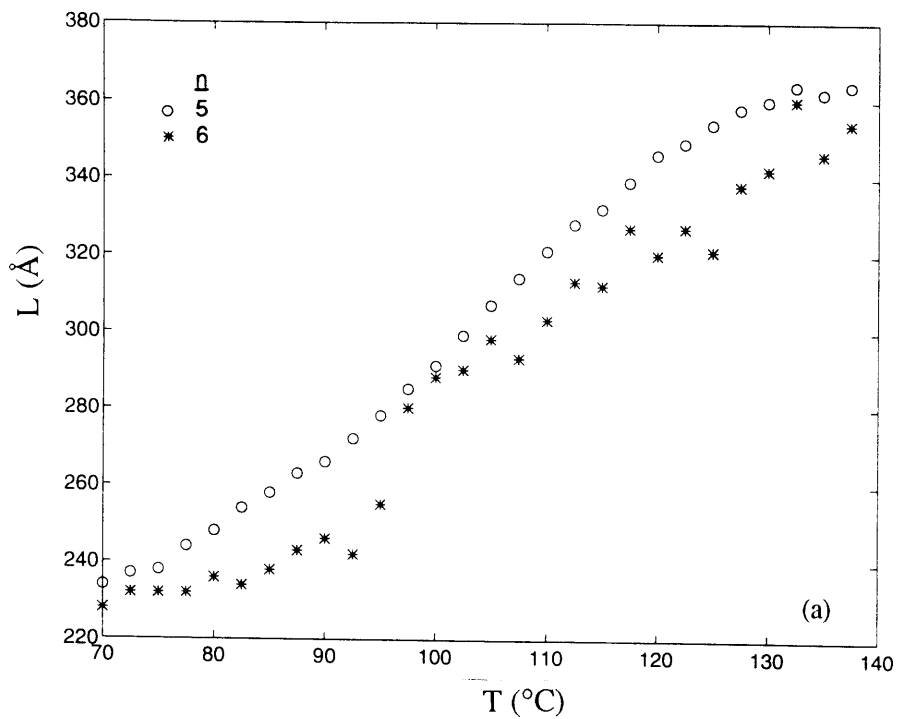
Figure 4.6   (a) Long period, (b) lamellar thickness, and (c) linear crystallinity

vs. temperature for HMS-5 and 6 during cooling at -5°C/min.
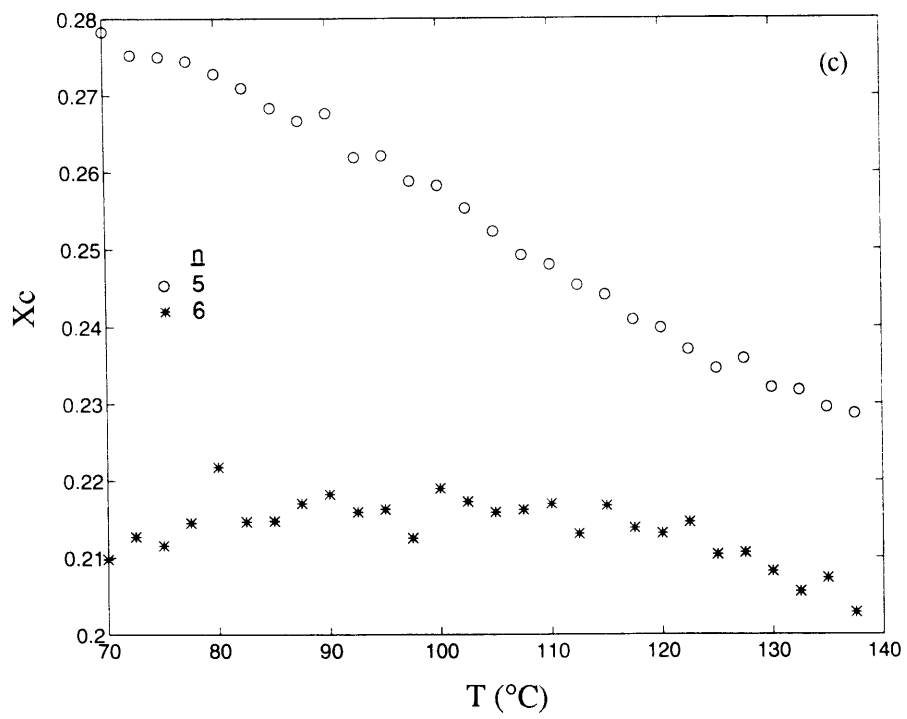
Figure 4.6, Continued

analysis was not applied to data taken above 140°C. The data collection time of 30 seconds results in temperature interval of 2.5°C for each data point. The intensity data represent an average over the temperature window. As temperature decreases below 140°C, the long period decreases steadily as shown in Figure 4.6a. Due to its low crystallinity, HMS-6 has a lower scattered intensity. The HMS-6 data are more noisy and the error of long period is high in the high temperature region.

Similar to what we observed in the room temperature SAXS (Figure 4.3a), the lamellar thickness of HMS-5 is always larger than HMS-6, as shown in Figure 4.6b. We also see two stages in the non-isothermal development of the lamellar thickness. At high temperature, l_c is increasing with decreasing temperature from about 140°C to 110°C; below 110°C, l_c steadily decreases. These trends are clearly seen in HMS-5, and weakly seen in HMS-6. The changes in lamellar thickness are much greater than what could be accounted for on the basis of thermal contraction during cooling.

In Figure 4.6c, the linear crystallinity of HMS-5 is always greater than that of HMS-6 over this temperature range. As temperature decreases, the linear crystallinity for HMS-5 increases from 0.23 to 0.28, while for HMS-6 the linear crystallinity is nearly flat. By the time the intensity shows a clear maximum (for T less than about 140°C) allowing K(z) to be determined unambiguously, significant linear crystallinity already exists. As shown in DSC cooling scans, the crystallization exotherm (lc-k) occurs at temperatures lower than 140 °C. Therefore, we consider the electron dense phase existing at this temperature actually represents the liquid crystalline phase.

The results shown in Figure 4.6 support the model of dual lamellar populations [95,105,106]. During isothermal crystallization, in the model of dual lamellar populations, initially "primary" crystals grow in a sea of amorphous melt forming the

superstructure of the spherulites. Other later forming "secondary" crystals grow in amorphous material of restricted mobility due to the entanglement effects caused by the primary crystals. The primary crystals may be thicker, more perfect, and higher melting. Secondary crystals may be thinner, less perfect, and lower melting. Here, we have to modify the model for our LCP system and for the nonisothermal conditions. During the first stage of crystallization (here, above 110°C) "primary" crystal lamellae form, which use the liquid crystalline phase as nucleation sites for crystal growth. During this stage, the long period decreases and lamellar thickness slightly increases as temperature decreases. In the second stage (below 110°C), smaller and less perfect crystal lamellae form from the isotropic phase, and therefore the average lamellar thickness and long period both decrease.

When cooling through the liquid crystalline phase transition, there exists a large fraction of electron dense phase, which is the nematic liquid crystalline phase. This phase serves as crystal nuclei for fast crystallization. From 140°C to 110°C, the crystallization mainly happens in this phase, therefore the linear crystallinity only slightly increases. The lamellar thickness increase in this temperature region can be ascribed to the "thickening" of the nematic crystal nuclei. We can imagine that the nematic phase is not very organized; therefore, the initial organized portion of the nematic phase serves as the crystal seed, which will draw the loosely-organized nematic liquid crystalline phase into the crystalline phase. This crystallization process is reflected in the major DSC crystallization exotherm, as shown in Figure 4.4.

The next series of figures refers to melting behavior of HMS materials which had been crystallized by cooling at -5°C/min from the melt to room temperature. Figure 4.7 shows DSC heating scans of HMS-5 to 9, for the purpose of comparison with SAXS data taken at the same heating rate. HMS-6 data are presented in Figure 4.8, while composite

113
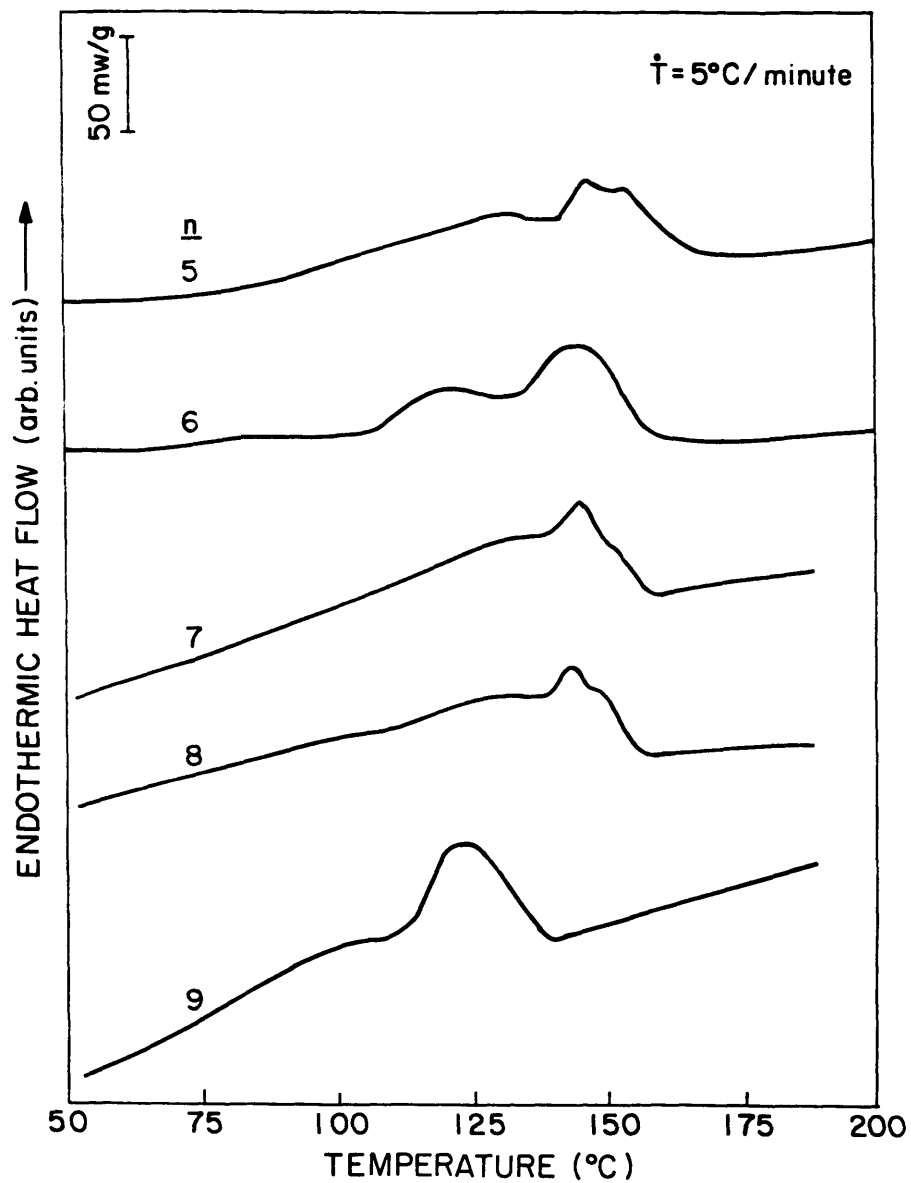
Figure 4.7   DSC thermograms of HMS-5 to 9 at 5°C/min heating rate.

114
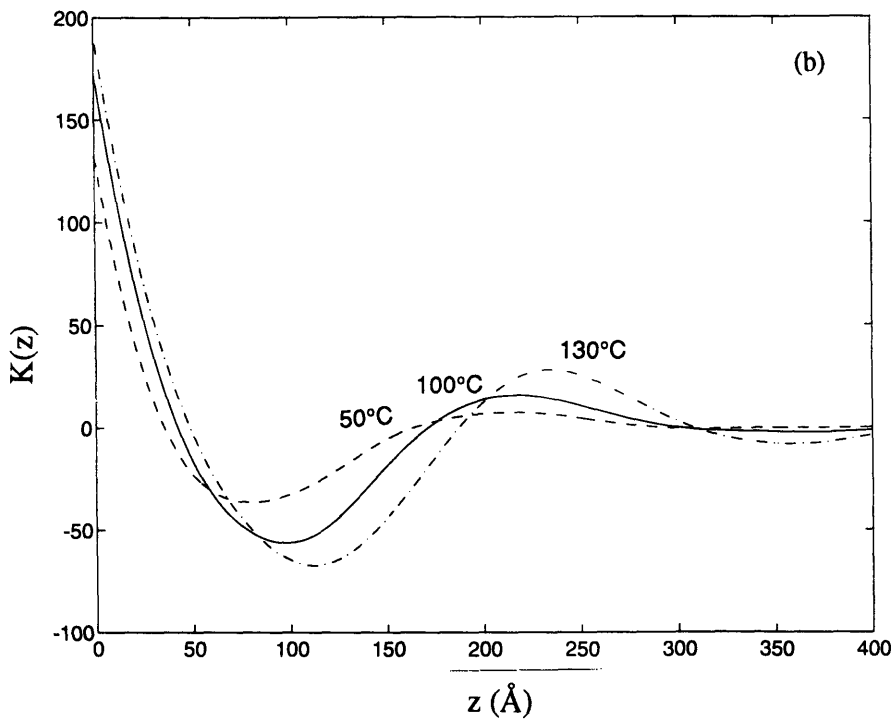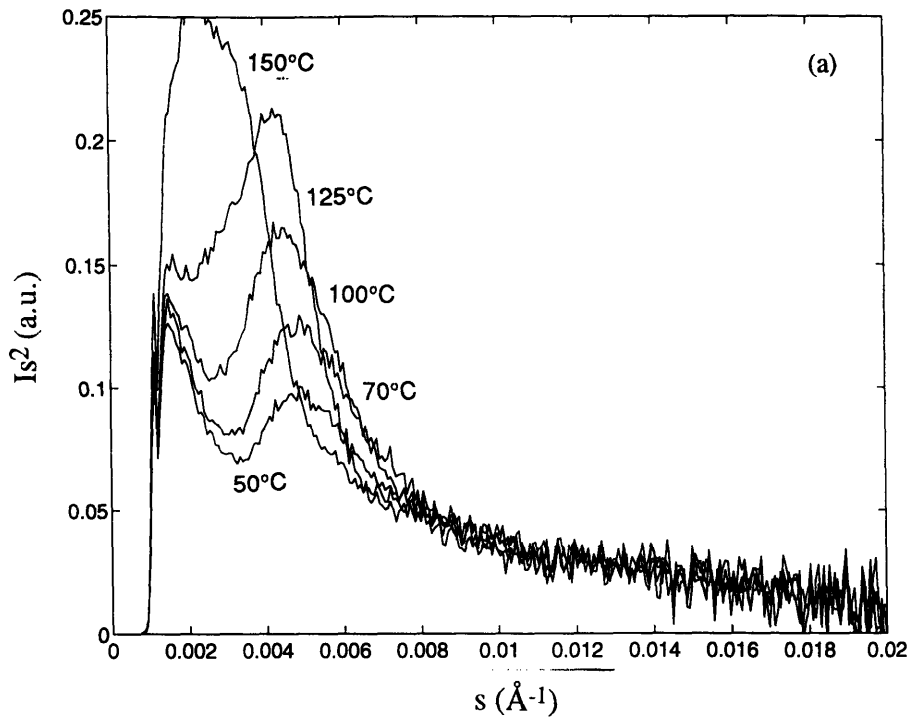
Figure 4.8   (a) Lorentz corrected SAXS intensity vs. s, (b) one-dimensional

electron density correlation function at several temperatures, and

(c) long period for HMS-6 during heating at 5°C/min.
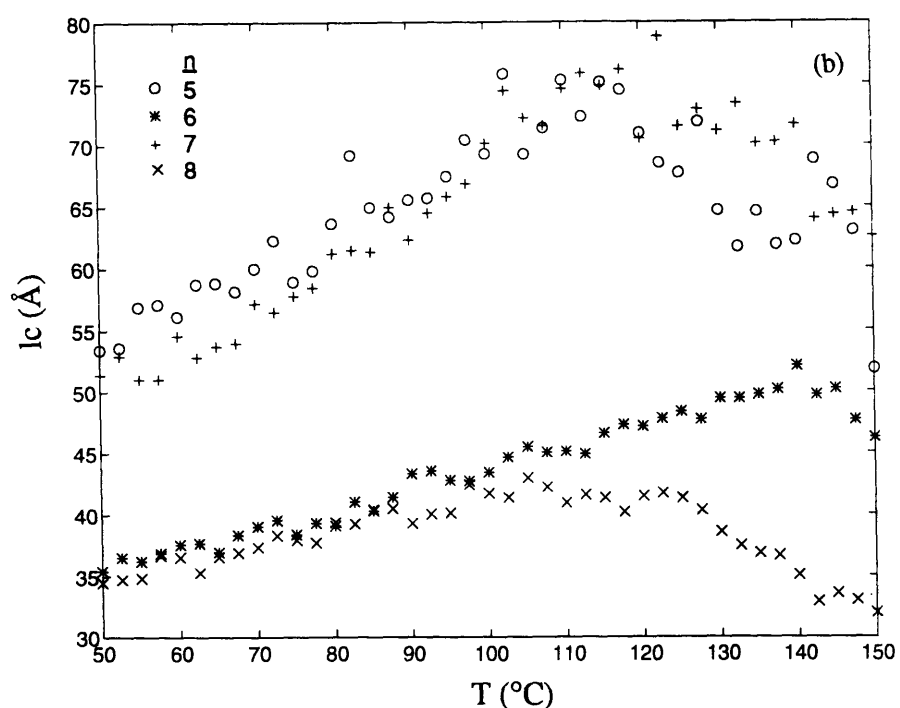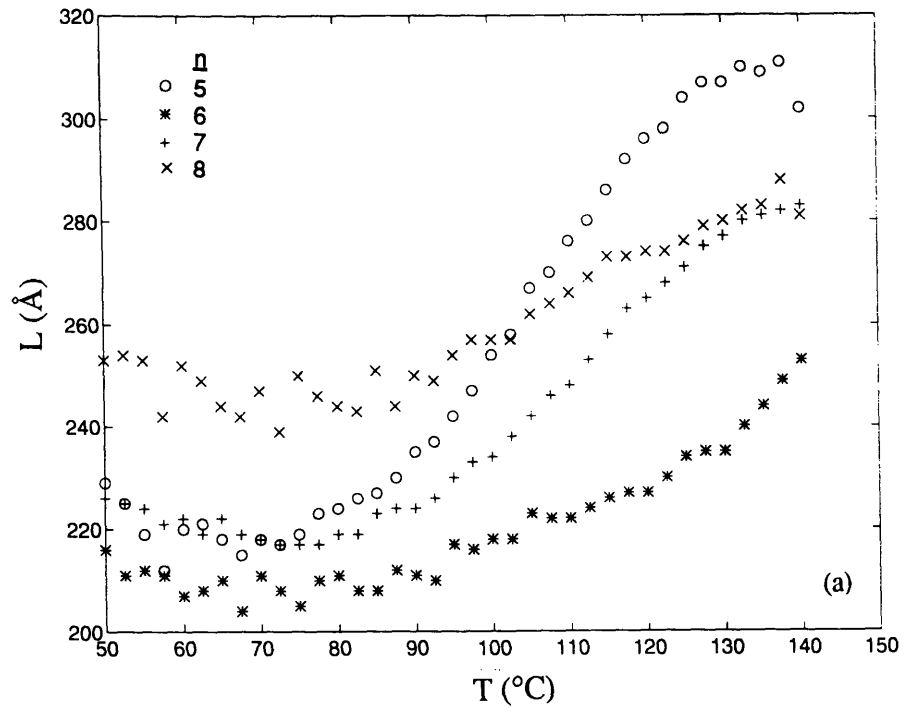
Figure 4.9   (a) Long period for HMS-6, (b) lamellar thickness, and

(c) linear crystallinity vs. temperature for HMS-5-8,

during heating at 5°C/min.
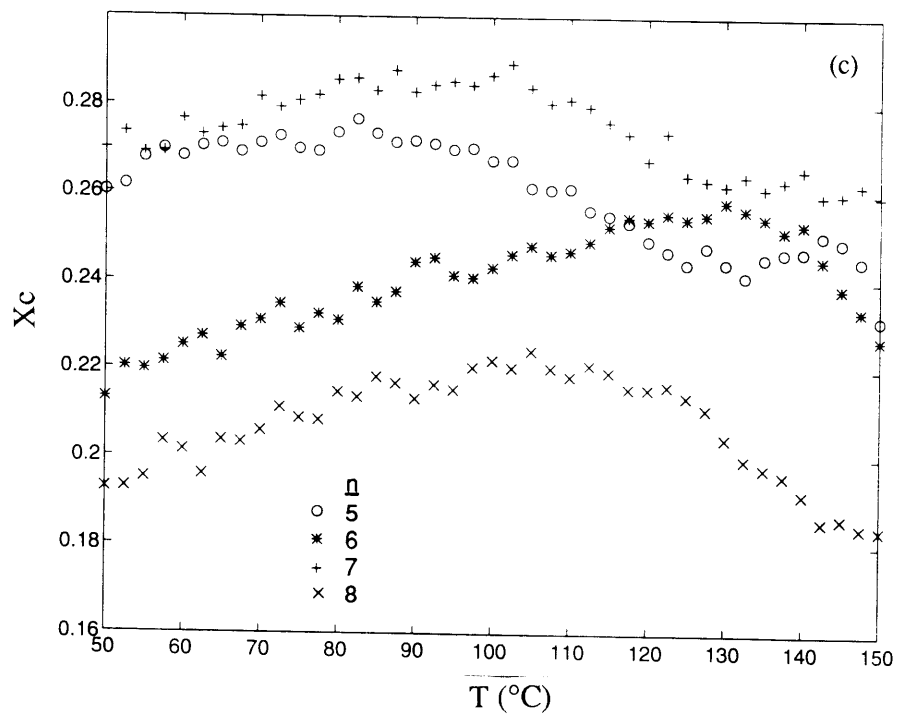
Figure 4.9, Continued

117

plots of HMS-5 through 8 are shown in Figure 4.9. In Figure 4.8a, we show the Lorentz corrected intensity versus s data at several temperatures during the heating scan for HMS-6. As temperature increases, the intensity increases. The position of the peak intensity maximum is constant in the beginning of heating, but decreases steadily once crystals start melting. We show K(z) versus z at several temperatures in Figure 4.8b. Figure 4.9a shows the long period (L) up to 140°C. Above 140°C, the long period data is not shown because of the higher error after the melting of the samples. Taking HMS-6 as an example, almost no melting occurs below 100°C, as seen from the nearly constant long period. But the lamellar thickness and linear crystallinity increase slightly from further crystallization of the sample, as shown in Figure 4.9b,c. Between 100-130°C there is slight melting, which causes the slight increase of long period. The lower melting crystals are imperfect crystals which crystallized mainly from the isotropic phase in the lower temperature range during the cooling. The average lamellar thickness and linear crystallinity still increase slightly, which suggest crystal reorganization during the heating scan. After 130°C, major melting of primary crystals occurs, which causes the drastic decrease of linear crystallinity and lamellar thickness, and the significant increase of long period. The melting history seen here approximately coincides with the DSC heating scan shown in Figure 4.7.

HMS-5 to 9 samples show similar melting behavior during the heating scan, except that HMS-9 has a lower melting temperature range, which is also consistent with our DSC study. Lamellar thickness and linear crystallinity versus temperature for HMS-5-8 are shown in Figure 4.9b,c, respectively. Notice that there is higher error in these two parameters after the samples start to melt. The odd-even effect holds clearly from the beginning of the heating scan to a temperature just before the melting.

4.3.3 Real-time SAXS during Isothermal Crystallization

In the real-time SAXS study of isothermal crystallization of HMS-5, the sample was melted and then cooled to 140°C. We show in Figure 4.10a the DSC exothermic heat flow vs. time at 140°C, and for comparison in Figure 4.10b the Lorentz corrected intensity (Is^2) vs. time at 140°C at s = 0.0025, where Is^2 has its maximum value. The Lorentz corrected intensity starts to increase when the temperature drops through the isotropic to mesophase transition although the cooling behavior is not shown here. Significant intensity has already developed through electron-dense phase formation by the time the temperature has reached 140°C. From the non-zero value of Is^2 at t = 0, we conclude that electron-dense phase formation happens as the material is cooled through the isotropic to mesophase transition. Once the isothermal crystallization temperature is reached, the intensity grows very fast in the early stage of crystallization before the time to maximum heat flow as observed in the DSC exothermic heat flow. The linear crystallinity, lamellar thickness and long period obtained from the one-dimensional electron density correlation function also quickly reach a final steady state value in the beginning of the isothermal crystallization. These facts suggest that the nematic phase serves as crystal nuclei for fast crystallization, as mentioned in Chapter 2 [99]. Table 4.2 shows the linear crystallinity, lamellar thickness and long period for HMS-5-8 isothermally crystallized at 140°C without cooling. An odd-even effect still can be observed for the linear crystallinity and lamellar thickness, probably because HMS-5 to 8 have similar crystallization behavior around 140°C, as shown in Chapter 2 [99].

By assuming the c-axis is perpendicular to the lamellar thickness, we list in Table 4.3 the estimated average number of monomer repeat units in crystal lamellae for HMS-5, 6, 7 and 8 isothermally crystallized at 140°C, and crystallized by cooling at -5°C/min from the melt to room temperature. We first note that the number of monomer repeat units in crystal lamellae is higher for samples isothermally crystallized at 140°C than for
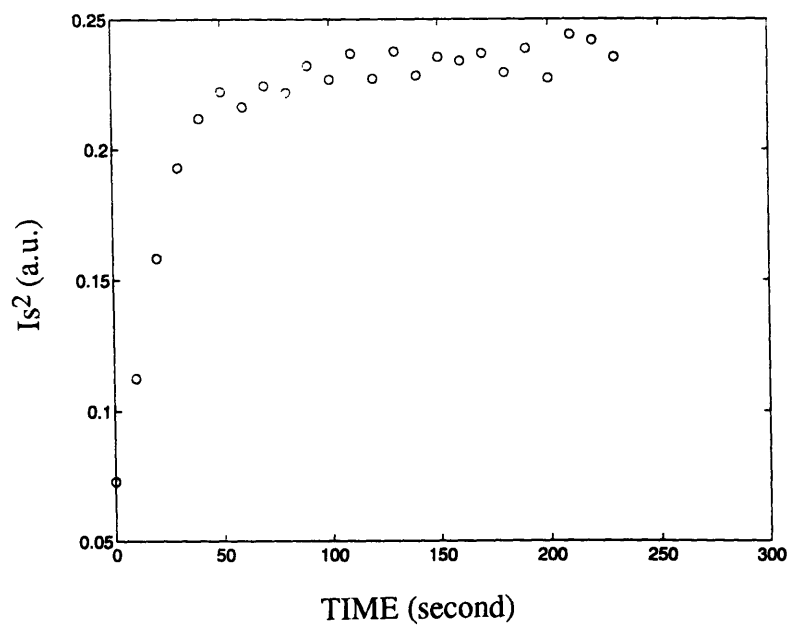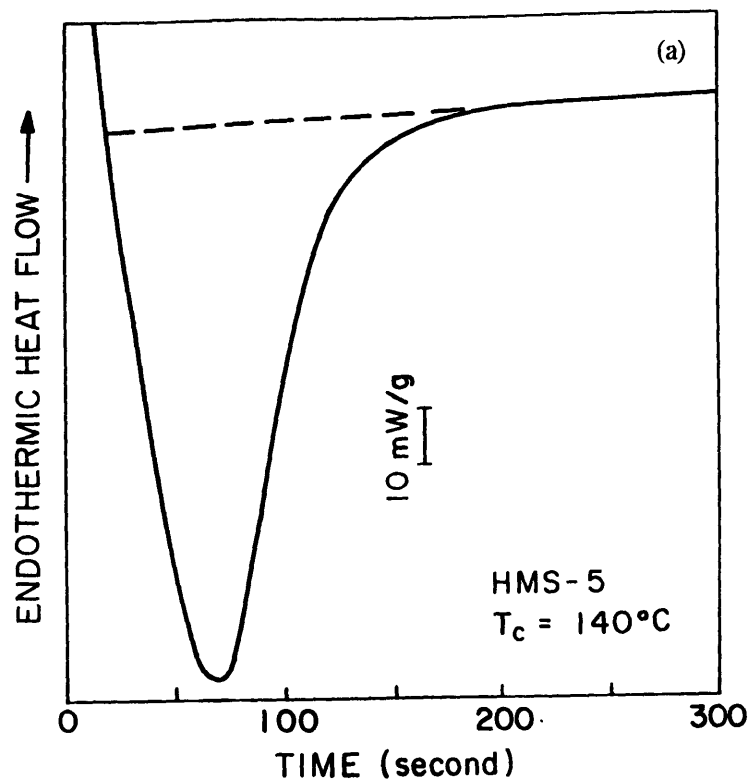
Figure 4.10   (a) DSC exothermic heat flow vs. time during isothermal

crystallization, (b) Lorentz corrected SAXS intensity vs. time

at s = 0.0025, for HMS-5 at 140°C.

Table 4.2

Long period, Linear Crystallinity and Lamellar Thickness
for HMS-5-8 Isothermally Crystallized at 140°C

Sample n	$L(\text{Å})$ ($\pm 5\text{Å}$)	X_c (± 0.01)	$l_c(\text{Å})$ ($\pm 2\text{Å}$)
5	380	0.24	89
6	360	0.22	57
7	355	0.24	82
8	370	0.21	55

Table 4.3

Monomer Repeat Unit Length and Estimated Number
of Monomer Repeat Unit in Crystal Lamellae for HMS-5-8

Sample n	Monomer length m	l_c^* / m	$l_c^\dagger / m$
5	23.4	3.8	1.9
6	24.4	2.3	1.4
7	25.6	3.2	1.8
8	26.8	2.1	1.1

* isothermal crystallization at 140°C.
† crystallization by cooling at -5°C/min from the melt to room temperature.

121

samples non-isothermally crystallized by cooling from the melt. As mentioned above, the nematic liquid crystalline phase serves as crystal nuclei and the major crystallization occurs from the scattered nematic phase. It is clear that the crystallization at high temperature such as 140°C without cooling avoids the further crystallization from the isotropic phase at the lower temperature; therefore, the lamellar thickness is higher and linear crystallinity is lower.

In Table 4.3, we can see that the lamellae of HMS-5 and 7 consist of more repeat units than the lamellae of HMS-6 and 8. As described above, the organized portion of the nematic phase serves as crystal nuclei, which later form crystal lamellar from the nematic phase. Therefore, we suggest that the size of both crystal nuclei and nematic phase are larger for the odd than the even series HMS polycarbonates. We ascribe the odd-even effect of lamellar thickness to the different degree of regularity of dipole orientation for HMS-5 and 7 compared with HMS-6 and 8. As shown in Chapter 3 [90], because of the extended conformation adopted by HMS-5 to 8 polymer chains within the crystalline phase, for HMS-5 and 7, consecutive carbonate dipoles on the chain point in nearly the same direction, while for HMS-6 and 8, consecutive dipoles point in nearly opposite directions. The favorable dipole orientation for the odd series must affect both the formation of the nematic liquid crystalline phase and the growth of crystal lamellar. Therefore, the lamellar thickness and even linear crystallinity are higher for the odd series than the even series.

In Table 4.1, we notice that HMS-9, 10 and 12 have a pretty high value of lamellar thickness, but their melting temperature is lower than HMS-n, for n ≤ 8 [99]. We ascribe the transition temperature drop to the greater length of the extended methylene spacer compared with the length of the mesogen, which causes a less perfect crystal structure and no formation of spherulites big enough to be observed under the

optical microscope [99].

4.4 CONCLUSIONS

The changes in linear crystallinity, lamellar thickness and long period during non-isothermal crystallization and melting can be explained by the model of dual lamellar thickness. The major crystals crystallize using the nematic liquid crystalline phase as crystal nuclei. The secondary crystals form from the isotropic phase at lower temperature. An odd-even effect is observed in lamellar thickness and linear crystallinity, in which both parameters are lower for α-methyl stilbene polycarbonates with odd-numbered methylene spacer. We suggest this alternation is caused by the different degree of regularity of the carbonate dipole orientation in the extended polymer chain conformation for the odd and even series.

Chapter 5

Characterization of DMS Polycarbonates and Comparison between HMS and DMS Polycarbonates

5.1. INTRODUCTION

As mentioned in Chapter 1, a series of polycarbonates has been synthesized by Dr. Schreuder-Gibson with stilbene mesogen, mono- or di- substituted with methyl or ethyl groups. These are referred as HMS-n, DMS-n, HES-n, DES-n, respectively. Chemical structures of these polymers are shown in Figure 1.5. The polycarbonates with heptane flexible spacer were chosen for comparison of the effect of different mesogen substitution on their properties [51]. Polycarbonates with ethyl substituted stilbene mesogen (HES-7 and DES-7) are amorphous, while polycarbonates with methyl substituted stilbene mesogen (HMS-7 and DMS-7) are semicrystalline and appear to be liquid crystalline under the optical microscope. Their different behavior was suggested in Dr. Schreuder-Gibson's work [51] to relate to the stilbene cross section size. This chapter concentrates on the characterization of DMS-n. The flexible spacer number ranges from n = 4-10, 12.

As described in Chapters 2 and 3, we determined that HMS polycarbonates actually can only form monotropic liquid crystalline phases. As mentioned in Chapter 1, the insertion of substituents on the mesogen will lower the stability of the liquid crystalline phase because of the steric effect. And in fact, α,β-dimethyl stilbene polyesters do not have an enantiotropic liquid crystalline phase while α–methyl stilbene polyesters do [14,21,49]. Therefore, it is not too surprising that DMS polycarbonates only have a virtual liquid crystalline phase, as described in this Chapter.

124

5.2. EXPERIMENTAL SECTION

5.2.1 Materials

The synthesis of DMS polycarbonates was performed in Dr. Schreuder-Gibson's group [51] and followed the method of Sato [84]. The synthesis is described in the Appendix. The resultant LCPs were soluble in chloroform and obtained as fine white powders. All polymers studied here have reasonably high molecular weight, in the range from 14,200 to 32,800 with distributions (M_w/M_n) close to 2 as reported previously [51].

5.2.2 Differential Scanning Calorimetry (DSC)

Thermal properties of materials were studied using a Perkin-Elmer DSC-4 or DSC-7. Indium was used to calibrate the temperature and the heat of fusion. The studies that were done included heating and cooling at fixed rates, and the effect of crystallization temperature on both crystallization time and melting temperature.

The first approach involved heating and cooling at fixed rates over a wide temperature interval. The sample was heated to 200°C and held at that temperature for 2.5-3 minutes, then cooled at a rate of 10°C/min to 40°C, then heated at 10°C/min to 200°C. This study was done for all DMS-n samples. For the purpose of comparison, HMS-7 was also studied in the same way. In addition, HMS-7 and DMS-7 were cooled and heated at 5, 20, and 50°C/min. HMS-7 was also cooled at 2°C/min. This study was designed to test the dependence of the isotropic to mesophase transition temperature on cooling rate.

The next study was isothermal crystallization for HMS-7 and DMS-7. The sample was melted at 200°C for about 3 minutes, then quenched at -50°C/min to a crystallization temperature T_c and held isothermally until the crystallization was finished.

125

The T_Cs were specifically chosen in advance to keep the crystallization times comparable. Because DMS-7 has lower crystallization temperature than HMS-7, we chose a crystallization temperature in the range from 120 to 132°C for DMS-7 and from 136°C to 147°C for HMS-7. Exothermic heat flow as a function of time was large enough to be measured in the chosen temperature for both materials. Here we were interested in the isothermal crystallization kinetics.

The next study involved immediate rescan after isothermal crystallization for HMS-7 and DMS-7. After staying at T_C isothermally until crystallization was finished, the sample was immediately heated at 5°C/min to 190°C without cooling. This immediate rescan technique avoids the formation of imperfect crystals during cooling to room temperature, and thus results in a cleaner endothermic response.

5.2.3 Wide Angle X-ray Scattering

A Rigaku RU-300 rotating anode x-ray generator was used to examine films of DMS-7 in $\theta/2\theta$ reflection mode.. The diffractometer has a diffracted beam graphite monochromator. Copper K_α radiation was used (λ=1.54Å) with a step scan interval of 0.1 degree, at a rate of 1 degree/minute, over the 2θ range from 3 to 53 degrees. Powder was dissolved in chloroform and several drops of the solution were placed onto quartz substrates. The thin films were run "as-is" without any other thermal treatment.

Wide angle X-ray scattering was also performed at room temperature using a Philips PW1830 X-ray generator operated at 45kV and 45mA with Ni-filtered CuK_α radiation (λ = 1.54Å). The Statton camera used in this study consists of a pinhole collimator over which the sample is placed, and a flat film (Kodak DEF-5) to record the scattering pattern. The sample to film distance is calibrated using Si powder reference standard (from National Institute of Standards & Technology) rubbed on the sample

surface. The first 2θ value for Si is 28.44Å. HMS-7 and DMS-7 fiber was hand drawn from the mesophase using tweezers. This fiber cooled rapidly in air, and will be referred to as raw fiber. Raw fiber was subsequently annealed below the melting temperature. WAXS was performed on both the raw and annealed fibers. CERIUS^{TM}, a commercial software package distributed by Molecular Simulations Inc., was used for indexing of experimental X-ray diffraction patterns and determination of the crystal structure.

5.2.4 Small Angle X-ray Scattering

The X12B beam line at Brookhaven National Synchrotron Light Source (NSLS) was used to obtain small angle X-ray scattering data in transmission mode. For high temperature work, a Mettler hot stage was supported in the X-ray beam path by an aluminum holder, and the beam passed through the sample, which was sealed between two pieces of Kapton^{TM} tape. A gas-filled two-dimensional histogramming wire detector was used. For isotropic samples, circular integration of the intensity was used to enhance the signal to noise ratio. For oriented fiber samples, sectorial integration of the intensity was used with 10° interval in each section. The beam profile was treated according to pinhole geometry. SAXS data were taken on two separate trips. The sample to detector distance was 1.39 m or 1.85 m, and was calibrated by cholesterol meristate and collogen fiber. X-ray wavelength was 1.38Å or 1.53Å.

SAXS scans at room temperature were taken for DMS-5 to 8, which were non-isothermally crystallized by cooling at 5°C/min from the melt to room temperature. Real-time SAXS data were taken for an isothermal crystallization study. DMS-7 and 8 samples were melted at 190°C for 2.5-3 minutes, then cooled at 20°C/min to 124°C and held there until crystallization was finished, which was predetermined by the DSC isothermal crystallization study. Data were collected during cooling from 170 to 140°C and during the whole isothermal crystallization process. The data collection time was 10

seconds. Raw HMS-7 fiber was quickly heated from room temperature to 88°C, then heated at 20°C/min to 138°C. Similarly, raw DMS-7 fiber was quickly heated to 75°C, then heated at 20°C/min to 125°C. Data were collected during the 20°C/min heating process. The data collection time was 15 seconds.

SAXS intensity was corrected for background, sample adsorption, variation of incident beam intensity and thermal density fluctuations. The slope of Is^4 versus s^4 plot (where s is the scattering vector, $s = 2 \sin\theta/\lambda$) was used to get the diffraction intensity contribution from thermal density fluctuations [119,120]. The corrected intensity is used for quantitative analysis.

5.3. RESULTS

5.3.1 Differential Scanning Calorimetry

In the DSC cooling scan of DMS-4-10 and 12 cooling from melt, usually a broad exotherm with a low temperature tail is observed. In the reheating scan, a broad endotherm with a low temperature tail caused by the melting of less perfect crystals is observed. For the purpose of comparison, Figure 5.1a,b shows the cooling and reheating scans of DMS-7 and HMS-7. In both scans, the baseline of HMS-7 is tilted steeply down from left to right. DMS-7 has lower crystallization and melting temperature than HMS-7. Table 5.1 summarizes the melting and crystallization peak positions for DMS-4-10 and 12. These values can be compared to those of HMS-7 which are listed in Table 2.1. Unlike HMS polycarbonates, the transition temperatures of DMS polycarbonates do not have an obvious relationship with the flexible spacer. Nevertheless, for both HMS and DMS polycarbonates, the transition temperatures drop when the methylene spacer number when n is bigger than 8.

128
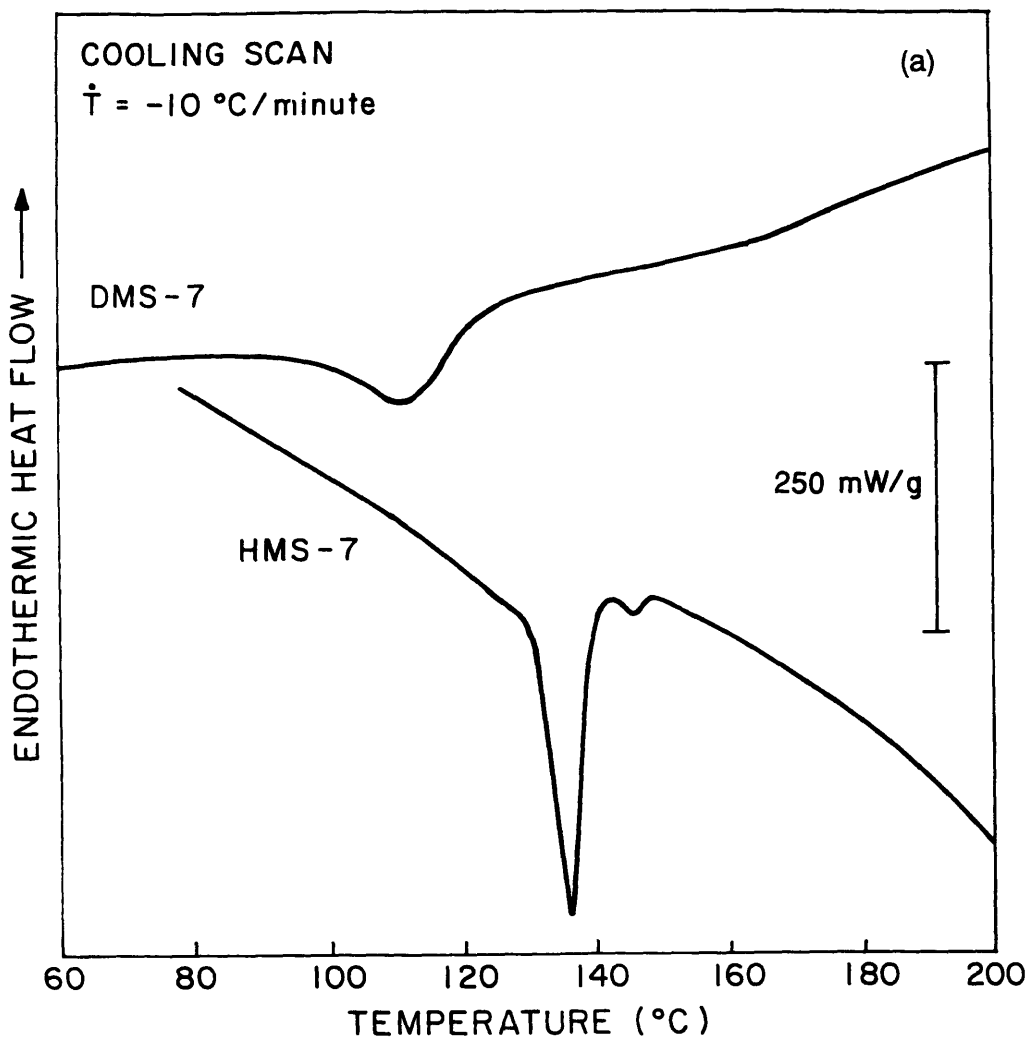
Figure 5.1   DSC thermograms of DMS-7 and HMS-7 at 10°C/min

(a) cooling and (b) heating.
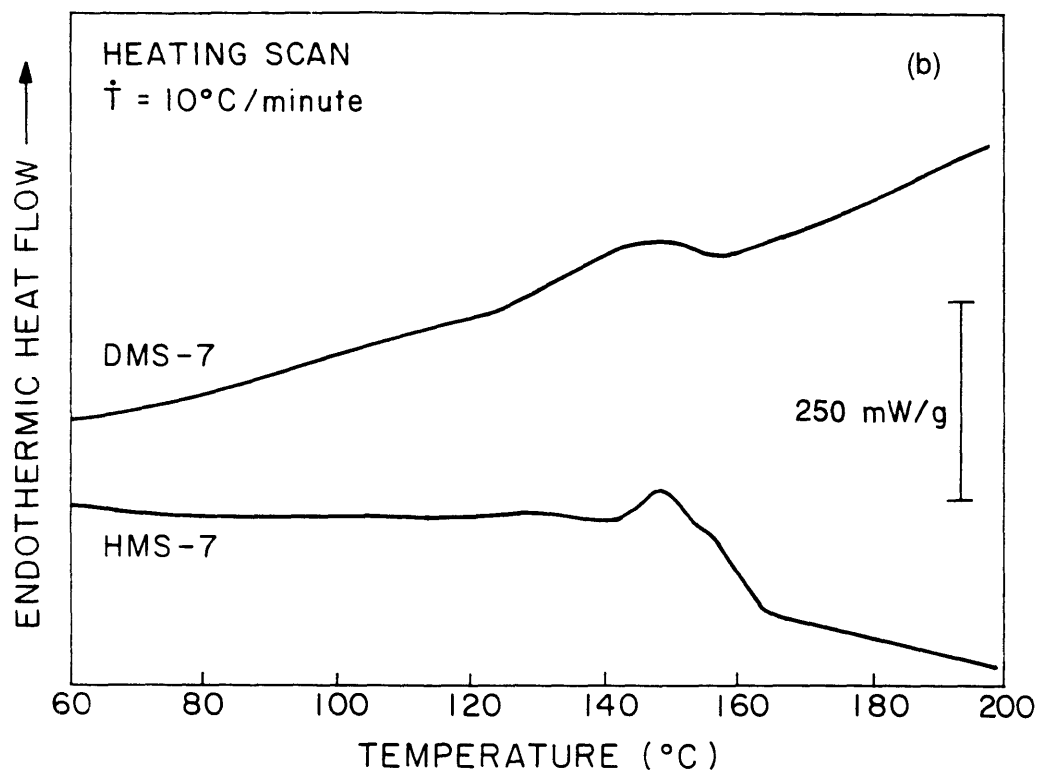
Figure 5.1, Continued

Table 5.1

**Thermal Transition Peak Temperatures for DMS Series Polycarbonates
at 10°C/minute Scan Rate**

Sample n	Crystallization Temp.(°C) T_c	Melting Temp.(°C) T_m
4	149	172
5	66	115
6	157	174
7	110	142
8	113	139
9	77	105
10	77	106
12	80	112

Figure 5.2a,b shows DSC cooling scans at various cooling rates for HMS-7 and DMS-7, respectively. As described in Chapter 2, HMS-7 has a monotropic liquid crystalline phase, which can be observed in cooling only provided that the crystallization process is suppressed for example, by increasing the cooling rate. The small higher temperature exotherm seen in Figure 5.2a represents the isotropic to liquid crystalline phase transition, whose position is less affected by the cooling rate, compared with that of the large lower temperature crystallization exotherm. Therefore, at a slow cooling rate like 2°C/min, the isotropic to liquid crystalline phase transition is covered by the crystalline phase transition. But at higher cooling rates, the liquid crystalline transition can be observed. In contrast, for DMS-7 shown in Figure 5.2b, higher cooling rates up to 50°C/min still can not separate the liquid crystalline transition from the crystalline phase transition.

In the DSC isothermal crystallization study, the time to maximum heat flow at several temperatures is obtained for DMS-7 and HMS-7, as shown in Figure 5.3a,b, respectively. The time to maximum heat flow of DMS-7 is less sensitive to the crystallization temperature increase than that of HMS-7.

The relationship between the melting point and the crystallization temperature is found from the Hoffman-Weeks equation [85] as:

$$T_m = T_m^0 \left(1 - 1/\gamma \right) + T_c / \gamma \qquad (1)$$

where T_m^0 is infinite crystal melting point and γ is the thickening factor of the crystal lamellae. HMS-7 and DMS-7 have similar values of thickening factor and infinite crystal melting point as shown in Table 5.2.
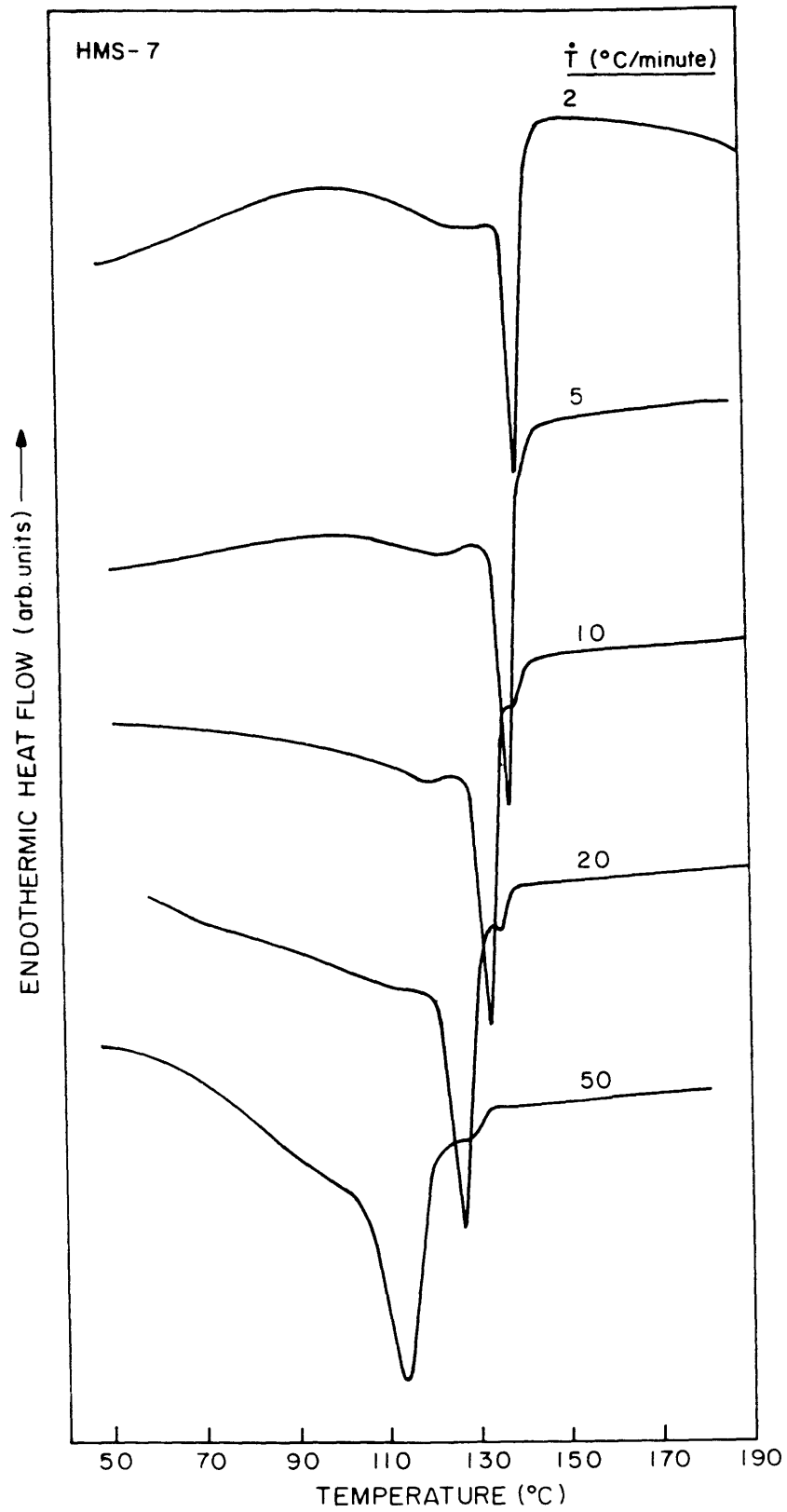
Figure 5.2   DSC thermograms of (a) HMS-7 and (b) DMS-7

at various cooling rates.

133
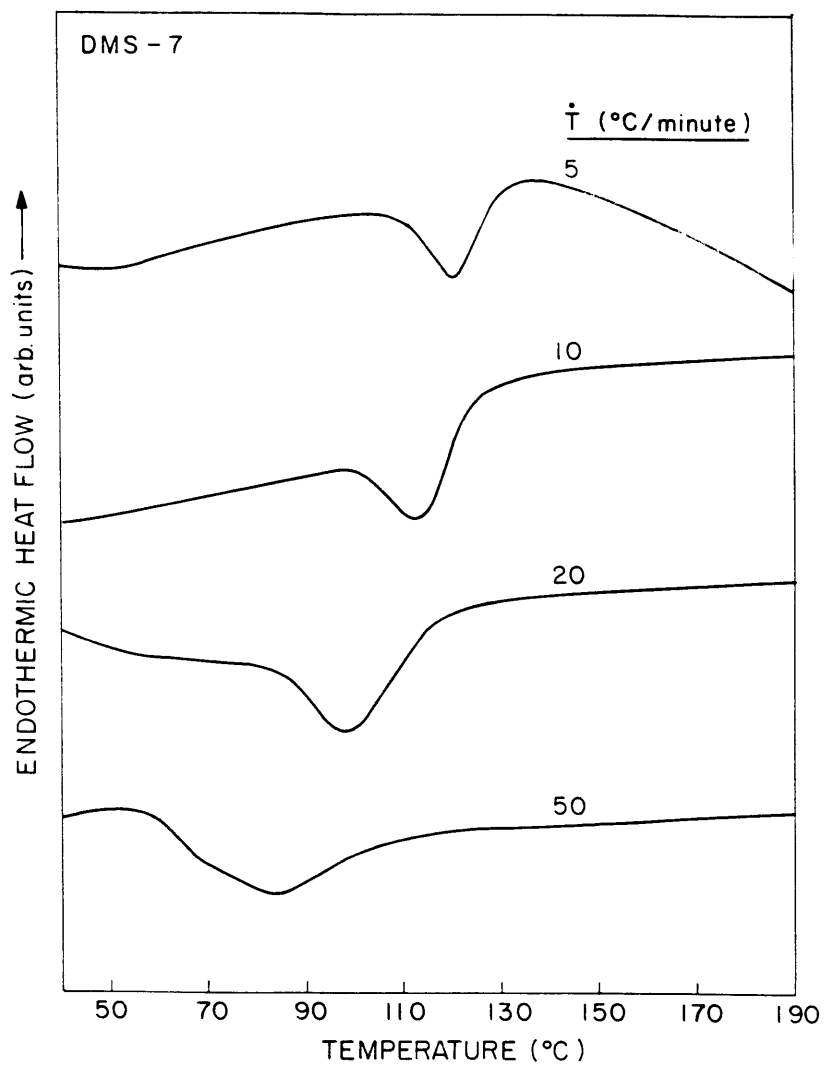
Figure 5.2, Continued

134
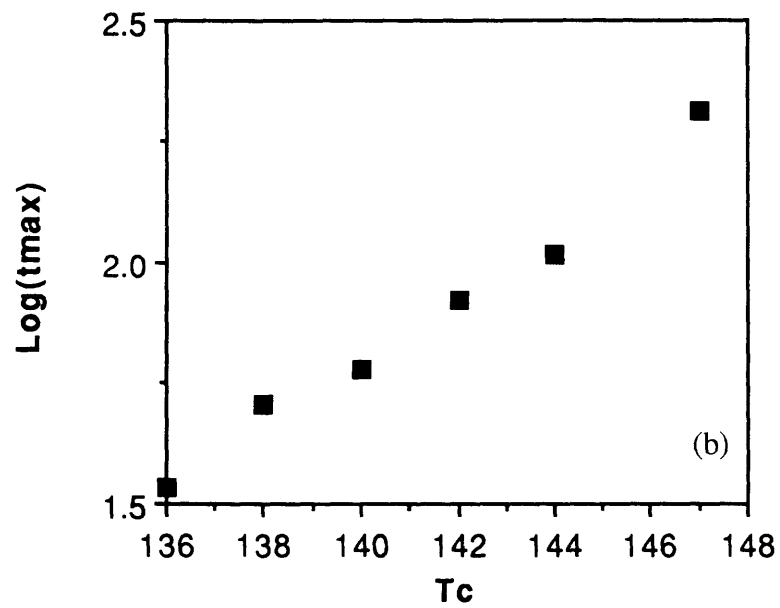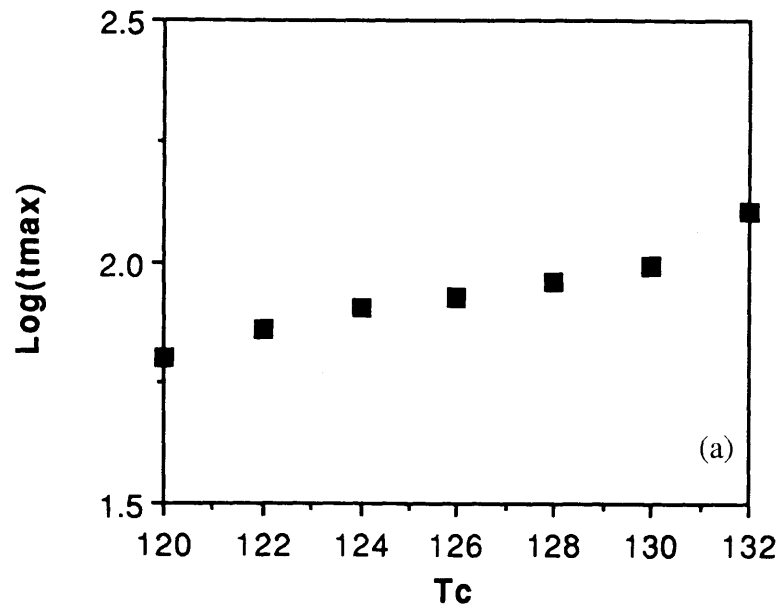
Figure 5.3   The time to maximum heat flow vs. temperature of (a) DMS-7
and (b) HMS-7.

Table 5.2

**Infinite Crystal Melting Point and Thickening Factor
for HMS-7 and DMS-7**

Sample	Infinite Crystal Melting Point, T_m° (°C)	Thickening Factor, γ
HMS-7	189	1.2
DMS-7	203	1.3

5.3.2 Wide Angle X-ray Scattering

Figure 5.4 shows WAXS reflection pattern of DMS-7 film as prepared without thermal treatment. The narrow single peak maximum located at d-spacing 4.4 Å suggests the existence of the nematic liquid crystalline order.

Figure 5.5a,b shows X-ray diffraction patterns of HMS-7 and DMS-7 raw fibers. HMS-7 raw fiber X-ray diffraction pattern in Figure 5.5a displays two strong equatorial reflections, which are associated with the (020) and (110) planes, as described in Chapter 3. Unlike HMS-7, DMS-7 raw fiber X-ray diffraction pattern in Figure 5.5b shows a diffuse ring with the maximum intensity on the equator. This pattern is similar to that of weakly ordered amorphous polymer, and indicates no strong orientation between adjacent DMS-7 polymer chains. Once the raw fiber is annealed, crystalline reflections are observed in HMS-7 and DMS-7, as shown in Figure 5.6a,b, respectively. HMS-7 has a monoclinic crystal structure with a = 9.4Å, b = 7.9Å, c = 25.6Å, α = 90°, β = 34.3°, γ = 90°, as described in Chapter 3. For DMS-7, an orthorhombic crystal structure with a = 4.8Å, b = 9.1Å, c = 25.7Å, α = β = γ = 90°, can be identified. The calculated scattering angle, 2θ, and corresponding d-spacings are shown in Tables 5.3, for direct comparison with the experimental data.

DMS-7 can be compared to an HMS polycarbonate having similar crystalline unit cell structure. Both DMS-7 and HMS-5 are orthorhombic. Notice that (0 0 l) reflections exist with l = odd in DMS-7 whereas no such reflections are seen in HMS-5 (see Table 3.1). Absence of (0 0 l) with l odd in HMS-5, is a signature of intermeshed structure in which adjacent chains are located at (0,0,0) and (1/2,1/2,1/2) positions. In DMS-7, existence of (0 0 l) for l odd indicates that this polymer does not have an intermeshed structure.
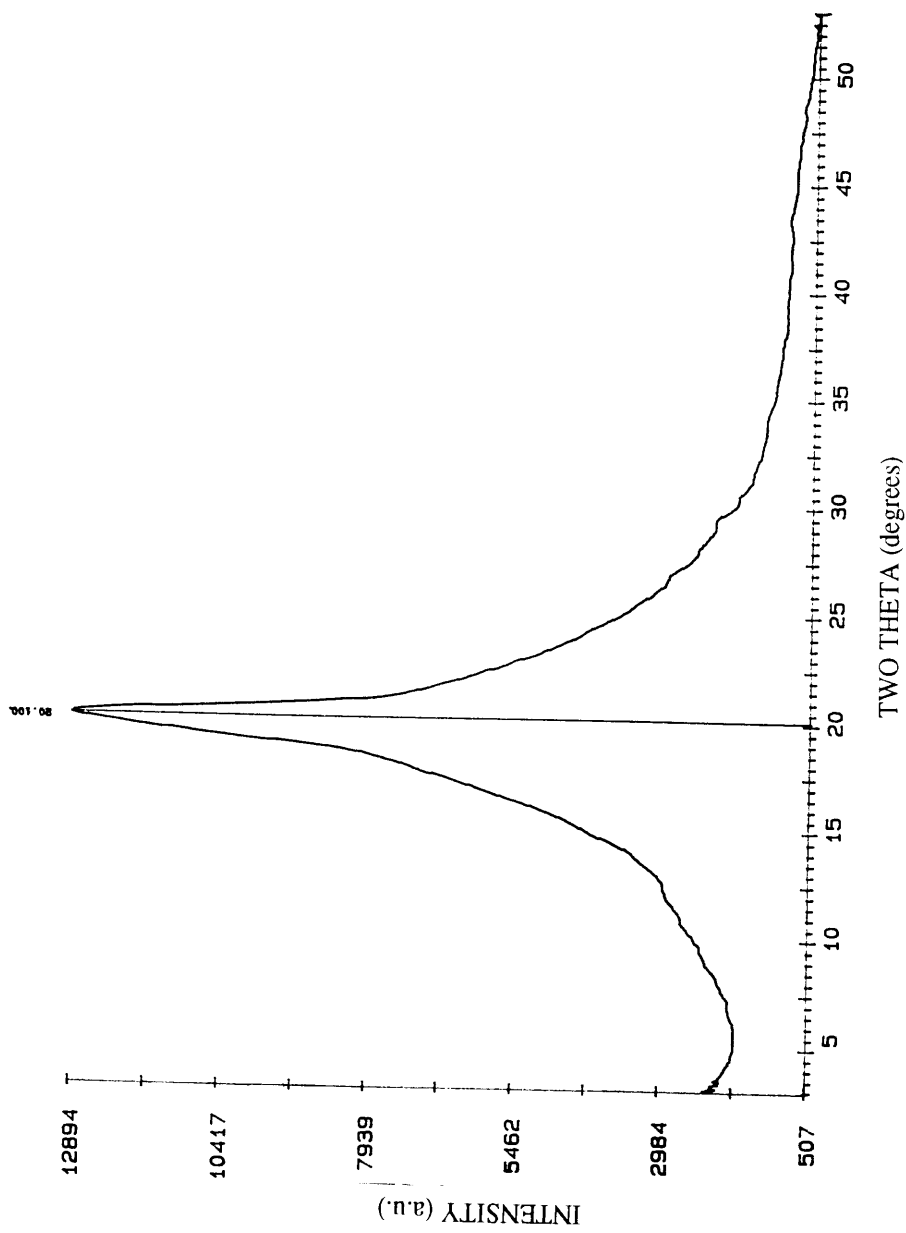
Figure 5.4   WAXS intensity versus two theta for DMS-7.

Figure 5.5   Flat film WAXS of hand drawn raw fibers:

a.) HMS-7, b.) DMS-7. Fiber axis is vertical.

Figure 5.5, Continued
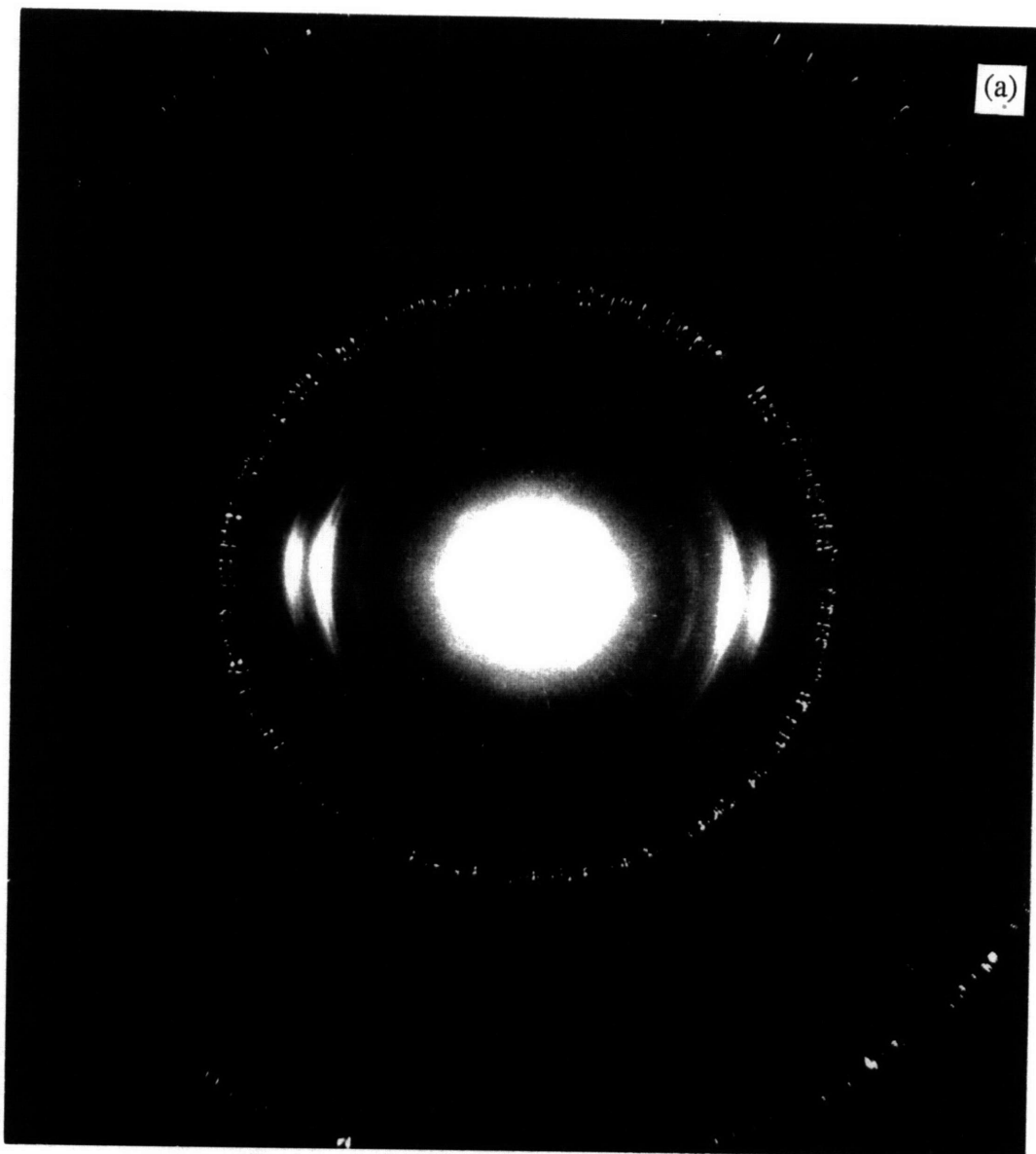
Figure 5.6   WAXS of hand drawn annealed fibers: a.) HMS-7, b.) DMS-7.

Fiber axis is vertical. Spotty ring is from Si calibration standard.

Figure 5.6, Continued

142

Table 5.3

Experimental and Calculated Crystallographic Parameters

of a Crystal Unit Cell of DMS-7

Miller Index*	2θ (°)		d-spacing (Å)	
(h k l)	data	Calc.	data	Calc.
(1 1 0)	20.8 (±0.3°)	20.9	4.3 (±0.1Å)	4.2
(0 1 1)	10.4 (±0.2°)	10.3	8.5 (±0.1Å)	8.6
(0 2 0)	19.5 (±0.2°)	19.5	4.5 (±0.1Å)	4.6
(2 0 0)	36.6 (±0.7°)	37.5	2.5 (±0.1Å)	2.4
(0 1 2)	11.8 (±0.2°)	11.9	7.5 (±0.1Å)	7.4
(0 0 3)	10.2 (±0.2°)	10.3	8.6 (±0.1Å)	8.6
(1 3 0)	34.6 (±0.5°)	35.0	2.6 (±0.1Å)	2.6
(0 0 4)	13.8 (±0.2°)	13.8	6.4 (±0.1Å)	6.4
(1 2 4)	29.9 (±0.5°)	30.4	3.0 (±0.1Å)	2.9
(1 1 5)	27.0 (±0.3°)	27.3	3.3 (±0.1Å)	3.3
(0 0 7)	23.4 (±0.7°)	24.2	3.7 (±0.1Å)	3.7

* Miller indices are assigned based on orthorhombic structure with lattice parameters a = 4.8Å, b = 9.1Å, c = 25.7Å, $\alpha = \beta = \gamma = 90°$.

5.3.3 Small Angle X-ray Scattering

We show in Figure 5.7a,b the Lorentz corrected SAXS intensity (Is^2) versus s data at room temperature of DMS-7 and HMS-7, respectively, which had been cooled at 5°C/min from the melt to room temperature. Considering that spherulites have been observed by optical microscopy [51], we assume that DMS polycarbonates have a lamellar structure in which stacks of lamellae alternate with amorphous material. Then the one-dimensional electron density correlation function, K(z), is obtained by discrete Fourier transform of the corrected intensity, as described in Chapter 4. z is a dimension along the normal to the lamellar stacks. In Figure 5.8a,b, we show K(z) versus z for DMS-7 and HMS-7, respectively. Long period, lamellar thickness and linear crystallinity are obtained according to the method proposed by Strobl and Schneider [121], as described in Chapter 4 .

In Table 5.4, we list linear crystallinity, lamellar thickness and long period at room temperature for crystallized DMS-5 to 8 and HMS-7 cooled at 5°C/min from the melt to room temperature. DMS-6, 7 and 8 have similar values of linear crystallinity. But DMS-7 has higher value of lamellar thickness and long period. HMS-7 has lower values of linear crystallinity and lamellar thickness than DMS-7.

In Figure 5.9a, we show Lorentz corrected intensity (Is^2) versus s data for the real-time SAXS study of isothermal crystallization of DMS-7. The sample was melted and then cooled to 124°C. The first scan at the bottom, marked T = 154°C, is from the melt. The second scan from the bottom, marked t = 0, represents the initial stage of isothermal crystallization at 124°C. Notice that by the time the cooling process from 154°C to 124°C is completed, significant intensity has already developed. Electron-dense phase formation does happen during the cooling process as DMS-7 is cooled through the isotropic to liquid crystalline transition. This i-lc transition can not be separated from the

144
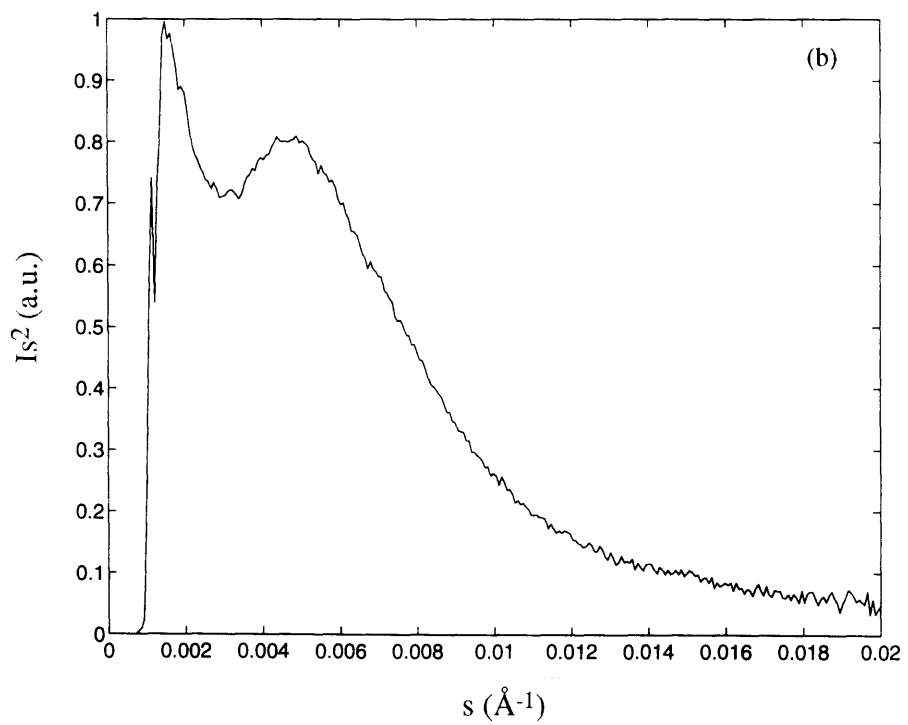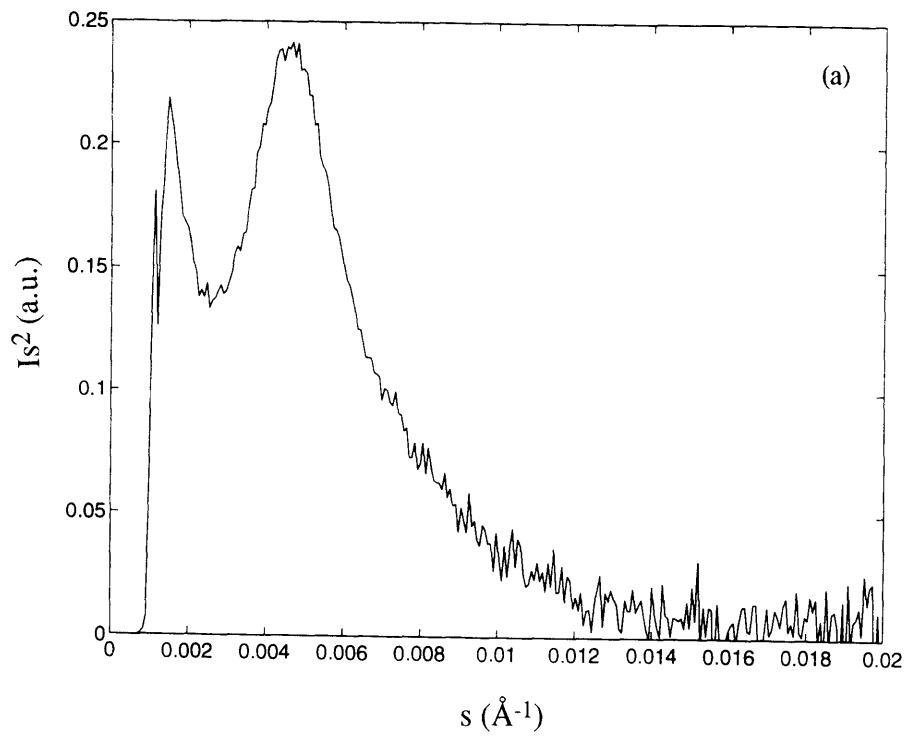
Figure 5.7   Lorentz corrected SAXS intensity vs. s at room temperature for

(a) DMS-7 and (b) HMS-7 cooled at -5°C/min from the melt.
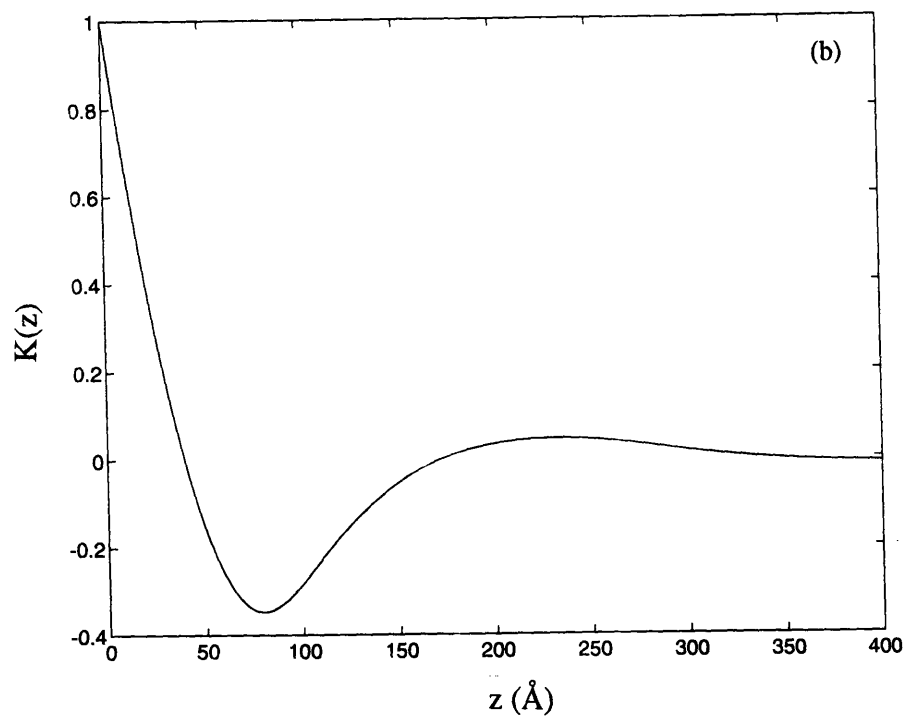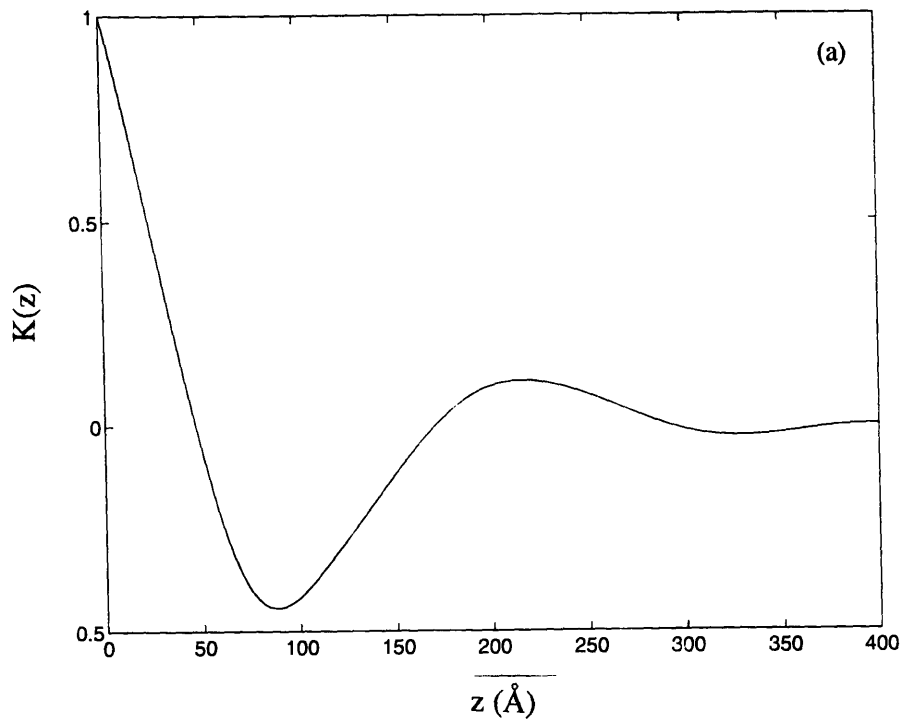
Figure 5.8   One-dimensional electron density correlation function, K(z) vs. z:

(a) DMS-7, (b) HMS-7 at room temperature.

146

Table 5.4

Long period, Linear Crystallinity and Lamellar Thickness for Crystallized DMS-5-8 and ΓMS-7 Cooled at 5°C/min from Melt to Room Temperature

Sample	$L(\text{Å})$ $(\pm 5\text{Å})$	Xc (± 0.01)	$lc(\text{Å})$ $(\pm 2\text{Å})$
DMS-5	230	0.20	32
DMS-6	189	0.28	45
DMS-7	218	0.29	67
DMS-8	191	0.28	47
HMS-7	234	0.25	46
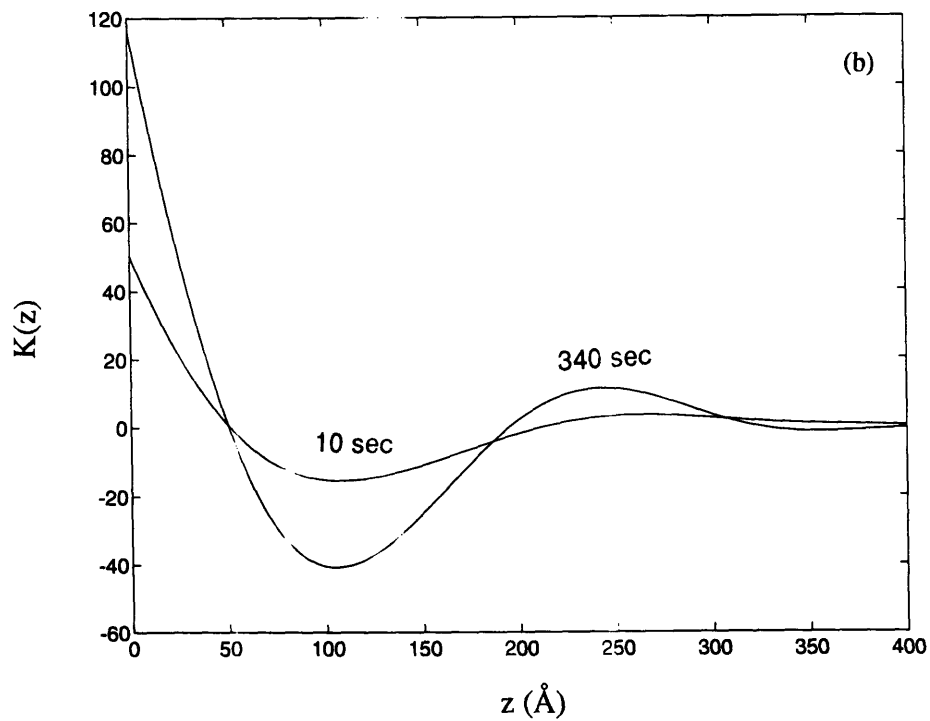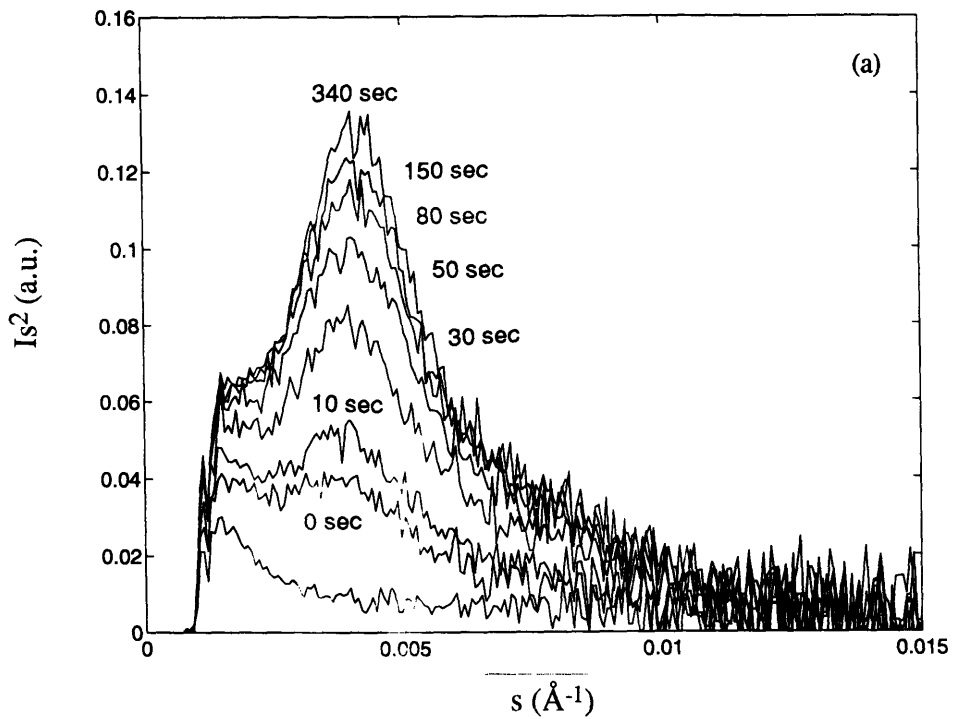
Figure 5.9   (a) Real-time Lorentz corrected SAXS intensity vs. s,

(b) one-dimensional electron density correlation function,

for DMS-7 isothermal crystallized at 124°C for the time indicated.

lc-k crystalline transition, as described above. Also, from our DSC study of isothermal crystallization kinetics, we know the time to maximum exothermic heat flow is 81 seconds, for DMS-7 crystallized at 124°C. The intensity grows very fast before 81 seconds. We apply the one-dimensional electron density correlation function to the intensity data. Figure 5.9b shows K(z) versus z in the beginning and late stages of isothermal crystallization of DMS-7. The linear crystallinity, lamellar thickness and long period quickly reach a final steady state value in the beginning of the isothermal crystallization. Table 5.5 shows the linear crystallinity, lamellar thickness and long period for DMS-7 and 8 isothermally crystallized at 124°C without cooling. DMS-7 and 8 have similar values of linear crystallinity, lamellar thickness, and long period. In comparison, HMS-5 to 8 have similar isothermal crystallization behavior at 140°C like DMS-7 and 8 at 124°C, as described in Chapter 4. But HMS-5 to 8 have much higher final values of lamellar thickness and long period.

The annealed HMS-7 and DMS-7 fibers show nice fiber SAXS patterns, which looks like one of the general SAXS patterns of uniaxial oriented fibers, as shown in Figure 5.10 [122]. The intensity maxima is located on the meridian and elongates in the direction of the equator, which is caused from the finite-size crystal lamellae aligning with c-axis parallel to the meridian direction, as shown in Figure 5.11a,b [122]. The plot of the intensity of the meridian section versus s are shown in Figure 5.12a,b for annealed DMS-7 SAXS fiber pattern taken at 125°C and annealed HMS-7 SAXS fiber pattern taken at 108°C, respectively. Figure 5.13a,b shows the resultant K(z) versus z. Table 5.5 lists linear crystallinity, lamellar thickness and long period for annealed DMS-7 and HMS-7 fibers. Annealed DMS-7 and HMS-7 fibers have similar values of lamellar thickness, but DMS-7 has higher linear crystallinity and lower long period.

Table 5.5

Long period, Linear Crystallinity and Lamellar Thickness for Isothermally Crystallized Samples and Annealed Fibers

Sample	L(Å) (±5Å)	Xc (±0.01)	lc(Å) (±2Å)
Isothermally Crystallized at 124°C			
DMS-7	245	25	55
DMS-8	251	24	53
Annealed Fiber			
HMS-7	196	24	39
DMS-7	173	27	40
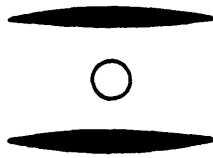
Figure 5.10   Schematic presentation of the SAXS fiber pattern.

The fiber direction is vertical, the circle in the middle of the

pattern represents the shadow of the beam stop.

(Figure taken from Ref. 122, Figure 7.19)

(a)

(b)
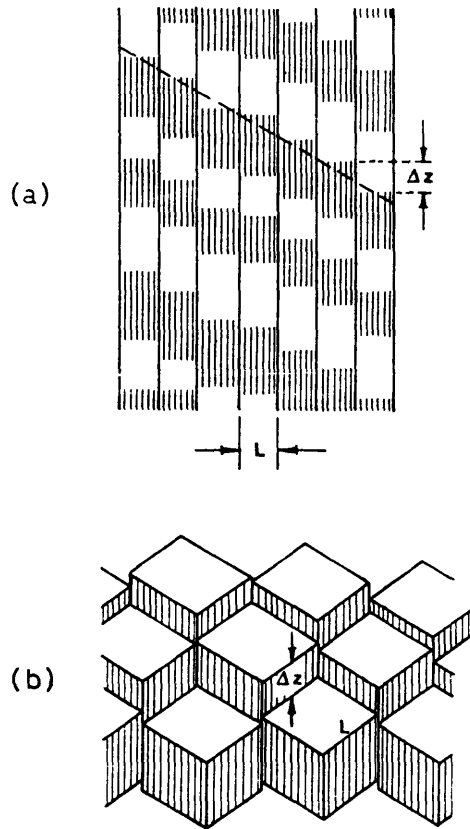
Figure 5.11   Schematic presentation of the paracrystalline fibrillar model,

proposed by Hosemann [123]. The striation indicates

the direction of the chains in the crystalline regions.

(a) Single row of microfibrils. (b) Part of a layer of crystalline

blocks [124]. (Figure taken from Ref. 122, Figure 7.22)

151
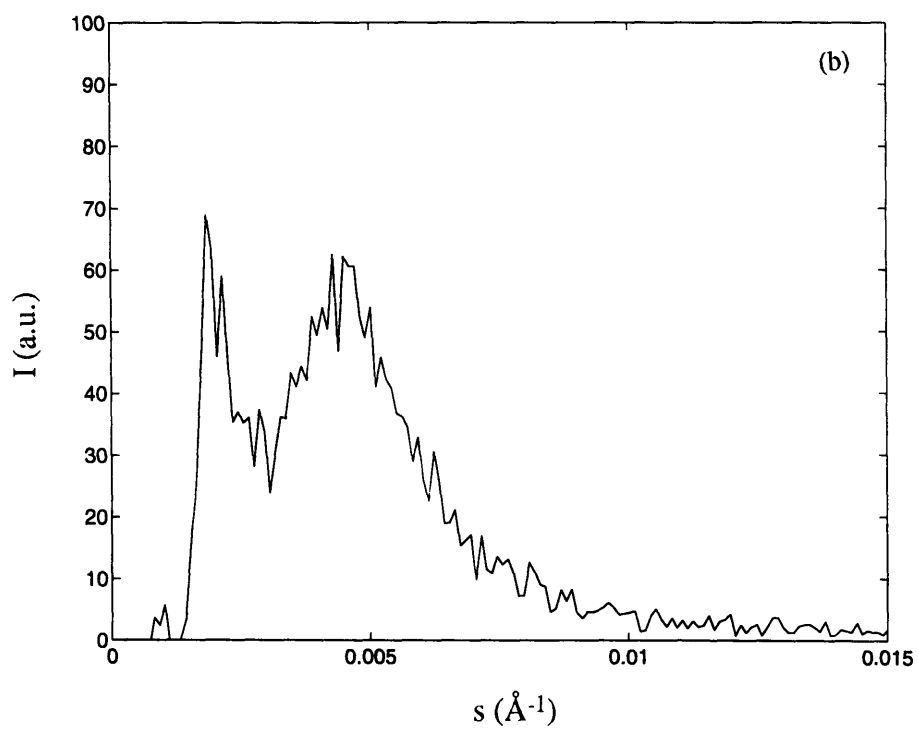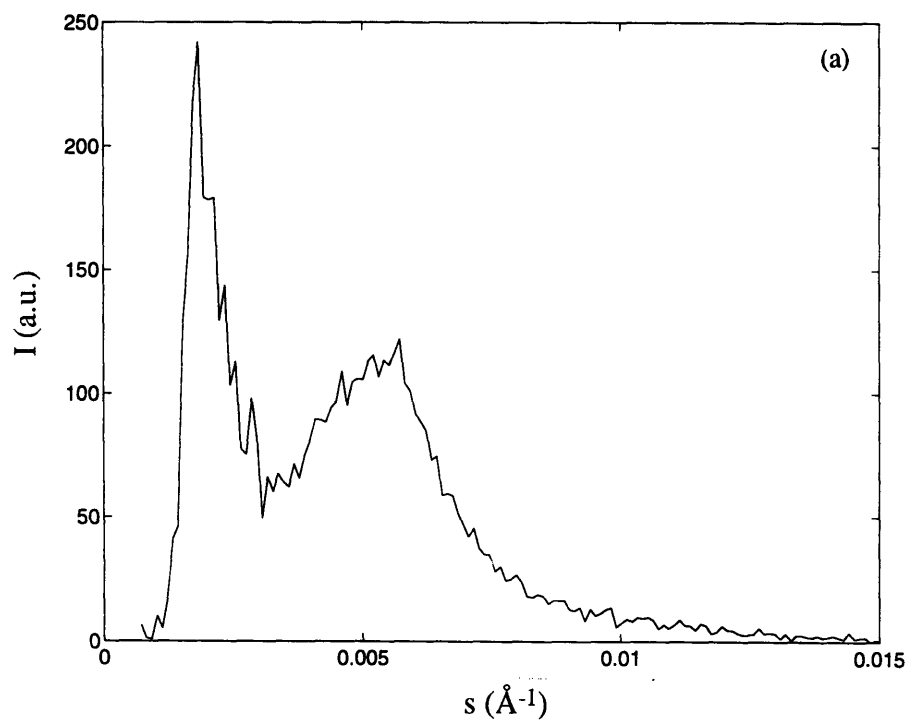
Figure 5.12   SAXS intensity of the meridian section vs. s for annealed fiber,

(a) DMS-7 at 125°C, (b) HMS-7 at 108°C.
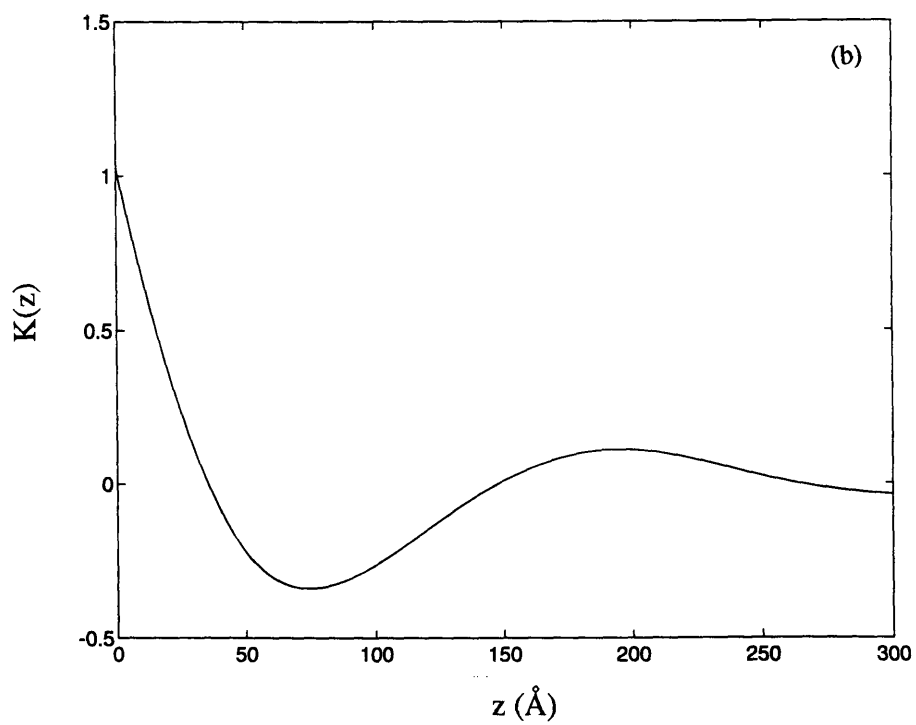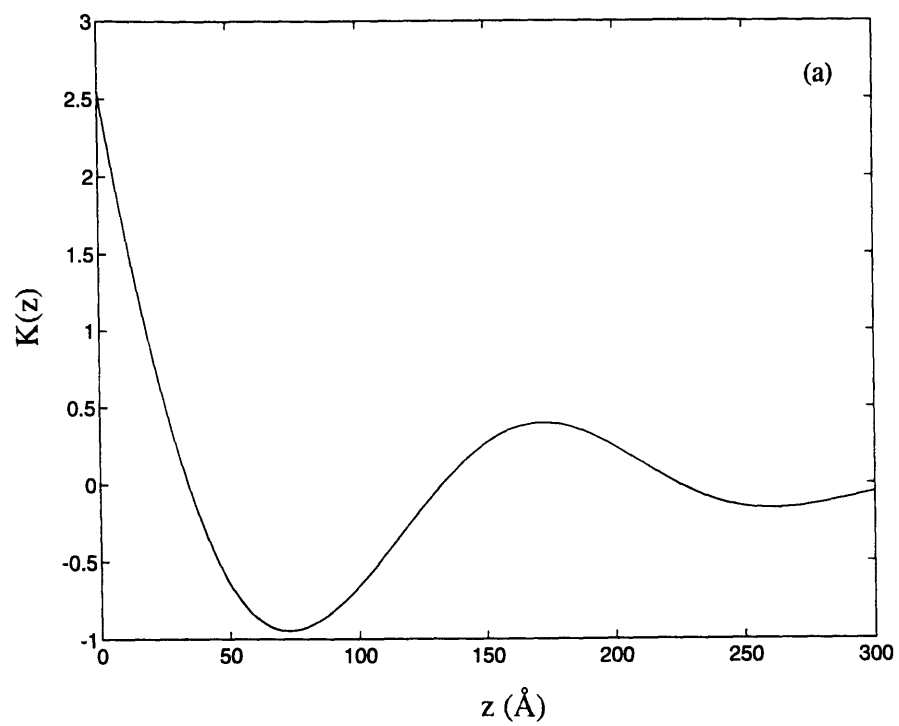
Figure 5.13   One-dimensional electron density correlation function for annealed

fiber, (a) DMS-7 at 125°C, (b) HMS-7 at 108°C.

5.4. DISCUSSION

As described in Dr. Heidi Schreuder-Gibson's work [51], the cross-section of the stilbene unit of DMS polycarbonates is 8.6 Å, which is much larger than that of HMS polycarbonates, at 6.5 Å. Therefore, we expect some differences in behavior between the two groups of polycarbonates. First of all, we notice that unlike HMS polycarbonates, DMS polycarbonates have only one broad exotherm. Also, the liquid crystalline phase transition can not be separated from the crystalline phase transition even at higher cooling rates. These facts suggest that DMS polycarbonates have less stable liquid crystalline phases than HMS polycarbonates do. The second lateral substituent on the mesogen further reduces the thermal stability of the liquid crystalline phase. This phenomenon has been observed in other LCPs [14,21,49], as described in Chapter 1.2.1 and 1.2.2. The second lateral substituent on the mesogen separates the polymer chains further, which reflects in the larger crystal unit cell dimension for DMS-7 compared with HMS-7. The unit cell parameters relating to interchain distances are b and $a\sin\beta$ (where $\beta = 90°$ for DMS-7). The area of the basal area, the product of b and $a\sin\beta$ parameters, is 41.9 $Å^2$ for HMS-7, which is smaller than 43.6 $Å^2$ for DMS-7.

As mentioned in 1.1.2, both the asymmetric shape and anisotropic molecular force are both important to the stability of the liquid crystalline phase. For DMS polycarbonates, not only the shape asymmetry but also the interaction between polymer chains is reduced. Therefore, as shown in Figure 1.3b, the free energy of the liquid crystalline phase should be even higher than that of the crystalline phase and the isotropic phase for DMS polycarbonates, compared with HMS polycarbonates. Consequently, T_{lc-i} of DMS polycarbonates is pushed to even lower temperature and the virtual mesophase behavior is enhanced.

154

The times to maximum heat flow observed in the isothermal crystallization study are less sensitive to temperature for DMS-7, compared with HMS-7. This result might also relate to the second lateral substituent on the mesogen. According to the kinetic theory of crystallization [125], the growth rate of crystals is proportional to $\exp(-K_g/T\Delta T)$, if crystallization happens in the temperature range of nucleation rate control. K_g is a parameter proportional to $1/\Delta f$, where Δf can be treated as the free energy difference between the crystalline phase and the liquid crystalline phase, which serves as crystal nuclei here. The growth rate of the HMS-7 crystalline phase is more sensitive to crystallization temperature change than the DMS-7 crystalline phase, which suggests that the Δf between the crystalline phase and the liquid crystalline phase should be smaller for HMS-7 than for DMS-7. This further supports that the separation of adjacent DMS polycarbonate polymer chains lowers the stability of the liquid crystalline phase.

The closeness of adjacent polymer chains of HMS-7 compared to those of DMS-7 is also reflected in the raw fiber WAXS pattern. DMS-7 raw fiber pattern only shows a single diffuse maximum on the equator, which is characteristic of a nematic mesophase. However, HMS-7 raw fiber pattern displays two equatorial reflections, which reflect a higher level of order in the interchain packing.

Because of the steric effect of the second lateral substituent on the mesogen, DMS polycarbonates do not seem to have "odd-even" property oscillation with the methylene spacer length, unlike HMS polycarbonates which do show such oscillation. DMS-7 does not exist in a stable intermeshed structure like HMS-7 does. It is our supposition that the steric effect of the second methyl substitution on the mesogen reduces the carbonate dipole interaction between adjacent polymer chains. Therefore, the transition temperatures do not change regularly with the methylene spacer length for DMS

polycarbonates. DMS-7 and 8 seem to have close crystallization and melting transition temperatures. When DMS-7 and 8 are isothermally crystallized at 124°C, they have similar values of linear crystallinity, lamellar thickness, and long period. Though the lamellar thickness and long period are higher for DMS-7 than DMS-8 when both are cooled at 5°C/min from the melt, it is probably because a large population of less perfect crystalline lamellae are formed during the cooling process for DMS-8.

In general, DMS polycarbonates have slightly higher linear crystallinity than HMS polycarbonates, as observed in several experiments described above. For example, annealed DMS-7 and HMS-7 have similar values of lamellar thickness, but DMS-7 has lower long period value because of slightly higher linear crystallinity. We suggest that the higher degree of structural symmetry for DMS than HMS polycarbonates might be the reason for the higher linear crystallinity of DMS polycarbonates.

5.5. CONCLUSIONS

The steric effect of the second lateral methyl substituent on the stilbene mesogen lowers the stability of the liquid crystalline phase of DMS polycarbonates. DMS polycarbonates do not have "odd-even" property oscillation with the methylene spacer length, unlike HMS polycarbonates which do. We suggest that this may be caused by the possible loss of carbonate dipole interaction caused by the steric effect.

156

Chapter 6

Summary and Suggestions for Future Work

In summary of this research, the flexibility of the carbonate linkage causes the monotropic liquid crystalline behavior of α-methyl stilbene polycarbonates. Both thermal and structural properties are affected by the chemical composition of α-methyl stilbene polycarbonates compared with α-methyl stilbene polyesters and polyethers. The low transition temperatures reflect the entropic effect given by the carbonate linkage, which increases chain flexibility. Furthermore, the structural studies using WAXS reveal that the enthalpic effect from the carbonate dipole interaction between polymer chains is also an important factor that causes the fast crystallization from the liquid crystalline phase. In addition to the carbonate linkage, the methylene flexible spacer length obviously plays an important role in the crystalline structure and crystallization kinetics. For HMS-7 and 8 the close match of the length of the methylene flexible spacer with that of the α-methyl stilbene mesogen causes fast crystallization from the liquid crystalline phase. When the length of the flexible spacer is higher than that of the α-methyl stilbene mesogen, that is, when the flexible spacer number n exceeds 9, the crystal structures change. Therefore, for $n \geq 9$, the melting temperatures drop, reflecting the reduced degree of perfection of the crystal structure.

An obvious odd-even effect is seen in the crystal structure parameters from WAXS and the crystal structure dimensions from SAXS for HMS-5 to 8, which has never been found before. The reason causing the odd-even effect is that HMS-5 to 8 have stable "intermeshed" crystal structure, in which the disposition of the carbonate dipoles is different from n-even to n-odd. However, there is no odd-even effect observed in the melting transitions, probably because the broad melting endotherms obscure this effect.

157

Finally, the second methyl substitution on the mesogen in the DMS polycarbonates possibly causes a reduction of the carbonate dipole interaction between the polymer chains and therefore results in a loss of the odd-even effect.

For commercial applications, thermotropic LCPs offer an advantage since they can be extruded by melt processing from the liquid crystalline state to form highly oriented fibers with high tensile strength. A broad temperature range of liquid crystalline phase stability is desirable so that the processing temperature can be easily controlled. α-methyl stilbene polycarbonates have low transition temperatures, which is an advantage for lowering the energy cost in the melting processing. However, our α-methyl stilbene polycarbonates only have a monotropic liquid crystalline phase with a narrow temperature stability range unlike α-methyl stilbene polyesters and polyethers which have a broader more stable enantiotropic liquid crystalline phase. Therefore, in order to have possible use for α-methyl stilbene polycarbonates as fiber forming materials, it is desired to broaden the temperature range of the liquid crystalline phase stability. One possible way is to copolymerize α-methyl stilbene polycarbonates with α-methyl stilbene polyesters or polyethers. The resulting copolymer might have a liquid crystalline phase with a broadened, more stable temperature range, because the crystallization of each component might be depressed to lower temperature. Also, this approach might improve the mechanical properties of α-methyl stilbene polycarbonate fibers like increasing their toughness.

For applications as a reinforcement material, a main chain thermotropic LCP with the "intermeshed" crystal structure is better than that with the "layered" crystal structure. The reason is that in the "layered" structure, the methylene flexible spacer has more space and freedom for conformational changes, which generally reduces the stiffness of polymers. On the other hand, in the "intermeshed" crystal structure, the methylene

158

flexible spacer directly contacts the rigid mesogen, which causes a more extended conformation of the methylene spacer and therefore a higher stiffness. For our liquid crystalline α-methyl stilbene polycarbonates, the "intermeshed" crystal structure can only exist when the length of the methylene spacer is smaller than that of the mesogen. Similar effect of the length of the methylene spacer on the crystal structure has also been observed in α-methyl stilbene polyethers [71]. Therefore, for the application of the main chain thermotropic LCPs containing the methylene flexible spacer as a reinforcement material, we suggest that the methylene spacer length should be chosen to be lower than that of the mesogen.

For future research, the liquid crystalline behavior of main chain thermotropic LCPs, especially monotropic ones, is very complex. Here we have focused on just one type of monotropic LCP. Future work might include other mesogens containing rigid groups such as anthracene or naphthalene. We could investigate how monotropic liquid crystalline behavior is related to mesogen type. The question of what specific chain chemistry leads to monotropic vs. enantiotropic behavior would be addressed by such studies.

In our research, DSC, wide and small angle X-ray scattering, optical microscopy and TEM have already given us macroscopic and microscopic understanding of the formation of the liquid crystalline phase and the crystallization from the liquid crystalline phase in our liquid crystalline stilbene polycarbonates. However, it is still helpful to use other techniques, such as solid state nuclear magnetic resonance (NMR) and modulated differential scanning calorimetry. High temperature NMR with decreasing and increasing temperature can give us the information on the chain conformation following the phase transition. By giving a sinusoidal temperature oscillation, modulated differential scanning calorimetry (MDSC) can resolve heat flow into the reversible and non-

reversible parts, which are related to heat capacity and kinetic processes, respectively. For example, the glass transition is a polymer chain relaxation process, which gives a non-reversible endothermic heat flow response. The crystallization and melting behavior is complicated in our LCPs. MDSC might separate the undistinguished thermal transitions observed in conventional DSC.

Furthermore, in our research, we are able to explore the relationship between the chemical structure variations, especially the methylene spacer length, and the morphology of the liquid crystalline phase and the crystalline phase for α-methyl stilbene polycarbonates. It might be interesting to investigate if the methylene spacer length plays a similar role in α-methyl stilbene polyesters and polyethers, which have not been studied thoroughly.

Another possible area of future work is investigation of the mechanical properties of extruded LCP fibers. It might be interesting to determine the role of chemical structure variations on the mechanical behaviors. The chemical variations can include: changes in flexible spacer length, linking group chemistry, and maybe substitution on the mesogen. The investigation of the relation between the mechanical behavior and morphology change by SAXS is a potential research field.

Bibliography

1.   Kwolek, S. L.; Morgan P. W.; Schaefgen J. R. In *Liquid Crystalline Polymers, Encyclopedia of Polymer Science and Engineering;* John Wiley & Sons, 1985, Vol 9.
2.   Demus, D.; Richter, L. *Textures of Liquid Crystals;* Verlag Chemie, Weinheim, 1978.
3.   Kleman, M. *Liquid Crystals and Plastic Crystals;* Gray, G. W. and Winsor P. A. Eds; Horwood, Chichester, 1974, Vol. 1; P. 76.
4.   Noel, C. In *Liquid Crystal Polymers: From structure to applications;* Collyer A., Ed.; Elsevier Science Publishers LTD, England, 1992; Chapter 2, P. 58.
5.   Thomas, E. L. and Wood, B. A. *Faraday Discuss. Chem. Soc.* **1985**, 79, 229.
6.   Flory, P. J. *Proc. R. Soc. London Ser.* **1956**, A 234 , 60.
7.   Ref 6, p.73.
8.   Flory, P. J.; Ronca, G. *Mol. Cryst. Liq. Cryst.* **1979**, 54, 289.
9.   Flory, P. J. In *Liquid Crystal Polymers I, Advances in Polymer Science Series*; Gordon, M. Ed.; Spring-Verlag, New York, 1984, Vol. 59; P. 1.
10. Aharoni, S. M. *Macromolecules* **1988**, 21, 1941.
11. Aharoni, S. M. *Macromolecules* **1989**, 22, 686.
12. Percec, V.; Keller, A. *Macromolecules* **1990**, 23, 4347.
13. Keller, A.; Ungar, G.; Percec, V. In *Liquid-Crystalline Polymers*; Weiss , R. A. and Ober, C. K., Ed.; ACS Symposium Series 435, 1989; Chapter 23.
14. Sirigu, A. In *Liquid Crystallinity in Polymers: Principles and Fundamental Properties*; Ciferri, A., Ed.; New York, 1991; Chapter 7.
15. Asrar, J.; Thomas, O; Zhou, Q.; Blumstein, A. *Proc. Macro-IUPAC,* Amherst, 1982.
16. Blumstein, A.; Vilasagar, S.; Ponrathnam. S.; Clough, S.B.; Blumstein, R.B.; Maret, G. *J. Polym, Sci., Polym. Phys. Ed.*, **1982**, 20, 877.
17. Jo, B.W.; Lenz, R.W.; Jin, J.I. *Makromol. Chem. Rapid Commun.* **1982**, 3, 23.
18. Lenz, R.W. *Pure Appl. Chem.* **1985**, 57, 1537.
19. Lenz, R.W. *Faraday Disc. Chem. Soc.* **1985**, 79, 21.
20. Limura, K.; Koide, N.; Ohta, R. *Rep. Prog. Polym. Phys. Jpn.* **1981**, 24, 231.
21. Roviello, A.; Santagata, S.; Sirigu, A. *Makrmol. Chem. Rapid Commun.* **1983**, 4, 281.
22. Zhou, Q.-F.; Lenz, R.W. *J. Polym. Sci., Polym. Chem. Ed.*, **1983**, 21, 3313.
23. Anton, S.; Lenz, R. W.; Jin, J. I. *J. Polym. Sci., Polym. Chem. Ed.* **1981**, 19, 1901.
24. Aharoni, S. M. *Macromolecules* **1988**, 21,1941; **1989**, 22, 686; **1989**, 22, 1125.
25. Aharoni, S. M.; Correale, S. T.; Hammond, W. B.; Hatfield, G. R.;Murthy, N. S. *Macromolecules* **1989**, 22, 1137.
26. Blumstein, A.; Thomas, O. *Macromolecules* **1982**, 15,1264.
27. Blumstein, R. B.;Stickles, E. M.; Blumstein, A. *Mol. Cryst. Liq. Cryst.* **1982**, 82, 205.
28. Cheng, S. Z. D.; Janimak, J. J.; Sridhar, K.; Harris, F. W. *Polymer* **1989**, 30, 494; **1990**, 31,1122.
29. de Abajo, J.; de la Campa, J.; Kricheldorf, H. R.; Schwarz, G. *Makromol. Chem.* **1990**, 191, 537.
30. Griffin, A. C.; Havens, S. J. *J. Polym. Sci., Polym. Phys. Ed.* **1981**, 19, 951.
31. Jonson, H.; Werner, P. E.; Gedde, U. W.; Hult, A. *Macromolecules* **1989**, 22, 1683.
32. Krigbaum, W. R.; Astar, J.; Toriumi, H.; Ciferri, A.; Preston, J. *J. Polym. Sci.,*

Polym. Phys. Ed. **1982**, 20, 109.

33. Krigbaum, W. R.; Watanable, J. *Polymer* **1983**, 24, 1299.
34. Kricheldorf, H. R.; Huner, R. *Makromol. Chem., Rapid. Commun.* **1990**, 11, 211.
35. Kricheldorf, H. R.; Domschke, A.; Schwarz, G. *Macromolecules* **1991**, 24, 1011.
36. Kricheldorf, H. R.; Jahnke, P. *Eur. Polym. J.* **1990**, 9, 1009.
37. Kricheldorf, H. R.; Schwarz, G.; de Abajo, J.; de la Campa, J. G. *Polymer* **1991**, 32, 942.
38. Kricheldorf, H. R.; Huner, R. *J. Polym. Sci., Polym. Chem.* **1992**, 30, 337.
39. Lenz, R. W.; Jin, J. I. *Macromolecules* **1981**, 14, 1405.
40. Laus, M.; Caretti, D.; Angeloni, A. S.; Calli, G.; Chiellini, E. *Macromolecules* **1991**, 24,1459.
41. Moore, J. S. Stupp, S. I. *Macromolecules* **1987**, 20, 273, 282; **1988**, 21, 1222.
42. Ober, C. K.; Jin, J. I.; Lenz, R. W. *Polym. J.* **1982**, 14, 9.
43. Sigaud, G.; Yoon, D. Y.; Griffin, A. C. *Macromolecules* **1983**, 16, 875.
44. Stupp, S. I.; Moore, J. S.; Martin, P.G. *Macromolecules* **1988**, 21, 1228.
45. Smyth, G.; Valles, E. M.; Pollack, S. K.; Grebowickz, J.; Stenhouse, P. J.; Hau, S. L.; MAcknight, W. J. *Macromolecules* **1990**, 23, 3389.
46. Sato, M. *J. Polym. Sci., Polym. Chem.* **1988**, 26, 2613.
47. Viney, C.; Yoon, D. Y.; Reck, B.; Ringsdorff, H. *Macromolecules* **1989**, 22,4088
48. Jackson, W. J.; Morris, J. C., *J . Appl. Polym. Sci. Appl. Polym. Symp.* **1985**, 41, 307.
49. Ruviello, A; Sirigu, A. *Makromol. Chem.* **1982**, 183, 895.
50. Percec, V.; Shaffer, T. D.; Nava, H. *J. Polym. Sci., Polym. Lett.* **1984**, 22, 637.
51. Bluhm, A. L.; Cebe, P.; Schreuder-Gibson, H. L.; Stapler J. T.; Yeomans, W. *Mol. Cryst. Liq.* Cryst. **1994**, 239, 123.
52. Donald, A. M.; Windle, A. H. *Liquid Crystalline Polymers*; Cambridge Univ. Press, Cambridge, 1992.
53. Muller, K.; Kothe, G. *Ber. Bunsenges. Phys. Chem.* **1985**, 89, 1214.
54. Samulski, E. T.; Gauthier, M. M.; Blumstein, R.; Blumstein, A. *Macromolecules* **1984**, 17, 479.
55. Bruckner, S.; Scott, J. C.; Yoon, D. Y.; Griffin, A. C. *Macromolecules* **1985**, 18, 2709.
56. Martins, A. F.; Ferreira, J. B.; Volino, F.; Blumstein, A.; Blumstein, R. B. *Macromolecules* **1983**, 16, 279.
57. Furuya, H.; Abe, A. *Polym. Bull.* **1988**, 20, 467.
58. Abe, A. *Macromolecules* **1984**, 17, 2280.
59. Yoon, D. Y.; Bruckner, S. *Macromolecules* **1985**, 18, 651.
60. Napolitano, R.; Pirozzi, B.; Tuzi, A. *Eur. Polym. J.* **1988**, 24, 103.
61. Auriemma, F.; Corradini, P.; Tuzi, A. *Macromolecules* **1987**, 20, 293.
62. Jin, J. I.; Choi, E. J.; Ryu, S. C.; Lenz, R. W. *Polym. J.* **1986**, 18, 63.
63. Griffin, A. C.; Britt, T. R. *Mol. Cryst. Liq. Cryst. Lett.* **1983**, 92, 149.
64. Donald, A. M.; Viney, C.; Windle, A. H. *Polymer* **1983**, 24, 155.
65. Bedford, S. E.; Windle, A. H. *Polymer* **1990**, 31, 616.
66. Chen, S.; Jin, Y.; Hu, S.; Xu, M. *Polymer* **1987**, 28, 208.
67. Hoff, M.; Keller A.; Odell J. A.; Percec, V. *Polymer* **1993**, 34, 1800.
68. Ref. 51, Chapter 2, P. 15.
69. Pardey, R.; Zhang, A.; Gabori, P. A.; Harris, F. W.; Cheng, S. Z. D.; Adduci, J.; Facinelli, J. V.; Lenz, R. W. *Macromolecules* **1992**, 25, 5060.
70. Campoy, I; Marco, C.; Gomez, M. A.; Fatou, J. G. *Macromolecules* **1992**, 25, 4392.
71. Unger, G.; Keller, A. *Mol. Cryst. Liq. Cryst.* **1987**, 155, 313.
72. Biswas, A., Gardner, K. H. and Wojtkowski, P. W. In *Liquid-Crystalline*

Polymers; Weiss, R. A. and Ober, C. K., Ed.; ACS Symposium Series 435, 1989; Chapter 19, P. 256.

73.   Papadimitrakopoulos, F.; Hsu, S. L.; MacKnight, W. J. *Macromolecules* **1992**, 25, 4761.

74.   Papadimitrakopoulos, F.; Sawa, E.; MacKnight, W. J. *Macromolecules* **1992**, 25, 4682.

75.   Percec, V.; Tsuda, Y. *Macromolecules* **1990**, 23, 3509.

76.   Percec, V.; Yourd, R. *Macromolecules* **1989**, 22, 524.

77.   Percec, V.; Yourd, R. *Macromolecules* **1989**, 22, 3229.

78.   Cheng, S. Z. D.; Yandrasits, M. A.; Percec, V. *Polymer* **1991**, 32, 1284.

79.   Yandrasits, M.; Cheng, S. Z. D.; Zhang, A.; Cheng, J.; Wunderlich, B.; Percec, V. *Macromolecules* **1992**, 25, 2112.

80.   Fujishiro, K.; Lenz, R. W. *Macromolecules* **1992**, 25, 81.

81.   Blumstein, R. B.; Blumstein, A. *Mol. Cryst. Liq. Cryst.* **1988**, 165, 361.

82.   Blumstein, A. *Polym. J.* **1985**, 17(1), 277.

83.   Dobbs, E. C.; Goldberg, L.; Lawson, W.; Robinson R. *Proc. Roy. Soc.* **1939**, B127, 140.

84.   Sato, M.; Nakatsuchi, K.; Ohkatsu, Y. *Makromol. Chem., Rapid Commun.* **1986**, 7, 231.

85.   Hoffman, J. D.; Weeks, J. J. *J. Res. Natl. Bur. Stand.* **1962**, 66, 13.

86.   Carpaneto, L., Marsano, E., Valenti, B.; Zanardi, G. *Polymer* **1992**, 33, 3865.

87.   Warner, S. B.; Jaffe, M. *J. Cryst. Growth* **1980**, 48, 184.

88.   Papadimitrakopoulos, F.; Kantor, S. W.; MacKnight, W. J. In *Fiber and Polymer Science, Recent Advances;* Fornes, R. E., Gilbert, R. D., Eds.; VCH Publishers, 1992.

89.   Cebe, P.; Carbeck, P.; Schreuder-Gibson, H. *Polym. Preprints* **1992**, 33(1), 331.

90.   Cheng, Y.-Y.; Brillhart, M.; Cebe, P.; Schreuder-Gibson, H. L.; Bluhm, A. L.; Yeomans, W. submitted to *Mol. Cryst. Liq. Cryst.*

91.   Butzbach, G. D., Wendorff, J. H.; Zimmermann, H. J. *Polymer* **1986**, 27, 1337.

92.   Bisvas, A.; Blackwell, J. *Macromolecules* **1988**, 21, 3146.

93.   Bisvas, A.; Blackwell, J. *Macromolecules* **1988**, 21, 3152.

94.   Bisvas, A.; Blackwell, J. *Macromolecules* **1988**, 21, 3158.

95.   Bassett, D. C.; Olley, R. H.; Al Raheil, I. A. M. *Polymer* **1988**, 29, 1745.

96.   Blundell, D. J.; Osborn, B. N. *Polymer* **1983**, 24, 953.

97.   Cebe. P.; Hong, S.-D. *Polymer* **1986**, 27, 1183.

98.   Cheng, S.; Cao, M.-Y.; Wunderlich, B. *Macromolecules* **1986**, 19, 1868.

99.   Cheng, Y. -Y.; Cebe, P.; Schreuder-Gibson, H. L.; Bluhm, A. L.; Yeomans, W. *Macromolecules* **1994**, 27, 5440.

100.   Spells, S. J.; Hill, M. J. *Polymer* **1991**, 32, 2716.

101   Schouterden, P.; Vandermarliere, M.; Riekel, C.; Koch, M. H. J.; Groeninckx, G., Reynaers, H. *Macromolecules* **1989**, 22, 1137.

102.   Russell, T. P.; Koberstein, J. T. *J. Polym. Sci. Polym. Phys. Edn* **1985**, 23, 1109.

103.   Santa-Cruz, C.; Stribeck, N.; Zachmann, H. G. ; Balta Calleja, F. J. *Macromolecules* **1991**, 24, 5980.

104.   Bark, M.; Schulze, C.; Zachmann, H. G. *Am. Chem. Soc. Div. Polym. Chem. Polym. Prepr.* **1990**, 31, 106.

105.   Hsiao, B. S.; Gardner, K. H.; Wu, D. Q.; Chu, B. *Polymer* **1993**, 34, 3986.

106.   Hsiao, B. S.; Gardner, K. H.; Wu, D. Q.; Chu, B. *Polymer* **1993**, 34, 3996.

107.   Wang, J.; Alvarez, M.; Zhang, W.; Wu, Z.; Li, Y.; Chu, B. *Macromolecules* **1992**, 25, 6943.

108.   Huo, P. P.; Cebe, P.; Capel, M. *J. Polym. Sci. Polym. Phys. Edn* **1992**, 30, 1459.

109.   Huo, P. P.; Cebe, P. *Colloid Polym. Sci.* **1992**, 270, 840.

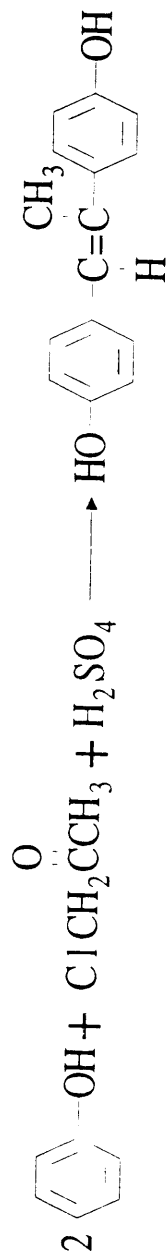110.   Huo, P. P.; Friler, J. B.; Cebe, P. *Polymer* **1993**, 34, 4387.

111. Hsiao, B. S.; Sauer, B. B.; Biswas, A. *J. Polym. Sci. Polym. Phys. Edn.* **1994**, 32, 1459.
112. Unger, G.; Keller, A. *Polymer* **1986**, 27, 1835.
113. Russell, T. P.; Brown H. R. *J. Polym. Sci. Polym. Phys. Edn* **1987**, 25, 1129.
114. Song, H. H.; Wu, D. Q.; Chu, B.; Satkowski, M.; Ree, M.; Stein, R. S.; Phillips, J. C. *Macromolecules* **1990**, 23, 2380.
115. Tashiro, K.; Satkowski, M.; Stein, R. S.; Li, Y.; Chu, B.; Hsu, S. L. *Macromolecules* **1992**, 25, 1809.
116. Cheung, Y. W.; Stein, R. S.; Chu, B.; Wu, G. *Macromolecules* **1994**, 27, 3589.
117. Nojima, S.; Kato, K.; Ono, M.; Ashida, T. *Macromolecules* **1992**, 25, 1922.
118. Lopez-Cabarcos, E.; Gonzalez-Arche, A.; Balta-Calleja, F. J.; Bosecke, P.; Rober, S.; Bark, M.; Zachmann, H. G. *Polymer* **1991**, 32, 3097.
119. Glatter, O.; Kratky, O. *Small Angle X-ray Scattering*, Academic Press, New York, 1982.
120. Koberstein, J. T.; Morra, B.; Stein, R. S. *J. Appl. Cryst.* **1980**, 13, 34.
121. Strobl, G. R.; Schneider, M. *J. Polym. Sci. Polym. Phys. Edn.* **1980**, 18, 1343.
122. Balta-Calleja, F. J.; Vonk, C. G. *X-ray Scattering of Synthetic Polymers*; Jenkins, A. D., Ed.; Elsevier Science Publishers B. V., 1989; Chapter 7.
123. Ferrevo, A.; Ferracini, E.; Hosemann, R. *Polymer* **1984**, 25, 1747.
124. Vonk, C. G. *Colloid Polym. Sci.* **1979**, 257, 1021.
125. Hoffman, J. D.; Davis, G. T.; Lauritzen, J. I. In *Treatise on Solid State Chemistry*; Hannay, N. B., Ed.; Plenum Press, New York, 1976.
126. Zaheer, S. H. J. Chem Soc., **1954**, 3360.

Appendix

Synthesis of Stilbene Polycarbonates

The polymerization method used to synthesize stilbene polycarbonates according to the method of Sato et al. [84] was described in detail by Dr. Schreuder-Gibson [51]. Her description is summarized as follows. The reactions were run in a side-arm test tube (23mm O. D. by 20 cm) which had a nitrogen inlet tube at the top for flushing while heating the reactants at atmospheric pressure, at which time the side-arm was vented through a water bubbler. In a typical reaction, equimolar (0.002 mol) proportions of the alkylene diphenyl dicarbonates and a stilbene were combined with 20 mg zinc acetate as catalyst. The reaction tube and the mixture of the alkylene diphenyl dicarbonates and a stilbene were placed in a Woods metal bath at 100°C under nitrogen for 1-2 hours. The mixture was then heated to 190°C for 2.5 hours, then house vacuum was applied and heating continued at 200°C for 2 hours, with a final heating to 210°C for 1 hour at high vacuum. The cooled reaction mixture was stirred with chloroform. The chloroform solution was filtered and added to the filtrate, which caused the polymer to separate. Yields were generally in the range of 50%. The follow two pages showing synthesis scheme were given by Dr. Schreuder-Gibson.
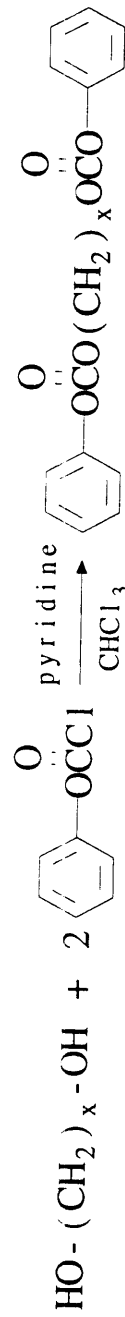
Synthesis of Stilbene Monomer

$$2 \ \langle\text{C}_6\text{H}_5\rangle\text{-OH} + \text{ClCH}_2\overset{\text{O}}{\overset{\|}{\text{C}}}\text{CH}_3 + \text{H}_2\text{SO}_4 \longrightarrow \text{HO-}\langle\text{C}_6\text{H}_4\rangle\text{-}\overset{\text{CH}_3}{\underset{\text{H}}{\text{C}=\text{C}}}\text{-}\langle\text{C}_6\text{H}_4\rangle\text{-OH}$$

4,4'-dihydroxy-α-methyl stilbene-trans

Ref: Zaheer, S.H., et al, *J. Chem. Soc. Lond.*, 1954, 3360 (1954)

Synthesis of Dicarbonate Monomer

$$\text{HO-(CH}_2)_x\text{-OH} + 2 \ \langle\text{C}_6\text{H}_5\rangle\text{-}\overset{\text{O}}{\overset{\|}{\text{OCC}}}\text{l} \xrightarrow[\text{CHCl}_3]{\text{pyridine}} \langle\text{C}_6\text{H}_5\rangle\text{-}\overset{\text{O}}{\overset{\|}{\text{OCO}}}(\text{CH}_2)_x\overset{\text{O}}{\overset{\|}{\text{OCO}}}\text{-}\langle\text{C}_6\text{H}_5\rangle$$

Ref: Sato, M., et al, *Makromol. Chem. Rap. Comm.*, 7, 231 (1986)

Synthesis of Polymer from Dihydroxy-α -Methyl Stilbene

$$\text{HO}-\overset{CH_3}{\underset{H}{C=C}}-OH + OCO(CH_2)_xOCO \xrightarrow{Zn(OAc)_2} \left[\overset{CH_3}{\underset{H}{C=C}}-OCO(CH_2)_xOCO \right]_n$$

Ref: Sato, M., et al, *Makromol. Chem. Rap. Comm.*, **7, 231 (1986)**